THE UNIVERSITY OF MANITOBA

OPTICAL STUDIES OF $TmCrO_3$ SINGLE CRYSTALS

by

© C.P. WONG

A THESIS

SUBMITTED TO THE FACULTY OF GRADUATE STUDIES

IN PARTIAL FULFILLMENT OF THE REQUIREMENTS FOR THE DEGREE

OF DOCTOR OF PHILOSOPHY

DEPARTMENT OF PHYSICS

WINNIPEG, MANITOBA

June 1981

OPTICAL STUDIES OF $TmCrO_3$ SINGLE CRYSTALS

BY

C.P. WONG

A thesis submitted to the Faculty of Graduate Studies of the University of Manitoba in partial fulfillment of the requirements of the degree of

DOCTOR OF PHILOSOPHY

TABLE OF CONTENTS

CHAPTER Page

ABSTRACT

The compounds $RCrO_3$, where R is a rare earth element or Yttrium, crystallize as orthorhombically distorted perovskites with the space group Pbnm. At sufficiently low temperatures these compounds order antiferromagnetically (Néel temperatures between 100-300 K) in one of a few temperature-dependent spin configurations, most commonly the $\Gamma_2(F_x)$ and $\Gamma_4(F_z)$, which have a net weak ferromagnetic moment along the $\vec{a}$ and $\vec{c}$ crystallographic axes respectively. Different experimental techniques have been applied to study the magnetic properties of these compounds. In particular, bulk magnetization and susceptibility, specific heat studies and optical absorption spectroscopy have been employed to study the field and temperature induced spin reorientation. Of these methods, optical absorption spectroscopy is the most direct and complete. This technique yields the energy levels and the group representation labels of both the R^{3+} and the Cr^{3+}, from which, in principle, all the physical quantities of interest can be calculated. This method also provides a very visual display of spin reorientation since energy level positions and selection rules depend critically on the spin configuration.

$TmCrO_3$ has been studied using magnetization and susceptibility methods. But optical studies have only been

conducted in the region ~13700 cm^{-1} (~7300 Å) where excitons due to the Cr^{3+} have been observed for many orthochromites. However the magnetization studies yield representation labels for the lowest two crystalline levels of Tm^{3+} which are different from that deduced for the similar levels of Tm^{3+} in $TmFeO_3$. These studies also do not determine unambiguously the stable spin configuration at ~4.2 K, although the exciton studies do indicate that the possible stable spin configuration at such temperatures is the $\Gamma_4(F_z)$. Finally, although magnon sidebands for excitons at ~13700 cm^{-1} have been reported for some orthochromites, they have not been reported for $TmCrO_3$.

The aim of this thesis is to determine the energy levels and group representation labels of Tm^{3+}, in single crystal $TmCrO_3$, corresponding to the optical transitions in the range 6000-8100 Å and to investigate the temperature and field induced spin reorientation at ~4.2 K. It also intends to investigate the possible occurrence of magnon sidebands of excitons at 13700 cm^{-1} and at other energies.

The results can be summarized as follows. Singlet states of the Tm^{3+} ground multiplet $^3H_6$ are found. In addition the positions of other Tm^{3+} levels in the $^3F_2$, $^3F_3$ and $^3F_4$ multiplets have been determined. The representation labels of most of the levels have also been determined. In particular the two lowest levels of Tm^{3+} have different representation

labels in agreement with the results deduced from magnetization studies. The stable spin configuration at zero field is found to be $\Gamma_4(F_z)$ in agreement with the results deduced from exciton studies of $TmCrO_3$. The magnon sidebands of the 13700 cm^{-1} excitons have been found and the magnon energies determined. They are close in value to those deduced for $YCrO_3$. Most important of all, magnon sidebands in the range 5000-5200 Å have been identified and the corresponding exciton positions predicted. No exciton transitions in this region have been reported in the literature for any orthochromites. Spin-flip type transitions involving Tm^{3+} and Cr^{3+} are also observed although the data are not sufficient for a more detailed understanding.

ACKNOWLEDGEMENTS

The author would like to take this opportunity to thank the following people; to his thesis advisor Professor A.H. Morrish for his supervision and encouragement throughout this research project; to Professor G. Tabisz and members of his group for very useful suggestions and sharing their equipment; to Professor A.C. Turnock, Geology Department, for the use of his equipment; to Drs. I. Yaeger and I. Maartense for numerous helpful discussions and providing the crystals (I.Y.); to Professor K. Aoyagi of Yamagata University, Japan, for sharing his unpublished results; to Dr. P. Picone for his suggestions and Dr. N. Saegusa for the translations of Japanese papers as well as very interesting discussions; to Mr. G. Roy and Mr. S-C Ho for invaluable technical assistance; to all the staff in the Electronics and Mechanical workshops for their suggestions; to Mrs. P. Giardino for her unbelievably efficient typing of the thesis. Finally the financial support received from the Physics Department of the University of Manitoba in the form of assistantships and research grants is gratefully acknowledged.

CHAPTER I

INTRODUCTION

1.1 The orthochromites

The present thesis intends to add to the intensive amount of research that has been done on the orthochromites, $RCrO_3$, where R is a rare earth element or Yttrium. The motivations for orthochromite research are both practical and fundamental. On the fundamental side, these compounds exhibit interesting phenomena as a result of the magnetic interactions of the R^{3+} and the Cr^{3+} ions, such as canted antiferromagnetism, a compensation point and spin-reorientation.

Different experimental techniques have been employed to study these compounds including magnetization and susceptibility, neutron diffraction and inelastic scattering, specific heat, optics (e.g. Faraday rotation), optical absorption spectroscopy and Raman spectroscopy. Absorption spectroscopy has the following advantages. First of all it yields not only information about the lower energy levels, but also about many excited states of both the R^{3+} and Cr^{3+} ions. Secondly this technique provides the microscopic parameters, the energy levels, which can be related to the macroscopic parameters, such as magnetization and specific heat, through statistical mechanics. Thirdly techniques like magnetization and specific heat do not separate the

contributions of the R^{3+} and Cr^{3+} ions. In contrast, optical spectroscopy displays separately (except for some accidental overlap of spectral lines) the R^{3+}, Cr^{3+} and R^{3+} - Cr^{3+} transitions. Finally the optical absorption technique also provides a very visual display of magnetic phase transitions, since energy level positions and selection rules depend critically on the temperature-dependent spin configurations.

1.2 Objective of this study

The aim of this thesis is to determine the energy and group representation labels of Tm^{3+} levels in $TmCrO_3$. In particular, it is intended to check the labels of the lowest two levels of Tm^{3+} (magnetization studies suggest these levels are of different representation whereas absorption studies of $TmFeO_3$ conclude that they are of the same representation). Another goal of this thesis is to determine the stable, zero field, spin configuration of $TmCrO_3$ at helium temperatures. Hence this work examines in detail the field- and temperature- induced spin reorientations through the observations of the various Tm^{3+}, Cr^{3+} and Tm^{3+}-Cr^{3+} transitions. Finally, since neither magnon sidebands of excitons at ~13700 cm^{-1} have been reported for $TmCrO_3$ nor magnon sidebands for the 'B' transitions of the Cr^{3+} ions for any $RCrO_3$, this thesis tries to investigate any such sidebands as well as spin-flip type of transitions involving both the Tm^{3+} and Cr^{3+} ions.

1.3 Relation to previous work

The work which will be reported in this thesis is a modest addition to the intensive research on $RCrO_3$, which began at the end of the sixties and is still being actively pursued, as witnessed by a series of papers on $YbCrO_3$ (Kojima et al, 1980 I, II, III). In this section the literature will be reviewed in the perspective of this thesis. In particular emphasis will be put on the optical absorption spectroscopy.

The research that has been done to determine the energy levels of R^{3+} in $RCrO_3$ as a main goal and as a means (complementary to other studies e.g. magnetization and specific heat) to study magnetic interactions and spin re-orientations will be reviewed. Cr^{3+} transitions, in particular, the excitons of the $^4A_2 \longrightarrow {}^2E$ single ion transitions (~13700 cm^{-1}) have been intensively studied together with their associated magnon sidebands. However, magnon sidebands and the associated excitons in the 'B' region of the Cr^{3+} single ion transitions (~5000 Å) have not been reported. These magnon sidebands are observed in this work; hence the literature on this region of transition will be briefly reviewed. Pair transitions, of the spin-flip type, involving both R^{3+} and Cr^{3+} ions have been reported only for $RCrO_3$ where R^{3+} is a Kramer's ion. Similar transitions for non-Kramer's ions have only been reported

for $HoCrO_3$ (Slobodsky, 1979) and in the present work. These will be reviewed. For very detailed and excellent reviews on $RCrO_3$ in general and their magnetic interactions in particular the following references are suggested: Nomura, 1978 and Hornreich 1978. The literature on $TmCrO_3$ will however be given detailed discussion separately in Chapter III.

Since the $RCrO_3$ compounds are structurally isomorphous with $YAlO_3$, and since the crystal fields on the rare earth ions at various sites, when introduced as impurities or in concentrated compounds, are weak, a good indication of the positions of the R^{3+} levels in $RCrO_3$ has been obtained by absorption studies of R^{3+} in $YAlO_3$ (Antonov et al, 1973). The effort was part of the work on the absorption and luminescence measurements as well as laser actions of some R^{3+} ions in $YAlO_3$. In conjunction with laser work, Weber, 1973 and Caird et al, 1975 have also produced fairly detailed energy level diagrams for both the R^{3+} and Cr^{3+} ions in $YAlO_3$ and other hosts. It was observed that not only the Cr^{3+} ions can have laser action when introduced in suitable hosts (e.g. ruby), they can also act as sensitizers to R^{3+} laser actions in $YAlO_3$. A most detailed review on lasers and excited states of rare earths is given by Reisfeld and Jørgensen, 1977.

The energy levels of R^{3+} in $RCrO_3$ have been determined in varying degrees of detail by optical absorption spectroscopy for the following orthochromites: $NdCrO_3$ (Hornreich et al, 1972, 1975), $ErCrO_3$ (Hasson et al, 1975; Courths et al, 1975, Kaneko et al, 1977). $YbCrO_3$ (Kojima, 1980I). However little is known about $CeCrO_3$ and $PmCrO_3$, whereas $PrCrO_3$ is totally opaque in the optical region. The lower energy levels of R^{3+} have also been obtained by inelastic neuton scattering (Shamir, 1977a, 1977b) and magnetization studies (see references of Hornreich, 1978).

The Cr^{3+} levels in various octahedral sites have been discussed by Wood et al, 1963, whereas Sugano et al, 1971 and Weber, 1974 have respectively reported the spectra of $YCrO_3$ and the energy level diagram of Cr^{3+} in $YAlO_3$ in the optical region.

Exciton magnon studies began with the orthochromites $YCrO_3$ and $LuCrO_3$, where both Y and Lu are non-magnetic. Up to the present, the following absorption studies on excitons ($\sim$13700 cm^{-1}) of Cr^{+} have been reported: $YCrO_3$ (Aoyagi et al, 1969; Allen, 1970; Tsushima and Aoyagi, 1970; Sugano et al, 1971; Aoyagi, 1974; Washimiya and Yamaguchi, 1975; Satoka and Washimiya, 1977), $LuCrO_3$ (Kajiura et al, 1975), $ErCrO_3$ (Meltzer, 1970; Meltzer and Moos, 1970), $DyCrO_3$ (Uesaka et al, 1971; Aoyagi, 1974),

$HoCrO_3$ (Meltzer and Moos, 1970), $YbCrO_3$ (Kojima et al, 1980 II, 1980 III), and $TmCrO_3$ (Aoyagi et al, 1976). Finally, the excitons of a number of orthochromites have been studied in great detail by Slobodsky, 1979. The results of these observations have the following characteristics in common. There are four exciton transitions which have a total Davydov splitting of less than 10 cm^{-1} and half widths of less than ~3 cm^{-1}. These transitions depend critically on the spin configurations and so are studied in connection with spin reorientations.

Magnon sidebands of the excitons have been reported for the following orthochromites: $YCrO_3$ (Van der Ziel and Van Uitert,1969a;Tsushima et al, 1970; Sugano et al, 1971; Aoyagi, 1974) and $LuCrO_3$ (Van der Ziel et al, 1969). Slobodsky, 1979 has also discussed magnon sidebands of these excitons in some detail. These observations show that the magnon sidebands are electric dipole in character, are allowed in all polarizations of the incident light, and are of half widths of ~ 30 cm^{-1}.

The 'B' transitions of Cr^{3+} occur often for Cr^{3+} as an impurity in a number of hosts: Ruby (Low, 1960; Kaplyanskii and Medvedev, 1968; Kaplyanskii and Przhevuskii, 1969; Kaplyanskii and Rozenbaum, 1972; Cohen and Bloembergen, 1964), MgO (Fairbank and Klauminzer,

1973) and Magnesium spinel (Sviridov et al, 1973). However the 'B' transitions for concentrated compounds have only been scantily reported in literature: Cr_2O_3 (McClure, 1962), $CrBr_3$ and $CrCl_3$ (Bermudez and McClure, 1979) and $YCrO_3$ (Sugano et al, 1971). (No excitons or associated magnon sidebands have ever been reported for these transitions). These observations show that the 'B' transitions are located at ~5000 Å. But unlike the rare earth ions, the Cr^{3+} ions are subjected to very strong crystal fields so the energy level positions at different sites could be very different.

Spin-flip transitions involving both R^{3+} and Cr^{3+} have been reported for the following orthochromites: $ErCrO_3$ (Meltzer, 1970), $DyCrO_3$ (Aoyagi, 1974; Aoyagi et al, 1977), and $YbCrO_3$ (Kojima et al, 1980 III) for the Kramer's ions and $HoCrO_3$ (Slobodsky, 1979) for a non-Kramer's ion. These observations show that these transitions are electric dipole, close to the 13700 cm^{-1} excitons, and have an anomalous shape with a sharp cut-off on the lowest energy side.

Spin reorientations have been observed spectroscopically with the R^{3+} transitions for the following orthochromites: $NdCrO_3$ (Hornreich et al, 1972), $ErCrO_3$ (Hasson et al, 1975; Courths and Hüfner, 1975; Kaneko et al,

1977), and $HoCrO_3$ (Courths and Hüfner, 1976). For spin reorientations observed with excitons see references given in connection with the discussion of excitons earlier. Spin reorientations observed with non-spectroscopic techniques have been reviewed in detail by Hornreich, 1978. The Faraday rotation technique has also been employed to determine whether there is a net component of magnetic moment along the propagation direction of the incident light. Polarized light with the $\vec{k}$ vector parallel and antiparallel to a component of magnetic moment in the direction of the $\vec{k}$ vector are rotated differently. The difference is proportional to the component of the magnetic moment. Thus this difference will vanish if a spin reorientation occurs so that there is no more net moment along the propagation direction. However,it should be noted that similar null results are also observed if the substance loses its moment as in a transition to the paramagnetic phase. The orthochromites studied with this technique are: $GdCrO_3$ (Zuk and Piotrowski, 1977) and $YCrO_3$ (Zuk and Piotrowski, 1978). Finally, the effect of ordering on Raman spectra have been reported for the following: $YCrO_3$ and $GdCrO_3$ (Udagawa et al, 1975) and $ErCrO_3$ (Ullrich et al, 1977). For a theoretical discussion of spin reorientations in rare earth orthochromites see Yamaguchi and Tsushima, 1973 and Hornreich, 1978 and references thereof.

CHAPTER II

SAMPLE PREPARATION AND THE EXPERIMENTAL SETUP

2.1 Sample preparation

The samples used in the present work were all prepared from crystals of several mm linear dimension. In this size the crystals are opaque. But they are beautifully green in transmitted light, when thinned and polished to a thickness of the order of 100 μm. For absorption spectroscopic work samples of this thickness and of several mm area are required. The crystallographic axes of the desired sample platelets can be determined by a knowledge of the external morphology of the crystal. The crystal grows with the habit that, when viewed along the c-direction, the crystal appears to be a parallelogram. The a and b axes are just the bisectors of the two angles of the parallelogram, which is easily recognized even with the unaided eye. To determine the a and b axes use is made of the fact that $TmCrO_3$ orders antiferromagnetically below 124 K with a weak ferromagnetic moment along the a-direction. Thus by cooling the crystal in liquid nitrogen (77.7 K) and using a small magnet the a-direction can be easily determined. The crystal with the known a and b directions is then glued onto the flat surface of the grinder (which is a metal cylinder) so that for the preparation of the a-b platelet the c axis is normal to

that surface, and similarly for the b-c platelet. These axes, e.g. a and b, are then marked on the grinder and the axis normal to the grinder surface is checked by taking Laue back reflection photographs. When the orientation of the bulk cyrstal is finished, the crystal is thinned down with sand papers of grids 240 - 600 to a thickness of about one mm and polished. After polishing,the crystal is removed and glued to a CaF_2 platelet of about 0.3 mm in thickness. The complex of the thinned crystal and CaF_2 is then reglued to another grinder with a small hole drilled parallel to the normal of the surface, and all the way through the grinder. Thus the transparency of the sample can be checked at all times. The CaF_2 is needed firstly to give a solid support to the very thin crystal and secondly to provide good thermal conductivity between the sample and the sample rod. When the crystal is sufficiently transparent it is polished again. By this time the crystal may be so thin that the parallelogram used to recognize the a and b axes has been lost. However the axes can be located again by viewing the sample between crossed polaroids. There will be complete extinction of transmitted light when either axis in the plane of the platelet is parallel to the easy axis of either the polarizer or analyser. Finally the sample plus CaF_2 is removed and glued onto the sample rod in the cryostat. There is no major difficulty in the preparation of the sample, except that, since these crystals are flux-grown,

occasionally pits filled with the flux will be encountered. Such pits will become holes in a thin sample. It is also important to have all surfaces cleaned and polished to achieve rigidity and to minimize loss due to scattering.

2.2 The experimental setup

The experimental setup is shown schematically in Figure 2.1. A tungsten lamp is used as the light source which illuminates the sample through the lens L_1 and L_2. Lenses L_3 and L_4 focus the light, after it has been reflected by the mirror, to the entrance slit of the spectrometer. The light entering the spectrometer exits through the exit slit to the N_2-vapour-cooled photomultiplier (EMI 9658F with S20 cathode). The output from the photomultiplier is further amplified before being recorded by the HP 680 strip chart record. Neon lines have been used for calibration. Light, when necessary, is polarized by a piece of polaroid. In the experiment it makes virtually no difference whether the polarizer is immediately in front of the sample or in the position shown.

2.2.1 The Czerny-Turner plane grating spectrometer

The schematic diagram of the spectrometer is shown in Figure 2.2. It consists of two mirrors M_1 and M_2 and a plane grating (600 lines/mm) which can be turned manually

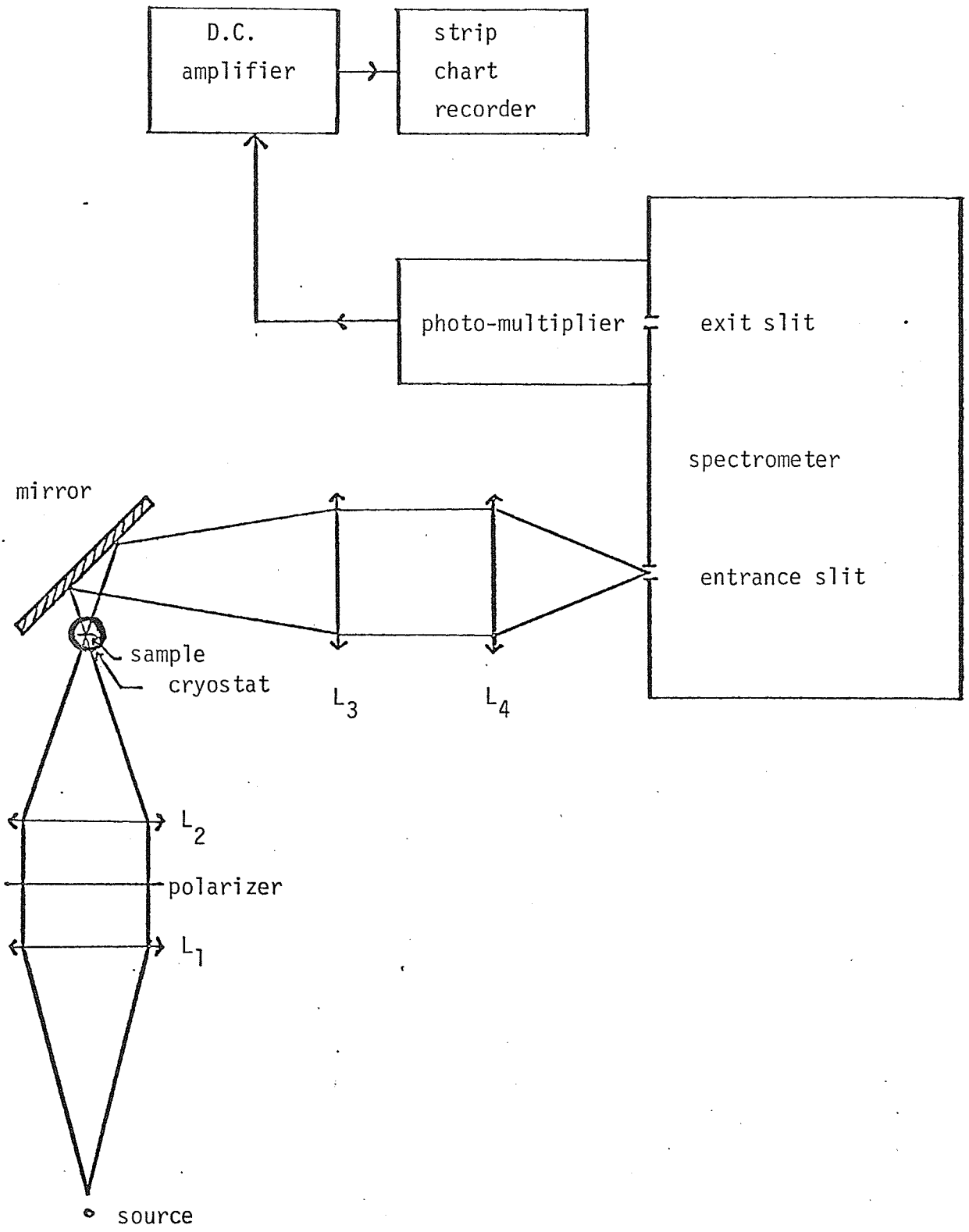

Figure 2.1: General setup of equipment

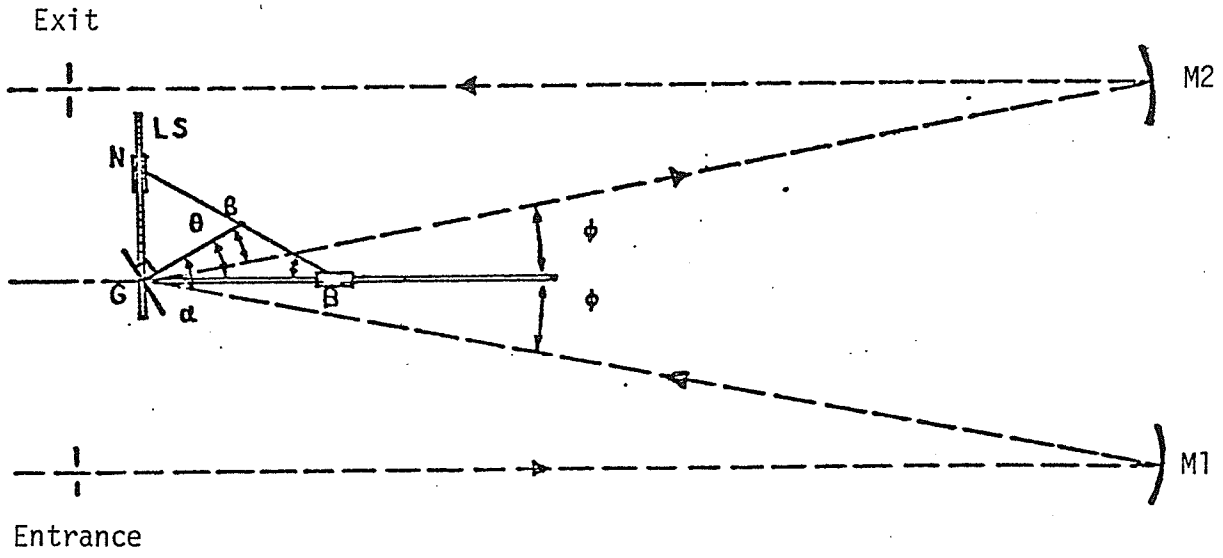

G = Grating B = Slide
N = Nut M1 & M2 = Mirrors
LS = Lead Screw

Figure 2.2: Schematic diagram of Czerny-Turner plane grating spectrometer

or by a motor so that any diffracted beam can be selected to pass through the exit slit to the photomultiplier. As the slide B moves away from the grating, NG decreases and the normal to the grating rotates toward GB.

Fundamental theory of the diffraction grating gives

$$m\lambda = d\ (\sin\alpha + \sin\beta)$$

where

m = order of diffracted beam,

λ = wavelength of diffracted beam,

d = grating spacing,

α = angle of incidence, and

β = angle of diffraction.

Both angles α and β are measured from the normal to the grating. However, this equation can be rewritten in terms of the constant angle ϕ ($\sim 7°$) and the variable θ which the normal to the grating makes with the line GB, as

$$m = d\ (2 \sin\theta \cos\phi)$$

where

$$\alpha = \theta + \phi$$

$$\beta = \theta - \phi$$

The resolving power $R_T = \lambda/\Delta\lambda$

$= \nu/\Delta\nu$

$= 2 \sin\alpha(W/\lambda) = mN$

where λ = wavelength,

W = width of ruling; total number of lines of grating is 600 x W = N,

ν = wavenumber,

m = order of diffraction,

N = total number of grating grooves.

Since resolution is a linear function of grating width (W), it is clear that if the source irradiates less than the full width of the grating, resolution will suffer. This dictates that the source or condensing lenses must fully illuminate the collimating mirror and hence the grating.

2.2.2 The optical helium cryostat

The cryostat is schematically shown in Figure 2.3. It consists mainly of a liquid helium compartment surrounding a central tube one end of which is the sample block. Outside this compartment and thermally isolated from it is the liquid nitrogen shield. Sample cooling is achieved through the flowing of liquid helium through the needle valve down the capillary tube and the evaporation of the liquid inside the sample block. The resultant vapour escapes through the central tube (the exhaust). By regulating the flow rate

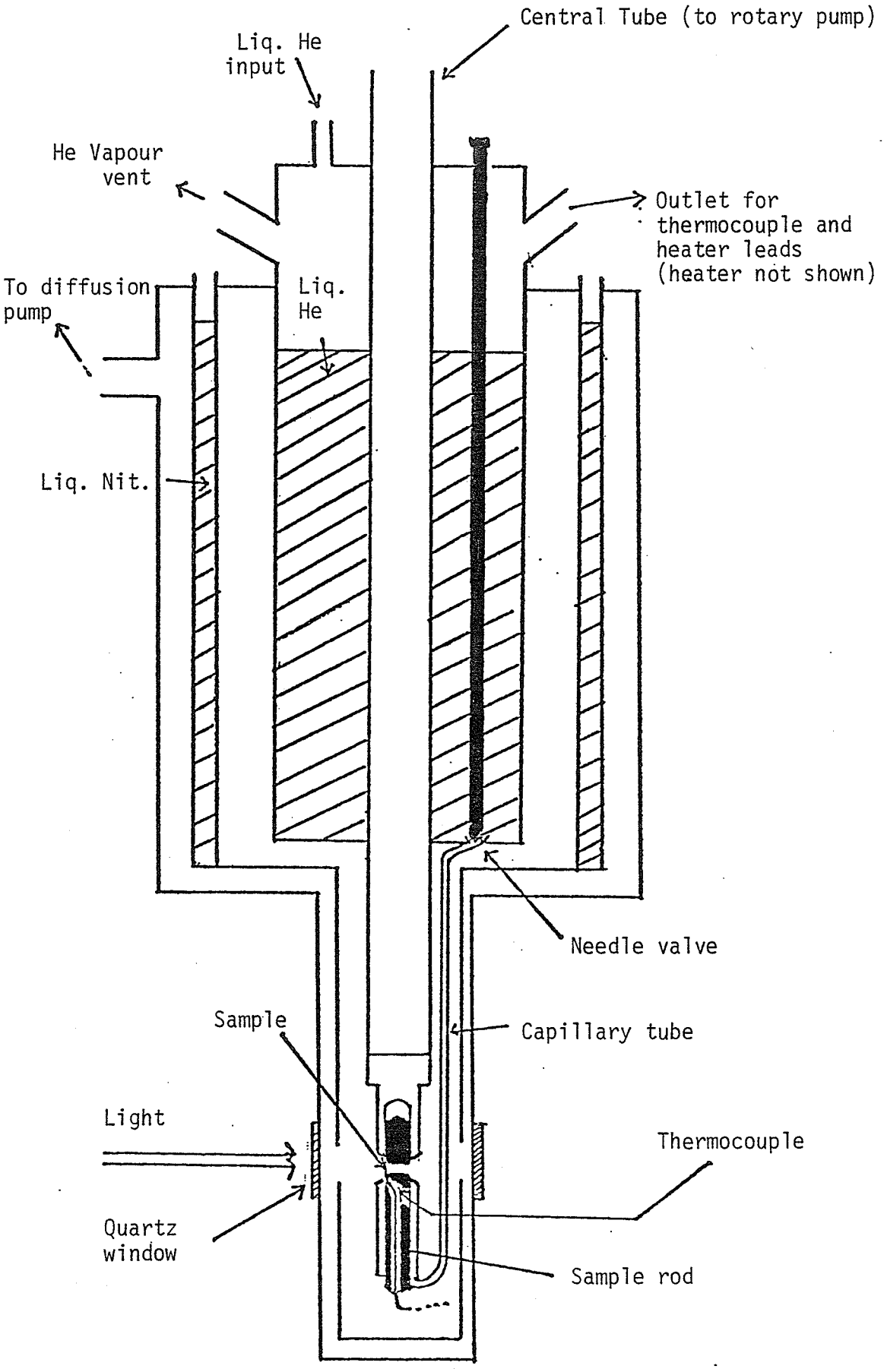

Figure 2.3: Schematic diagram of cryostat

with the needle valve and the exhaust rate with a pump, the temperature of the sample can be stabilized easily for above-helium temperatures. Such temperatures are measured by a thermocouple (Au + 0.03% Fe vs. Chromel) one junction of which is at the helium chamber and the other is at the sample. Temperatures below 4.2 K, obtained by pumping liquid helium, are measured by a calibrated carbon resistor glued next to the sample (not shown in Figure). There are two orthogonal pairs of quartz windows to allow light to illuminate the sample. To minimize heat losses there are radiation shields over the sample block (not shown) and at the lower end of the nitrogen shield.

CHAPTER III

Tm^{3+} CRYSTAL FIELD SPECTRA IN $TmCrO_3$

3.1 The lanthanides and lanthanide contraction

The rare-earth lanthanides constitute a group of chemically similar elements (Wybourne, 1965). In the atomic state, beginning with Lanthanum (Z = 57) and ending with Lutecium (Z = 71), they possess a common Xenon-like electronic structure, a number of 4f electrons and two or three outer electrons ($6s^2$ or $5d'\ 6s^2$). It is, however, the ionized state rather than the neutral state which has been the subject of intense investigation. In particular the triply ionized state attracts the most attention. In such states the electronic configuration is $4f^N\ 5s^2\ 5p^6$ with N = 0 for La ranging to N = 14 for Lu.

The compounds in which the rare-earth ions are triply ionized, e.g. the orthoferrites and orthochromites, are interesting and peculiar in that they have fairly sharp absorption lines in the visible or neighbouring spectral regions. Furthermore, the crystal spectra observed are very similar to the corresponding free ion spectra and these are often very useful guides to the analysis of the former. Thus it is helpful to understand the theory of the free ion spectra in order to have an understanding of the crystal spectra.

The reasons for the similarity in the free ion and the crystal spectra are worth noting and so will be described briefly before the theory of the free ion and the crystal

spectra are discussed. Such similar behaviour can be expected if some conditions can be satisfied. First, it is necessary to have a crystalline environment for the ions which does not fluctuate in time and which is identical for all the ions. Such is the case, if the crystal containing the ions is at very low temperature and the crystal is relatively free from structural defects. Secondly, the neighbouring ions of the same type should not interact markedly. Classically this means that the valence electrons must lie within some outer electrons or quantum mechanically that the wavefunctions of these electrons must not overlap appreciably. The rare-earth lanthanides satisfy this latter condition better than any other group due to the phenomenon called the lanthanide contraction (Wybourne, 1965). The contraction refers to the contraction of the wavefunction of the 4f shell because of the imperfect screening of one 4f electron by another and consequently the 4f shell behaves as an inner shell. That is why the configuration is written as $4f^N\ 5s^2\ 5p^6$. This peculiarity makes the lanthanides relatively insensitive to the change of their surroundings and hence sharp lines are expected. However insensitivity is only relative and the crystal spectra do reflect the environment surrounding the ions. Another effect of this environment is that the interaction among neighbouring ions of the same kind leads to a broadening of the spectral lines.

3.2 Free ions

As a starting point, the free-ion level scheme in triply-ionized lanthanides will now be discussed. In the free ion, the energy level scheme can be understood in terms of the electrostatic repulsion of the 4f electrons and the spin-orbit coupling of their spin- and orbital-angular momenta. For a first approximation, one may just consider the interaction among the 4f electrons themselves, since all the outer electronic shells are spherically symmetric and so their effect on all the terms of a 4f configuration is the same in first order. Consequently the Hamiltonian for the 4f energy levels can be written as

$$H = = \frac{\hbar^2}{2m} \sum_{i=1}^{N} \Delta_i - \sum_{i=1}^{N} \frac{Z^* e^2}{r_i} + \sum_{i<j}^{N} \frac{e^2}{r_{ij}} + \sum_{i=1}^{N} \xi(r_i)\, \vec{s}_i \cdot \vec{\ell}_i \qquad (3.1)$$

where N is the number of 4f electrons,

$Z^* e$ is the screened charge of the nucleus because the closed shells have been ignored,

$\xi(r_i)$ is the spin-orbit coupling function;

$$\xi(r_i) = \frac{\hbar^2}{2m^2 c^2 r_i} \frac{du(r_i)}{dr_i}$$

and

$u(r_i)$ being the potential in which the electron i is moving.

The first term is the kinetic energy of the 4f electrons and the second term represents their Coulomb interaction with the nucleus. Because there is an interaction, with the closed shells, that modifies this second term only in magnitude, but not in its symmetry, the real charge of the nucleus is replaced by a screened charge. It is also noted that these two terms being spherically symmetrical do not remove any of the degeneracies within the 4f electronic configuration and therefore can be neglected in this discussion. The third term represents the mutual Coulomb interaction (H_c) of the 4f electrons and their spin-orbit interactions (H_{so}). For the lanthanides, H_c and H_{so} can be of the same order of magnitude and hence must be considered together. This is called intermediate coupling.

To calculate the energy levels, it is necessary to diagonalize the matrix obtained with a certain set of basis functions. Commonly the basis chosen is the set of Russell-Saunders (R-S) eigenfunctions which truly diagonalize the matrix if $H_c >> H_{so}$. In the R-S approximation, the spin- and orbital-angular momenta of the electrons couple separately to form $\vec{S}$ and $\vec{L}$ vectors which then interact weakly by the spin-orbit interaction. But J will be a good quantum number whether or not the above inequality is satisfied and J states will be linear combinations of functions of S and L. The matrix elements appearing in the matrix will thus

involve

$$\langle 4f^N SLM_S M_L \left| \frac{e^2}{r_{ij}} \right| 4f^N S'L'M'_S M'_L \rangle \quad \text{and}$$

$$\langle 4f^N SLJM_J \left| \sum_{i=1}^{N} \xi(r_i)\, \vec{s}_i \cdot \vec{\ell}_i \right| 4f^N S'L'J'M'_J \rangle .$$

By using the tensor operator technique (Hüfner, 1978), which will not be dealt with here, it can be shown that the first type of matrix element is diagonal in L, M_L, S and M_S and that the second type of matrix element is diagonal in J and M_J. (In such calculations, the spin-orbit coupling parameter is assumed to be the same for all 4f electrons and is defined as the radial integral $\xi_{4f} = \int R^2_{4f}\, \xi(r)dr.$). Thus the matrix elements, sum of those of $\frac{e^2}{r_{ij}}$ and $\sum_{i=1}^{N} \xi(r_i)\vec{s}_i \cdot \vec{\ell}_i$, will not be diagonal in L and S. The elements which are diagonal in J, L, S are given by

$$\langle 4f^N \ldots . \left| H_{so} \right| 4f^N \ldots . \rangle = \xi \left(\frac{\lambda}{2}\right) [J(J+1) - L(L+1) - S(S+1)] \qquad (3.2)$$

where λ is a constant for a state with given L and S. This is just the formula leading to the Landé interval rule which states that in any Russell-Saunders multiplet the interval between neighbouring terms is proportional to the higher J of the pair.

The general matrix element being diagonal in J and M_J implies that J and M_J are good quantum numbers. Thus the spectra of the free ion will appear reasonably well separated into groups each of which is characterized by J and states of M_J which are degenerate. This degeneracy is however lifted, as will be discussed in the next section, when the ion is introduced into the crystal. The degree to which this degeneracy will be lifted depends on the ion site symmetry and on whether the number of electrons of the ion is even or odd.

3.3 Trivalent ions in a crystal field

Now the effect of the crystal environment on the rare-earth ion will be described and the powerful method of group theory will be introduced and used to relate the symmetry of the site to the lifting of degeneracy mentioned. When an ion is introduced into the crystal, the ion experiences an electric field from the other ions in the crystal. These latter ions include ions of the same element at the same or different type of sites or ions of other kinds. This electric field is known as the crystal field. The 4f shell, being partially filled and so aspherical, experiences an inhomogeneous field. This field has two effects on the 4f electrons. It distorts the closed shells of the rare-earth ions, it also removes the M_J degeneracy of the free ion 4f levels, and hence produces a major modification of the energy-level

scheme. However the crystal field interaction is smaller than the energy separation of the various free ion terms. So an understanding of the crystal field splitting can be obtained by applying the potential produced by the crystal to the free ion 4f wavefunctions.

In order to make the crystal field into a useful and reasonably simple and hence workable concept, certain assumptions are necessary. The ions firstly are considered static in the crystal; lattice vibrations and their effect on the energy levels are neglected. Such an assumption is valid clearly only at low temperature. Secondly the 4f electrons of one rare-earth ion are regarded as representative of all the rare-earth ions in the crystal and the interaction of the 4f electrons of adjacent rare-earth ions is neglected. Thirdly the crystal is assumed to consist of extended charge contributions, thus producing overlap of the charge contributions of the neighbouring ions and the 4f electrons. This is different from the simpler point charge model which assumes that the field is due to point charges surrounding the rare-earth ion concerned and hence there is no overlap of the kind mentioned. In the more complicated model there is, furthermore, transfer of electrons, since there is overlap. Fourthly, the 4f electrons of one ion are considered to be independent of one another; correlation of electron motion is thus neglected. The first assumption implies that problems

dependent upon phonon and rare-earth interactions, such as line width and temperature dependent line position, are ignored. The second assumption means that the interaction between the 4f electrons of different ions are negligible and is equivalent to saying that the rare-earth ion energy levels have no dispersion. The third assumption just reflects the inadequacy of the point charge model as already mentioned. Finally the fourth assumption is just introduced to simplify and make the problem mathematically tractable.

For the present purpose, it is sufficient to mention that with these assumptions and using tensor technique the matrix elements of the crystal field potential can be evaluated. The crystal field potential used is introduced as an expansion in terms of the crystal field parameters. One then calculates matrix elements of the type $\langle 4f^N SLJM_J | V | 4f^N S'L'J'M'_J \rangle$ which is clearly diagonal in S, since V, the crystal field potential, is not acting on the spin. Furthermore, it is only diagonal in S; the states of M_J are all mixed. There is a certain degree of J mixing too. However, such mixing can be ignored if the separation of various spin-orbit terms are much greater than the crystal field interaction. Thus the crystal field lifts the degeneracy of the M_J states, the degree to which the degeneracy will be lifted depends precisely on the site symmetry of the rare-earth ions. In the next section, it will be seen how selection rules can be formulated in terms

of a new quantum number, the group irreducible representation label.

3.4 Group theoretical considerations

3.4.1 Basic concepts of group theory (Tinkham, 1964)

To understand better what is going to be discussed, it is necessary to recall the meaning of certain terminologies in group theory.

a) Class - two group elements A and B are called conjugate if the relation $B = C^{-1} A C$ holds, where C is any member of the group. All group elements that are conjugate to each other are said to belong to a class. The identity element E clearly forms a class by itself since $C^{-1} E C \equiv E$. Physically speaking a class always contains those symmetry elements which have the same physical property.

b) Representation - for each group element, a matrix of a given size can be assigned in such a way that if AB = C is valid then $M_A M_B = M_C$. These matrices M_A, M_B ..... are said to form a representation of the group. It is possible to have representations by matrices of other sizes.

c) Irreducible representation - if a representation $\Gamma(A)$, $\Gamma(B)$, ... of group elements A,B, ... can be written in the form

$$\Gamma(A)=\begin{pmatrix}\Gamma_1(A) & 0 & 0 & 0\\ 0 & \Gamma_2(A) & 0 & 0\\ 0 & 0 & \Gamma_3(A) & 0\\ 0 & 0 & 0 & \Gamma_4(A)\end{pmatrix},\quad \Gamma(B)=\begin{pmatrix}\Gamma_1(B) & 0 & 0 & 0\\ 0 & \Gamma_2(B) & 0 & 0\\ 0 & 0 & \Gamma_3(B) & 0\\ 0 & 0 & 0 & \Gamma_4(B)\end{pmatrix},\ \Gamma(C)=\ldots \tag{3.3}$$

and similarly for the other elements of the group, where $\Gamma_1(A)$, $\Gamma_1(B)$, $\Gamma_1(C)$.... are matrices of one and the same size and $\Gamma_2(A)$, $\Gamma_2(B)$, $\Gamma_2(C)$..... form another set of matrices and similarly for $\Gamma_3(A)$, $\Gamma_3(B)$, $\Gamma_3(C)$...., (0 represents a zero matrix) the matrices $\Gamma_1 \equiv \{\Gamma_1(A), \Gamma_1(B), \ldots.\}$, $\Gamma_2 \equiv \{\Gamma_3, \Gamma_3(B), \ldots.\}$ etc. are said to form irreducible representations of the group. It is easily verified, by direct matrix multiplications, that if AB = C then $\Gamma_i(A)\ \Gamma_i(B) = \Gamma_i(C)$ for all i. So for each i, Γ_i is indeed a representation of the group. The original representation is said to be reducible and by a matrix transformation it has been reduced to matrices $\Gamma(A)$, $\Gamma(B)$,.... given above with the greatest number of zeros for non-diagonal elements, and with block sub-matrices along the diagonal, which cannot be simplified or reduced further. These block matrices are logically called the irreducible representations of the group. It can be shown that the number of classes is the same as the number of irreducible representations.

d) Character - the trace of any matrix is the sum of its diagonal elements. It is invariant under a matrix transformation and is known as the character of the group element represented by

the matrix. By definition of conjugation and class, elements of the same class have, therefore, the same character.

Using the above definitions, it can be shown that the number of times P_s, that an irreducible representation Γ_s (with character χ_{sr}) is contained in a reducible representation Γ (with character χ_r) is given by

$$P_s = \frac{1}{n} \sum_{r=1}^{C} h_r \chi_r \chi^*_{sr} \quad (^* \text{ denotes complex conjugation}) \qquad (3.4)$$

where n is the order of the group (the order of a group is the number of group elements in that group); C is the number of classes; and h_r is the number of elements that the class r contains.

3.4.2 Reducible representation D_J of the free ion and Kramer's Theorem

The different irreducible representations are matrices which may be of different sizes; the sizes of different sets of matrices are characterized by their different dimensions. This dimension has a very physical interpretation. It represents the degeneracy of a quantum system in a particular environment. For example a free ion is characterized by different values of J; each J has $2J + 1$ M_J values and hence each J level is

$2J + 1$ fold degenerate. Thus the irreducible representations of the free ion, reflecting the full rotational symmetry of space, are sets of matrices of dimension $2J + 1$, for all the allowable J values of the system. The representation is generally denoted by D_J for each J.

In a crystal, the symmetry is clearly less than that of the three-dimensional rotational group and the initially irreducible $2J + 1$ dimensional representation D_J becomes reducible and decomposes into blocks of sub-matrices corresponding to the irreducible representations of the new environment. Mathematically $D_J = \sum_s P_s \Gamma_s$, where the coefficients P_s can either be worked out using equation (3.4) or be obtained by inspection. In any case, the character χ_r of the reducible representation D_J has to be known. It is given by the formula

$$\chi_J(\alpha) = \frac{\sin[(J + \frac{1}{2})\alpha]}{\sin[\frac{\alpha}{2}]} \qquad (3.5)$$

where α is just any rotation by an angle α about an arbitrary axis; α takes the place of the label r which numbers the class. (The symmetry of the free ion is given by the full three-dimensional rotational group). Once introduced into a crystal, the ion enjoys only the symmetry allowed at the site and out of all the α's only a few would remain as symmetry elements e.g. if the site group just has a two-fold axis, α can be π and not $\frac{\pi}{2}$ or other values. Once $\chi_r \equiv \chi_J$ is obtained for those α's which are allowed, the P_s's can be obtained.

The lifting of the degeneracy of levels depends only partly on the symmetry of the site group. The degeneracy of the crystal-field levels also depends, in a very fundamental way, on whether the ions have an even or an odd number of electrons. For the even number electron case, a crystal site of sufficiently low symmetry would lift all the $2J + 1$ degeneracy for a given J. But due to the time reversal symmetry which is the basis of the Kramer's theorem (Tinkham, 1964), the energy levels of the odd-number-electron ion must be at least two-fold degenerate. Thus even in the lowest symmetry site, the levels can not be singlets. However this degeneracy due to time reversal can be lifted in the presence of a magnetic field which can be either externally applied or be just the internal molecular field which exists when the crystal becomes magnetically ordered. The concept of molecular field will be described more fully later in the section concerning magnetic interactions and magnetic symmetry in crystals containing rare-earth ions (section (3.5)).

3.4.3 Direct product representations and selection rules

In order to study theoretically the selection rules among crystal-field levels, the concept of the direct product of two representations must be introduced. If $\Gamma_i(A)$ and $\Gamma_j(A)$ are two representations of a group G, where A can be any element of the group, it can be shown that the direct product $\Gamma(A) = \Gamma_i(A) \times$

$\Gamma_j(A)$ is also a representation of the group. But $\Gamma(A)$ is in general reducible i.e. $\Gamma_i \times \Gamma_j = \sum_\ell a_{ij\ell}\, \Gamma_\ell$ and the character of $\Gamma_i \times \Gamma_j$ is given by $\chi = \chi_i \chi_j$. The concept of direct product representation is related to the selection rule as follows. It can be shown that the matrix elements $\langle \Psi_i | H_j | \Psi_f \rangle$ where Ψ_i is the initial state with representation Γ_i, Ψ_f is the final state with representation Γ_f and H_j is the Hamiltonian with representation Γ_j, can be non-zero only if $\Gamma_i^* \times \Gamma_j$ contains Γ_f at least once or equivalently $\Gamma_i^* \times \Gamma_j \times \Gamma_f$ contains Γ_1, the identity representation; Γ^* is the Hermitean conjugate of Γ. (The identity representation is the representation which uses the 1 x 1 unit matrix to represent every element of the group. The character of each element is unity and clearly if AB = C, $M_A M_B = 1 \times 1 = 1 = M_C$).

In the case of interest H_j is usually the electric dipole operator or the magnetic dipole operator. That is, one is talking about electric and magnetic dipole transitions respectively. The components of an electric dipole are proportional to $\vec{r} \equiv (x, y, z)$ and transform as the components x, y, z, i.e. as the components of a polar vector, whereas the components of a magnetic dipole transform as the components of an axial vector i.e. as the components of an angular momentum R_x, R_y, R_z. The way in which x, y, z and R_x, R_y, R_z are transformed is listed in the character table and so Γ_j can be obtained for the two operators.

The electric-dipole transition, which is strictly forbidden for the free ion, is however observable in the crystal-field spectra. To understand this, one must understand why such transitions are forbidden in free ions and see what happens to lift this selection rule. Since optical transitions take place between levels of a particular $4f^N$ configuration, the initial state and the final state are of the same parity. But the electric dipole operator is of odd parity. Therefore the transition matrix $\langle \Psi_i | \vec{r} | \Psi_f \rangle$ is of odd parity and must vanish. In a crystal, however, electric dipole transitions can occur if the $4f^N$ states have admixtures of $4f^{N-1}$ $n\ell$ configurations, where $4f^{N-1}$ $n\ell$ is such that it has opposite parity to $4f^N$. The admixture is produced by interactions that have odd parity. In the crystal there are two mechanisms that can produce these admixtures, namely odd parity crystal field components and crystal vibrations of odd symmetry. For a crystal with a center of inversion, the odd crystal field components are zero. Therefore there can be no electric-dipole transition induced by the crystal field. But the possibility of inducing it by odd symmetry vibrations remains. For a crystal without a center of inversion, there is of course no restriction and both mechanisms contribute. But in spite of the mixing which allows the forbidden transitions to occur, the parity is essentially that of the original $4f^N$ configuration, since the mixing is quite small, though

effective. Thus electric-dipole transitions can occur in the presence of perturbations, hence the name forced electric dipole transition. However there is no parity restriction on magnetic dipole transitions.

3.5 The effect of magnetic ordering and the magnetic group

In addition to the crystal-field potential, a rare-earth ion in a magnetic crystal also experiences magnetic interactions with the other rare-earth ions as well as the other magnetic ions present. These interactions are however very complicated and are best represented by the molecular field. But their effect on the crystal field split levels are very small for even-number-electron ions, since in low enough site symmetry all the M_J degeneracies are already lifted. All that the molecular field can do is to perturb the levels very slightly and the crystal field spectra are essentially unchanged. However the magnetic interactions can affect the crystal field levels by lifting selection rules for forbidden lines. This is possible, since in some magnetic configurations of the crystal the molecular field acting on the rare-earth ions can mix states of different representations. The magnetic configurations themselves are in turn determined by the symmetry of the crystal. When the crystal is not ordered, the symmetry of the crystal is given by the space group of the crystal and time reversal is a symmetry element. When

it is ordered, the magnetic space group however is the appropriate description. In the magnetic group, the time reversal operator is no longer an element of the symmetry group. In fact the original space group is split into two halves. Half of the elements remain as the symmetry elements of the magnetic group and the other half multiplied by the time reversal operator, form the new elements of the magnetic group (Cracknell, 1975). For the description of the spin configuration, it is convenient to simplify things further by using the magnetic point group instead of the magnetic space group (Dzyaloshinski, 1958). But specific descriptions of the magnetic configurations for these compounds will be discussed in a later selection (3.7).

3.6 Tm^{3+} in $TmCrO_3$

3.6.1 Site symmetry of Tm^{3+}

In this section, the general discussion presented previously will be illustrated with the specific rare-earth ion Tm^{3+} in $TmCrO_3$. Thulium has atomic number 69 and in the triply ionized state, it has the configuration $4f^{12}\ 5s^2 5p^6$. Spin-orbit interaction in the free ion splits the Russel-Saunders terms into multiplets with $^3H_6$ being the lowest. The excited state multiplets in ascending order of energy are $^3H_4$, $^3H_5$, $^3F_4$, $^3F_3$, $^3F_2$, $^1G_4$.... (Hüfner, 1978). Of these

only $^3H_6 \longrightarrow {}^3F_4$, $^3F_3$, $^3F_2$ and $^1G_4$ correspond to transitions in the visible region. In this work, detailed spectra and analyses of only the first three inter-multiplet transitions will be presented.

The crystal field spectra of Tm^{3+} indeed follow closely the free ion spectra, and various spectra of Tm^{3+} introduced as an impurity (Antonov, 1973) and in concentrated crystals (Malozemoff, 1970) show agreement in average level positions though the exact pattern of the splitting depends on the precise site group concerned. For ions at sites of the same symmetry, the representations of the levels in turn depend on the precise nature of the other magnetic ions present as will be seen later when $TmCrO_3$ and $TmFeO_3$ are compared.

According to Geller and Wood, 1956 and Geller, 1956, Bertaut and Forrat, 1956, the site group of Tm^{3+} in $TmCrO_3$ is $C_s(m) \equiv C_{1h}(m)$. This site group has only two classes, each containing one element. The two elements are the identity E and the plane of reflection, σ_h perpendicular to the c-crystallographic axis. Table 3.1 gives the character table of $C_s(m)$, (Tinkham, 1964).

Since there are only two classes, there are just two irreducible representations A_1 and A_2. (This small number of classes and irreducible representations simply reflects the low symmetry characteristics of the site involved).

		E	σ_h
R_z x, y	A_1	1	1
R_x, R_y, z	A_2	1	-1

Table 3.1: Character table of $C_s(m)$

Furthermore the representations are all one-dimensional as expected since the sum of the squares of the dimensions n_{A_1} and n_{A_2} of the respective irreducible representations has to be equal to the number of group elements (Tinkham, 1964); $n^2_{A_1} + n^2_{A_3} = 2$, n_{A_1} and n_{A_2} can only be 1). In other words the matrices representing the group elements are one by one matrices; the character is the same as the matrix. Table 3.1 also gives the way in which the components x, y, z of the polar vectors and the components R_x, R_y, R_z of the axial vectors are transformed. Suppose one has an incident electromagnetic wave with vectors $\vec{E}$ and $\vec{H}$. If $\vec{E}$ is parallel to the $\vec{x}$ or $\vec{y}$ direction (the x, y, z directions parallel respectively to the a, b, c axes of the crystal), and if the selection rule permits, an electric dipole moment proportional to x or y would be induced. Similarly $\vec{H}$ parallel to $\vec{z}$ will induce a magnetic dipole moment M_z. Therefore according to the second row of Table 3.1

$$E(\underline{\bar{X}}) = (+1)\ (\underline{\bar{X}})$$

$$\sigma_h(\underline{\bar{X}}) = (+1)\ (\underline{\bar{X}}) \qquad (3.6)$$

where $\underline{\bar{X}}$ is x, y, or M_z. In exactly the same manner $\vec{E}||\vec{z}$, and $\vec{H}||\vec{x}$ or $\vec{H}||\vec{y}$, if selection rules permit, will give rise to an electric dipole moment proportional to z and magnetic dipole

moments M_x or M_y respectively and according to the third row of Table 3.1

$$E(Y) = (+1)\ (Y)$$
$$\sigma_h(Y) = (-1)\ (Y) \qquad (3.7)$$

where Y is M_x, M_y or z.

It is also observed that the site group lacks a center of inversion and so parity is not a good quantum number. In other words, the wavefunctions are of mixed parity and even in the absence of odd component lattice vibrations, electric dipole transitions can occur. Of course the parity, as explained earlier, is still mainly determined by the $4f^{12}$ configuration. The effect of the low symmetry of the site and the fact that Tm^{3+} has an even number of electrons result in the lifting of all the degeneracy of the multiplets. Each multiplet $^{2S+1}L_J$ is expected to split into 2J + 1 levels each of which is characterized by one of the two irreducible representations A_1 or A_2.

3.6.2 Selection rules

Next the selection rules for transitions among the crystal-field split levels will be calculated. As mentioned previously, the transition from state with representation

Γ_i to one with Γ_j is induced by a perturbation of representation Γ_H. This means that the transition matrix element $\langle\Gamma_i|\Gamma_H|\Gamma_f\rangle$ is not equal to zero if the condition $\Gamma_1 \subset \Gamma_i^* \times \Gamma_H \times \Gamma_f$ is fulfilled. (In our new notation $\Gamma_1 \equiv A_1$). The details and the results of this test are presented in Table 3.2, Table 3.3 and Table 3.4. The details of the third row of Table 3.2 is given in Table 3.3. It should be mentioned that $\vec{E} \perp \vec{z}$ is included in Table 3.4 since sometimes it is of interest or of necessity to perform experiments with (110) platelets.

3.6.3 Reduction of the free ion representation

To analyse the crystal field spectra in order to obtain the energy level scheme, it is necessary to know for a given J how many levels can have labels A_1 and A_2 respectively. According to group theory, for a multiplet $^{2S+1}L_J$, with total number of levels 2J + 1, there should be J + 1 levels of representation A_1 and J levels of representation A_2 if J is even. For J odd there are J levels A_1 and J + 1 levels A_2. Thus

$$\begin{aligned} {}^3H_6 &= 7A_1 + 6A_2 \\ {}^3F_4 &= 5A_1 + 4A_2 \\ {}^3F_3 &= 3A_1 + 4A_2 \\ {}^3F_2 &= 3A_1 + 2A_2 \end{aligned} \qquad (3.8)$$

	Γ_i	Γ_H	Γ_f	$\Gamma_i^* \times \Gamma_H \times \Gamma_f$	$\lvert\Gamma_i\rangle \leftrightarrow \lvert\Gamma_f\rangle$
$\vec{H}\|\|\vec{z}$, $\vec{E}\|\|\vec{x}$, $\vec{E}\|\|\vec{y}$	A_1	A_1	A_1	A_1	allowed
$\Gamma_H = A_1$	A_1	A_1	A_2	A_2	forbidden
	A_2	A_1	A_1	A_2	forbidden
	A_2	A_1	A_2	A_1	allowed
$\vec{H}\|\|\vec{x}$, $\vec{H}\|\|\vec{y}$, $\vec{E}\|\|\vec{z}$	A_1	A_2	A_1	A_2	forbidden
$\Gamma_H = A_2$	A_1	A_2	A_2	A_1	allowed
	A_2	A_2	A_1	A_1	allowed
	A_2	A_2	A_2	A_2	forbidden

Table 3.2 Selection rules for electric and magnetic dipole transitions

	E	σ_h
A_1	1	1
A_2	1	-1
$A_1 \times A_1$	1	1
$A_1 \times A_1 \times A_2$	1	-1

Table 3.3 Details of third row of Table 3.2

$$A_1 \times A_1 \times A_2 = A_2 \not\supset A_1$$

$$\therefore \quad |A_1\rangle \leftrightarrow |A_2\rangle \quad \text{forbidden}$$

Transition	A_1 to A_1 or A_2 to A_2	A_1 to A_2 or A_2 to A_1
Electric dipole allowed	$\vec{E} \perp \vec{z}$, $\vec{E} \parallel \vec{x}$, $\vec{E} \parallel \vec{y}$	$\vec{E} \parallel \vec{z}$
Magnetic dipole allowed	$\vec{H} \parallel \vec{z}$	$\vec{H} \parallel \vec{x}$, $\vec{H} \parallel \vec{y}$

Table 3.4 Summary of electric dipole and magnetic dipole transitions

for J = 6, 4, 3 and 2 respectively.

To make things more transparent, the decomposition of $^3H_6$ will be shown. In this case J = 6 and the reducible representation is D_6 with character given by $X_6(\alpha) = \frac{\sin(6+1/2)\alpha}{\sin\alpha/2}$. At the site $C_s(m)$ α can only have values corresponding to E and σ_h; it must be 0 and π respectively. $C_s(m)$ is actually not a subgroup of the three-dimensional rotational group R. It is a subgroup of the three-dimensional rotational-inversion group. Since $\sigma_h = iC_2$, and for an even number of electrons $\chi(i) = +1$, therefore $\chi(\sigma_h) = \chi(C_2)$. That is why we have been able to decompose D_J as if $C_s(m)$ is a subgroup of R. The corresponding characters are $X_6(E) = 13$ and $X_6(\sigma_h) = 1$, since

$$X_J(E) = \lim_{\alpha\to 0} X_J(\alpha) = \frac{\sin(\frac{2J+1}{2})\alpha}{\sin\frac{\alpha}{2}} = \frac{\frac{2J+1}{2}\alpha}{\frac{\alpha}{2}} = 2J+1$$

$$X_6(\pi) = \sin(\frac{13\pi}{2}) = +1 \ . \qquad (3.9)$$

The details are summarized in the Table 3.5. Similarly one can calculate the decompositions for the other multiplets.

3.7 Spin configurations in the orthoferrites and the orthochromites

Now, given the details of the crystal field of $C_s(m)$ symmetry, the magnetic interactions and the spin configurations for the rare-earth orthochromites will be described. Since orthochromites are structurally isomorphic to orthoferrites the following discussion is applicable to both. Indeed the discussion is quite general and applies to compounds of the chemical formula RMO_3 where R is the rare-earth ion and M

	E	σ_h
A_1	1	1
A_2	1	-1
D_6	13	1

$$\therefore D_6 = 7A_1 + 6A_2$$

Table 3.5 Proof of $^3H_6 = 7A_1 + 6A_2$

can be either Chromium or Iron.

The orthochromites and the orthoferrites crystallize in an orthorhombically distorted perovskite structure (Space group Pbnm (D_{2h}^{16})) with four formula units per unit cell. There are four inequivalent M^{3+} sites and four inequivalent R^{3+} sites in each unit cell, each site belonging to one magnetic sublattice. The unit cell is given in Figure 3.1 where, for simplicity the oxygen sites are not shown. The eight inequivalent sites mentioned are related to one another by symmetry elements of the magnetic space group. However, as discussed earlier, it suffices, for the description of spin configurations, to use the magnetic point groups. Upon choosing as the basis of the irreducible representation the vectors

$$\vec{F} = \vec{N}_1 + \vec{N}_2 + \vec{N}_3 + \vec{N}_4$$

$$\vec{G} = \vec{N}_1 - \vec{N}_2 + \vec{N}_3 - \vec{N}_4$$

$$\vec{C} = \vec{N}_1 + \vec{N}_2 - \vec{N}_3 - \vec{N}_4$$

$$\vec{A} = \vec{N}_1 - \vec{N}_2 - \vec{N}_3 + \vec{N}_4 \quad , \text{(N=S for } M^{3+} \text{ ions and N=J for } R^{3+} \text{ ions)}$$

for the magnetic moments $\vec{S}_i$ of the M^{3+} ions and $\vec{J}_i$ of the R^{3+} ions, and applying space group theoretical considerations, the possible zero-field configurations $\Gamma_1 \ldots\ldots \Gamma_8$ are obtained. (For illustrations of these vectors see Bertaut,

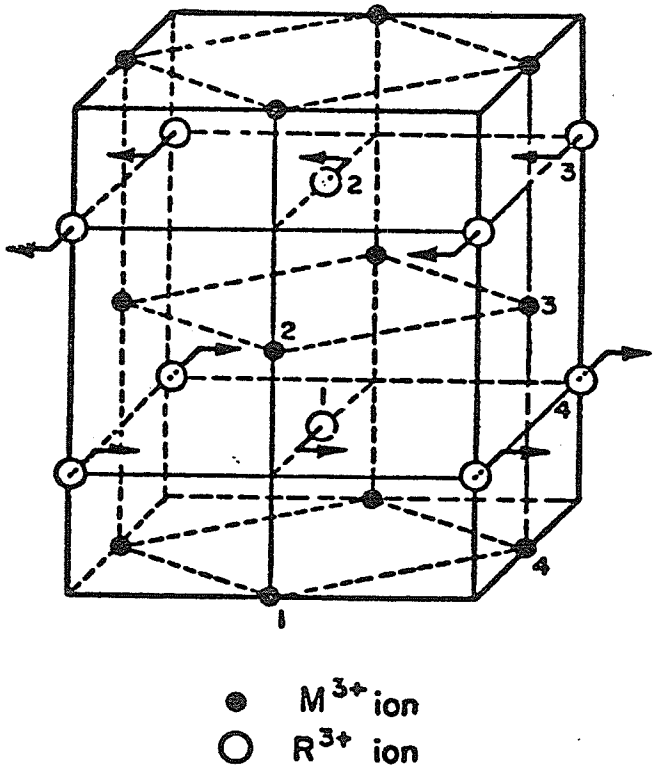

Figure 3.1: Schematic representation of the R^{3+} and M^{3+} sites in the orthorhombic unit cell of the rare earth perovskites. The arrows at the R^{3+} sites indicate the local deviation from the undeformed perovskite structure (after Gordon, 1976).

1963). The results are summarized in Table 3.6 (Malozemoff, 1970). F depicts coupling of ions with a net ferromagnetic moment whereas G, C, A are different forms of antiferromagnetic coupling of the ions.

The subscripts 1, 2, 3, 4 refer to the four inequivalent sites in each unit cell and E, I, C, R and σ stand for the identity, inversion, rotation, time reversal and reflection operators respectively. It is seen that the magnetic point group corresponding to Γ_1 consists of eight elements E, I, C_{2x}, C_{2y}, C_{2z}, σ_x, σ_y, σ_z. The configurations Γ_2 to Γ_8 all have half of these eight elements multiplied by the time reversal operator. In the case of the orthochromites the configurations of interest are usually Γ_1, Γ_2 and Γ_4 and so these will be examined in greater detail. These spin configurations are shown in Figure 3.2.

Γ_1 ------- In this configuration, the individual spins of M^{3+} ions all have non-vanishing x, y or z spin components but the R^{3+} ions individually have no x,y spin components and has only a non-vanishing z spin component. However the non-vanishing spin components cancel one another for both types of ions. Hence there is no net moment of either ion. For this reason, this spin configuration is normally written as $\Gamma_1(0)$.

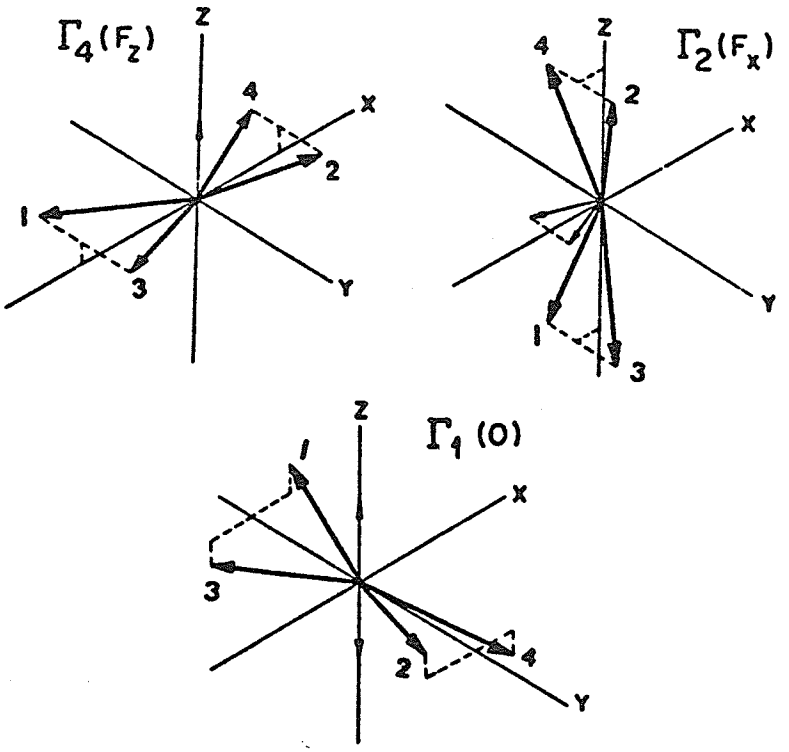

Figure 3.2: Schematic representation of the three coupled R-M zero field configurations in RMO_3 compounds. The arrows drawn by thick lines represent the M^{3+} moments, and those of the thin lines symbolize the R^{3+}moments (after Gordon, 1976).

Modes of Magnetic Coupling	Symmetry Elements	Compatible Spin Configurations			
		Basis Vector	M^{3+} ion	Basis Vector	R^{3+} ion
Γ_1	E, I, C_{2x}, C_{2y}	A_x	$S_{1x} = -S_{2x} = -S_{3x} = S_{4x}$	--	$J_{ix} = 0$
		G_y	$S_{1y} = -S_{2y} = S_{3y} = -S_{4y}$	--	$J_{iy} = 0$
	C_{2x}, σ_x, σ_y, σ_z	C_z	$S_{1z} = S_{2z} = -S_{3z} = -S_{4z}$	c_z	$J_{1z} = J_{2z} = -J_{3z} = -J_{4z}$
Γ_2	E, I, C_{2x}, σ_x	F_x	$S_{1x} = S_{2x} = S_{3x} = S_{4x}$	f_x	$J_{1x} = J_{2x} = J_{3x} = J_{4x}$
		C_y	$S_{1y} = S_{2y} = -S_{3y} = -S_{4y}$	c_y	$J_{1y} = J_{2y} = -J_{3y} = -J_{4y}$
	RC_{2y},RC_{2z},$R\sigma_x$,$R\sigma_y$	G_z	$S_{1z} = -S_{2z} = S_{3z} = -S_{4z}$	--	$J_{iz} = 0$
Γ_3	E, I, C_{2y}, σ_y	C_x	$S_{1x} = S_{2x} = -S_{3x} = -S_{4x}$	c_x	$J_{1x} = J_{2x} = -J_{3x} = -J_{4x}$
		F_y	$S_{1y} = S_{2y} = S_{3y} = S_{4y}$	f_y	$J_{1y} = J_{2y} = J_{3y} = J_{4y}$
	RC_{2x},RC_{2z},$R\sigma_x$,$R\sigma_z$	A_z	$S_{1z} = -S_{2z} = -S_{3z} = S_{4z}$	--	$J_{iz} = 0$
Γ_4	E, I, C_{2z}, σ_z	G_x	$S_{1x} = -S_{2x} = S_{3x} = -S_{4x}$	--	$J_{ix} = 0$
		A_y	$S_{1y} = -S_{2y} = -S_{3y} = S_{4y}$	--	$J_{iy} = 0$
	RC_{2x},RC_{2y},$R\sigma_x$,$R\sigma_y$	F_z	$S_{1z} = S_{2z} = S_{3z} = S_{4z}$	f_z	$J_{1z} = J_{2z} = J_{3z} = J_{4z}$
Γ_5	E, C_{2x}, C_{2y}, C_{2z}	--	$S_{ix} = 0$	g_x	$J_{1x} = -J_{2x} = J_{3x} = -J_{4x}$
		--	$S_{iy} = 0$	a_y	$J_{1y} = -J_{2y} = -J_{3y} = J_{4y}$
	RI, R_x, R_y, R_z	--	$S_{iz} = 0$	--	$J_{iz} = 0$
Γ_6	E, C_{2x}, σ_y, σ_z	--	$S_{ix} = 0$	--	$J_{ix} = 0$
		--	$S_{iy} = 0$	--	$J_{iy} = 0$
	RI, RC_{2y}, RC_{2z},$R\sigma_x$	--	$S_{iz} = 0$	a_z	$J_{1z} = -J_{2x} = -J_{3z} = J_{4z}$
Γ_7	E, C_{2y}, σ_z, σ_x	--	$S_{ix} = 0$	--	$J_{ix} = 0$
		--	$S_{iy} = 0$	--	$J_{iy} = 0$
	RI, RC_{2z}, RC_{2x},$R\sigma_y$	--	$S_{iz} = 0$	g_z	$J_{1z} = -J_{2z} = J_{3z} = -J_{4z}$
Γ_8	E, C_{2z}, σ_x, σ_y	--	$S_{ix} = 0$	a_x	$J_{1x} = -J_{2x} = -J_{3x} = J_{4x}$
		--	$S_{iy} = 0$	g_y	$J_{1y} = -J_{2y} = J_{3y} = -J_{4y}$
	RI, RC_{2x},RC_{2y},$R\sigma_z$	--	$S_{iz} = 0$	--	$J_{iz} = 0$

Table 3.6 Magnetic Configurations of the Orthoferrites and Orthochromites

Γ_2 -------- The M^{3+} ions have non-vanishing spin components along x, y, z but only the x spin components have the same sign for all the four ions; hence there is a net magnetic moment in the x direction. The R^{3+} ions have non-vanishing spin components along x, y directions and zero spin component along the z direction. The x components are of the same sign and so have a net moment in the x direction. This configuration is normally written as $\Gamma_2(F_x)$ or F_xG_z .... f_xc_y (G_z means that the antiferromagnetic axis of the coupling G is along the z direction; the non-capital letters denote similar quantities for the R^{3+} ions).

Γ_4 -------- The M^{3+} ions have non-vanishing components along x, y, z directions but only in the z direction is there a net magnetic moment. The R^{3+} ions have zero components along the x and y directions and non-vanishing z components having the same sign, and thus have a net magnetic moment in the z direction. This configuration is normally written as $\Gamma_4(F_z)$ or F_zG_x .... f_z (f_z means that the R^{3+} ions are polarized by the molecular field so that there is a net moment in the z direction paramagnetically; in general the R^{3+} ions do not order until down to helium temperatures).

It is seen that (Figure 3.2) basically the magnetic ordering is antiferromagnetic and canting of spins is the cause of the net magnetic moments.

It has been stated that different spin configurations have different molecular fields at the rare-earth sites. The molecular fields in the Γ_2 and Γ_4 configurations have been completely derived in the work on $TmFeO_3$ (Malozemoff, 1970). It suffices to say that for the $\Gamma_2(F_x)$ configuration, the molecular field on the rare-earth ions point in the x-y plane: - for sites 1 and 2 it points at some angle off the x-axis, and for sites 3 and 4 it points at the same angle on the other side of the x-axis. But the moments and molecular fields do not have to be collinear, because of the rare-earth g-factor anisotropy. For the $\Gamma_4(F_z)$ configuration, the molecular field points in the z-direction and is the same for all the four rare-earth sites.

It can be shown that fields along the z-direction mix states of similar representations, so that selection rules are preserved whereas fields in the x-y plane mix states of different representations and hence lift all selection rules. Thus in the $\Gamma_2(F_x)$ magnetic configuration all selection rules are lifted but there is no such mixing in the $\Gamma_4(F_z)$ since in this latter case, the molecular field is along the z-direction.

3.8 Known investigations on $TmCrO_3$ spin configurations

The spin configurations of $TmCrO_3$ have been investigated with various methods including neutron diffraction (Bertaut et al, 1966; Pataud and Sivardiere, 1970), magnetization and susceptibility measurements (Hornreich et al, 1973; Tamaki et al, 1977) and exciton studies (Aoyagi et al, 1976). All these studies consistently show that in the absence of an external field for temperatures higher than approximately 4.2 K, $\Gamma_2(F_x)$ is the stable configuration whereas below ~ 4.2 K, $\Gamma_4(F_z)$ could be the stable configuration. The findings of these studies will now be described.

Neuton diffraction studies have shown that below the Néel temperature, T_N, of 124 K, at which the Cr^{3+} spins order spontaneously, the Cr^{3+} spin structure is, in the notation of Koehler et al (1960) and Bertaut (1963), primarily G_{xz} at 80 K and G_x at 4.2 K. These data imply that at 80 K the weak-ferromagnetic moment should have components along both the $\vec{a}$ and $\vec{c}$ axes and at 4.2 K should be along the $\vec{c}$ axis. (G_{xz} signifies that the antiferromagnetic axis is in the x-z (a-c) plane).

In magnetization measurements (Hornreich et al, 1973) on $TmCrO_3$ single crystals, however, it was found that $TmCrO_3$ orders with the weak ferromagnetic moment in the $\vec{a}$ direction

indicating that the Cr^{3+} spin structure is G_zF_x. This configuration, according to these studies, is stable for $6 \leq T < 124$ K and probably also for $2.2 < T \leq 6$ K. But other magnetization measurements (Tamaki et al, 1977) seem to show that although the Cr^{3+} spins below 5 K undergo a temperature-induced spin reorientation to configurations which have a ferromagnetic moment along the $\vec{c}$ axis, the antiferromagnetic ordering is not simply given by G_x.

From the interaction of the Cr^{3+} spins with one another, the stationary states of the Cr^{3+} ions are more appropriately described by exciton levels. In orthochromites the very sharp lines around 13700 cm^{-1} region have been intensively studied. There are four such lines corresponding to transitions from the ground single ion level $^4A_2$ to the four exciton levels originating from the single ion excited level ^2E. These levels are spin configuration dependent and thus can be used to study these configurations. According to such studies on $TmCrO_3$ (Aoyagi et al, 1976), the stable configuration at 1.8 K is consistent with G_xF_z and for high enough temperature it is with G_zF_x.

So far the above discussions have been focused on stable zero-field spin configurations at different temperatures. The spin reorientation part has not been discussed. Details of

such reorientations induced by temperature and by a small external field will however be coherently presented later with the spectra of the Cr^{3+} ions, under the chapter on spin reorientation (Chapter IV).

To complete this section, the spin configurations of the Tm^{3+} ions will now be described. Neutron diffraction studies (Bertaut et al, 1966) report that Tm^{3+} spins order cooperatively at approximately 4 K, consistent with the ordering at 5 K reported by magnetization studies (Tamaki et al, 1977). However other magnetization measurements (Hornreich et al, 1973) show no evidence of ordering down to very low temperatures consistent with specific heat studies. In any case even if unordered, the Tm^{3+} spins can still be polarized by the molecular field due to the Cr^{3+} spins and these spin configurations still have to be compatible with that of the ordered Cr^{3+} spins. In conclusion, for high temperatures the spin configuration of $TmCrO_3$ is G_zF_x (Cr^{3+}) .. f_xc_y (Tm^{3+}) and at low temperature the configuration is probably some configuration with F_z and f_z.

3.9 Analyses of spectra of Tm^{3+} ions in $TmCrO_3$

This section will present the spectra of Tm^{3+} as a function of temperature. Indirectly some conclusions will be drawn about the spin configurations as a function of temperature from their effect on the selection rules of the

transitions.

3.9.1 Introduction

The lowest-temperature spectra are analysed first, since at these temperatures only the lowest crystal field state is populated. All transitions have the same initial states and so the same representation Γ_i (to be determined later). For a given polarization of the incident electromagnetic wave the representation Γ_H is also fixed. In other words the matrix element $\langle\Gamma_i|\Gamma_H|\Gamma_f\rangle$ is a function of the representation of the final state. But the final states, for a given J, are separated into two groups -- for J even, there are J + 1 states of A_1 and J states of A_2; for J odd, there are J states of A_1 and J + 1 states of A_2. Thus one expects to find for each J, 2J + 1 lines of relatively high intensity at the lowest-temperature spectra. Furthermore if the representations are indeed good quantum numbers, each spectral line should occur primarily in one polarization of the incident light. To sum up, by counting the number of lines in each of two orthogonal polarizations, the representation Γ_f of the final state can be deduced; the representation of the initial state has yet to be determined.

To determine the representation of the initial state Γ_i, one must know whether the 2J + 1 lines are of the type

A_1 to A_1 or A_2 to A_2 or of the type A_1 to A_2 or A_2 to A_1. If this is known, and the Γ_f for the final states are known, Γ_i is uniquely determined. To determine the type of transitions mentioned, in turn, it is necessary to know whether the transition is due to the electric field vector or due to the magnetic field vector of the electromagnetic wave. In other words the dipole nature of the transitions has to be determined. This can be done by comparing the spectra of two sample platelets, say a-b and b-c. Thus for the a-b platelet, the polarization of the incident light is either ($\vec{E}||\vec{x}$, $\vec{H}||\vec{y}$) or ($\vec{E}||\vec{y}$, $\vec{H}||\vec{x}$). If a certain transition is due to the $\vec{E}$ vector, it is electric dipole and according to Table 3.4 it must be of the A_i to A_i type, while if it is due to the $\vec{H}$ vector, it is magnetic dipole and so it must be of the type A_i to A_j. On the other hand, for the b-c platelet there can only be these two polarizations of the light: ($\vec{E}||\vec{y}$, $\vec{H}||\vec{z}$) or ($\vec{E}||\vec{z}$, $\vec{H}||\vec{y}$). Hence a line which occurs with ($\vec{E}||\vec{y}$, $\vec{H}||\vec{x}$) in the a-b platelet spectra and with ($\vec{E}||\vec{y}$, $\vec{H}||\vec{z}$) in the b-c platelet spectra must be due to $\vec{E}||\vec{y}$ and so must be electric dipole and so is either A_1 to A_1 or A_2 to A_2. But an electric dipole transition occurring with $\vec{E}||\vec{z}$ in the b-c platelet cannot appear in the a-b platelet spectra, since in this latter platelet $\vec{E}$ cannot be parallel to $\vec{z}$.

3.9.2 Analyses of spectra

The spectra will be presented and analysed, first for temperature above 5 K, where the zero-field configuration is $\Gamma_2(F_x)$ and then for temperature below 5 K down to 3.4 K with and without an external field.

3.9.2.1 Spectra at $T \geq 5K$, zero field

From the data presented in Figures 3.3 - 3.5 for the b-c platelet, most of the lines in the spectra can be identified as transitions from states of the ground multiplet, labelled I, II, III etc., to the states of an excited multiplet labelled a, b, c, etc., in order of increasing energy. To illustrate the identification technique, the spectra representing transitions from the $^3H_6$ to the $^3F_4$ multiplet will be examined. In the $^3H_6 \longrightarrow {}^3F_4$ spectra at 5 K, nine lines have been observed which are of a significantly higher intensity than the other lines and can be labelled Ia, Ib, ... Ii. These lines also appear primarily in either one polarization or the other. Thus the selection rules given in Table 3.4 are a good approximation in the $\Gamma_2(F_x)$ spin configuration and and the levels of the multiplet can indeed be identified with the irreducible representation labels A_1 or A_2; the five lines (Ia, Ic, Id, Ig, Ii) corresponding to the five levels (a, c, d, g, i) with Γ_f being A_1 and the four lines

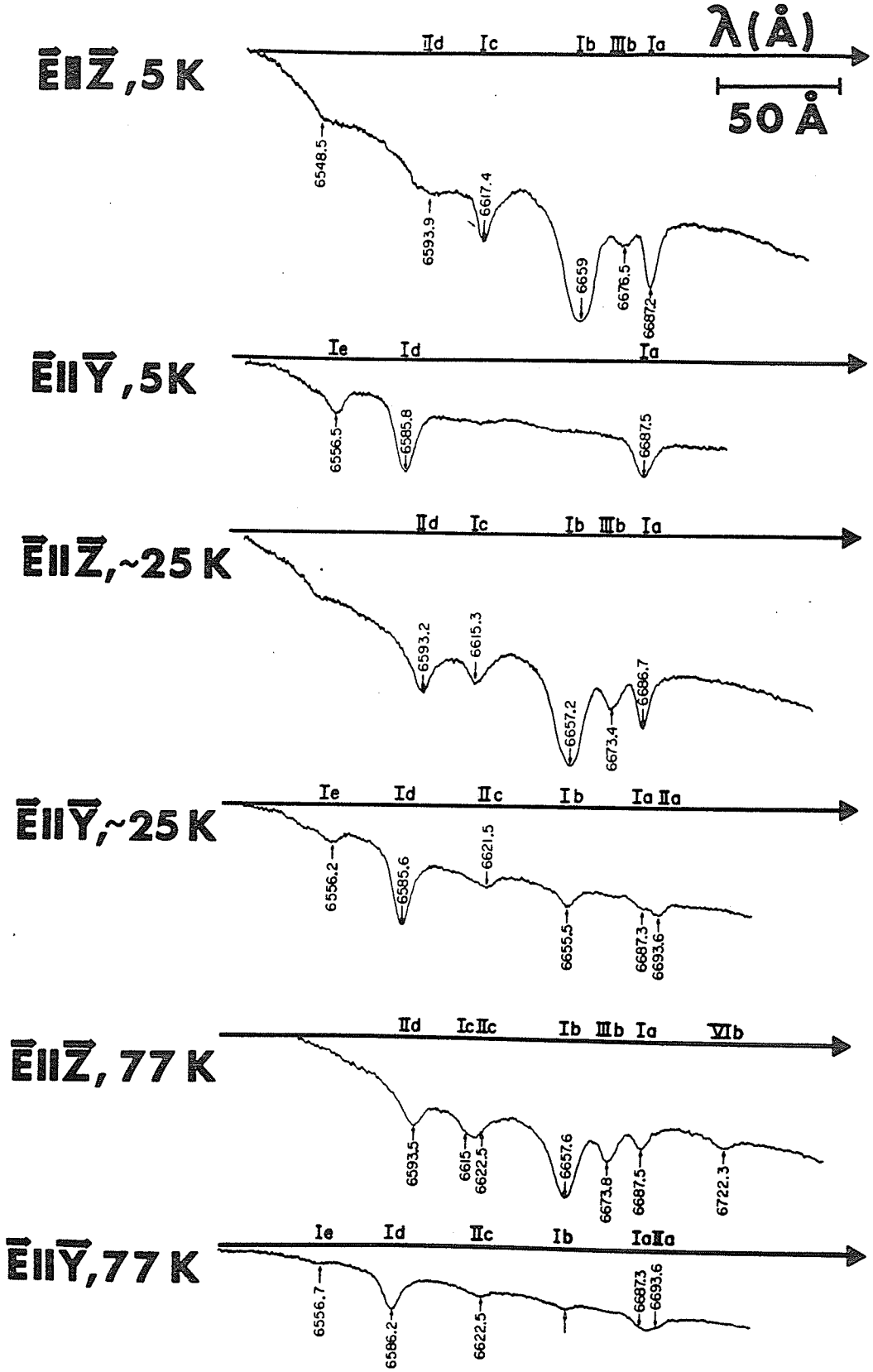

Figure 3.3: Absorption spectra of $^3H_6 \rightarrow {}^3F_2$ transitions of $TmCrO_3$, zero field

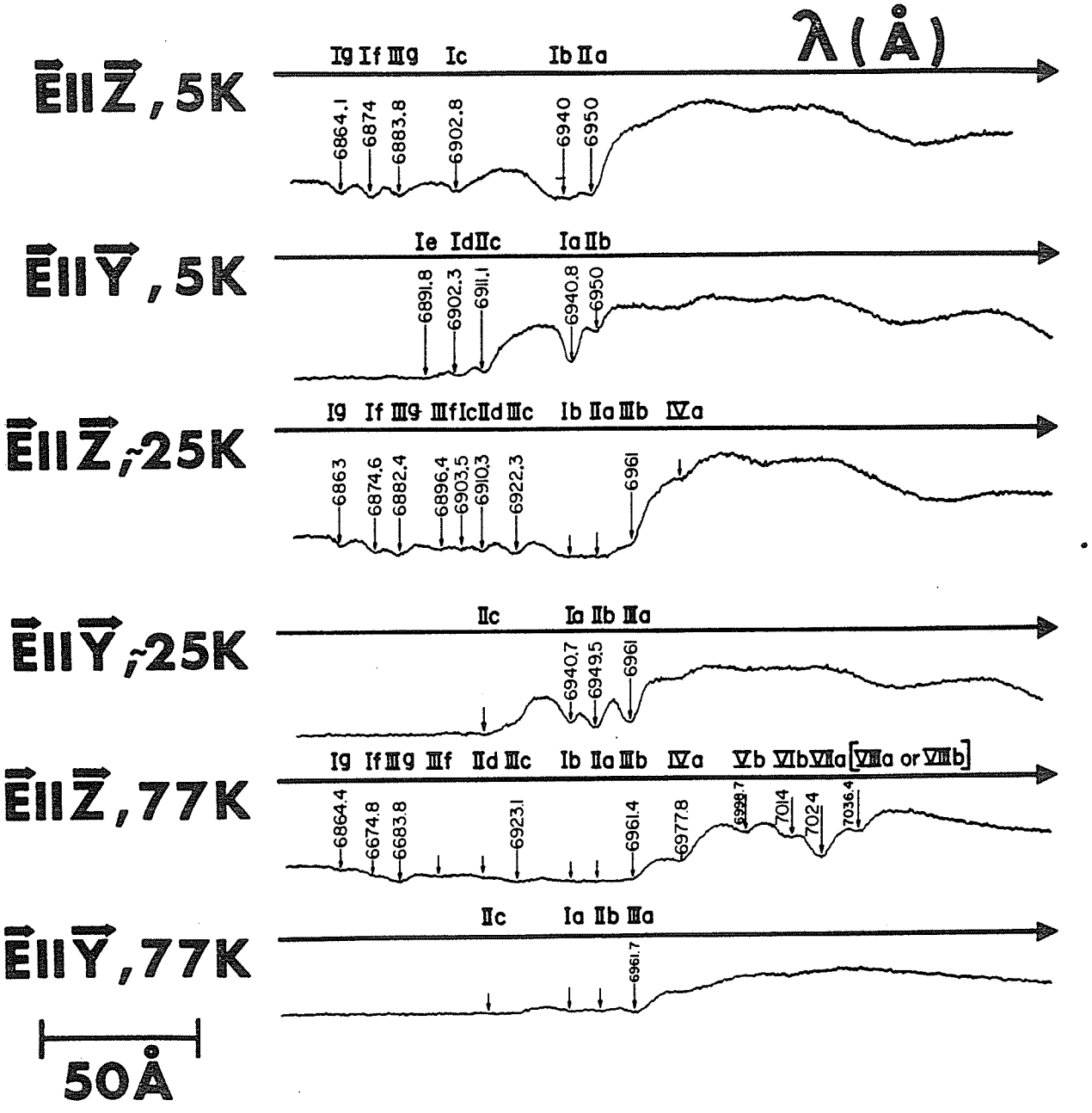

Figure 3.4: Absorption spectra of $^3H_6 \rightarrow {}^3F_3$ transitions of $TmCrO_3$, zero field

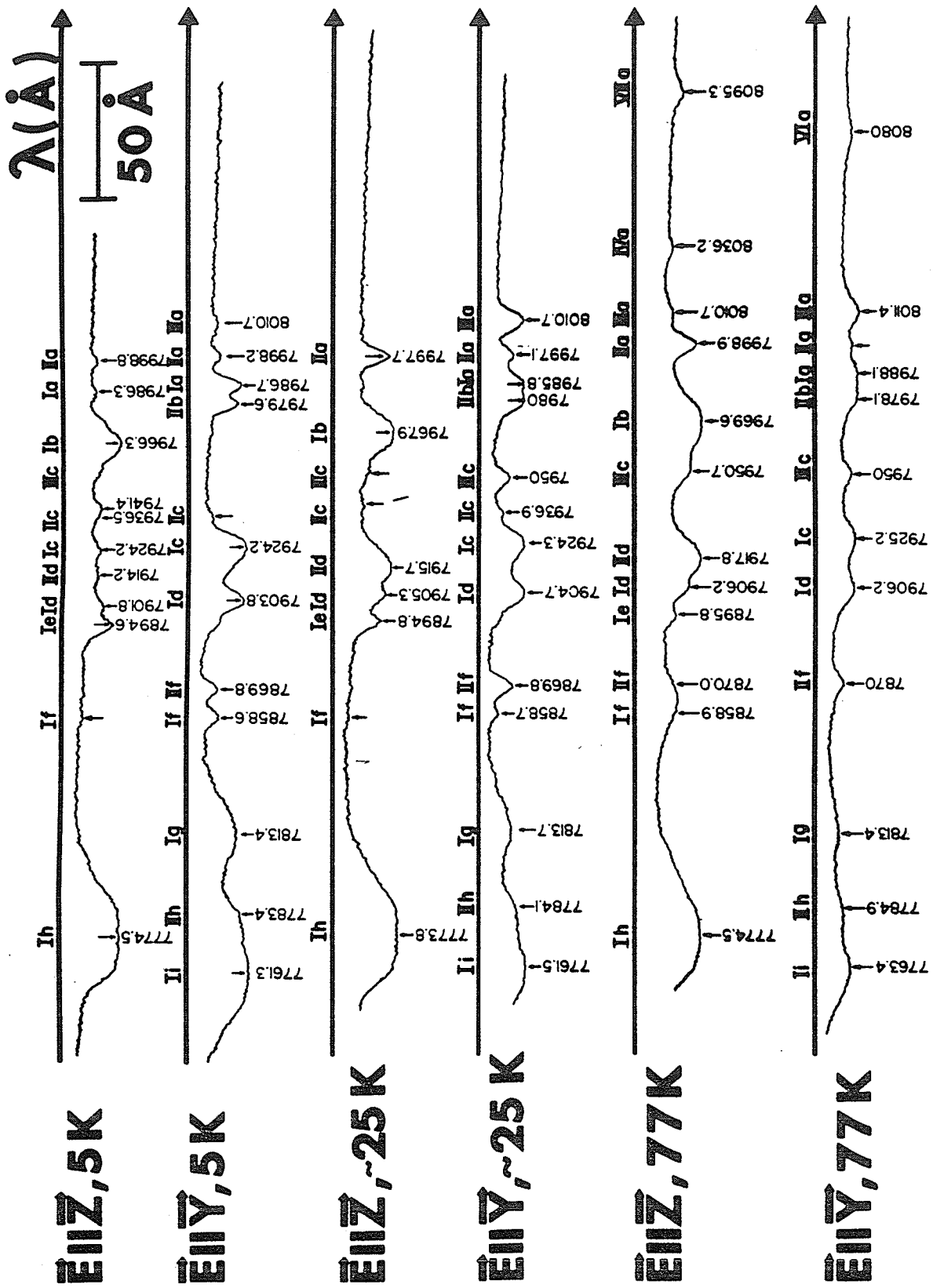

Figure 3.5: Absorption spectra of $^3H_6 \rightarrow {}^3F_4$ transitions of $TmCrO_3$, zero field

(Ib, Ie, If, Ih) correspond to the four levels (b, e, f, h) with Γ_f being A_2 (in the spectra shown 'If' seems to be in $\vec{E}||\vec{y}$; careful analysis with other spectra in different spectral regions at different temperatures show that it belongs to $\vec{E}||\vec{z}$). Since the lines appearing only in the ($\vec{E}||\vec{y}$, $\vec{H}||\vec{z}$) polarization for the b-c platelet also appear in the ($\vec{E}||\vec{x}$, $\vec{H}||\vec{y}$) and ($\vec{E}||\vec{y}$, $\vec{H}||\vec{x}$) polarizations for the a-b platelet spectra (not shown), it follows that the transitions are due to the $\vec{E}$ vectors and so the transitions are electric dipole. The five $\vec{E}||\vec{y}$ transitions, with Γ_f being A_1, are therefore, A_1 to A_1 type, a fact implying that the representation Γ_i of level I is A_1. Similarly the four $\vec{E}||\vec{z}$ transitions with Γ_f being A_2, are therefore A_1 to A_2 type, again yielding I as A_1.

At higher tempetures these relatively strong lines remain with about the same intensities. Most of the other lines increase in intensity with the increase in temperature. For example, at 25 K are the lines IIa, IIc, IId, IIf and IIh, which are about 20 cm^{-1} from the corresponding I lines. These II lines appear in different polarizations from the corresponding I lines. Hence, level II and level I are of different representations. The former therefore must be A_2, if the latter is A_1. Thus the representations of I and II agree exactly with the representations deduced for I and II from magnetization measurements (Hornreich et al, 1973). This result however is different from that reported for

$TmFeO_3$ (Malozemoff, 1970) where the representations of the corresponding levels are the same. At 25 K lines IIIa, IIIc of the same polarization as the corresponding I lines appear. Therefore III has the same representation A_1, as I. Also these III lines are about 45 cm^{-1} from the I lines. As the temperature increases further to 77 K more lines appear such as IVa, VIa and VIIa corresponding to the transitions from the other states of the ground multiplet. In an exactly similar way, the energy and the representations of the levels of the $^3F_3$ and $^3F_2$ multiplets have been deduced. These transitions, corresponding levels and representations are listed in Tables 3.7 - 3.10.

It is observed that the analyses of the $^3H_6 \longrightarrow {}^3F_3$ and $^3H_6 \longrightarrow {}^3F_4$ transitions yield I and II as A_1 and A_2 respectively, whereas the analysis of the $^3H_6 \longrightarrow {}^3F_2$ transitions yields I and II as A_2 and A_1 respectively. This "inconsistency" will however be understood and in fact, later, removed by analyses of spectra below 5 K. Before this inconsistency is removed, however, it seems appropriate to see why it arises. The crucial thing is the counting of the number of lines in each polarization of the light. Table 3.7 shows that for 5 K, in zero field, there are three lines in $\vec{E}||\vec{z}$ and two lines in $\vec{E}||\vec{y}$, hence the three final states for the former are A_1 and the two final states for the latter are A_2. But these are electric dipole transitions, and so

Wavelength (Å)	Identification	Ground-state energy separation (cm^{-1})	Polarization[a] $\vec{E} \parallel \vec{Z}$, $\vec{E} \parallel \vec{Y}$
6687.1	Ia		M
6657.9	Ib		S
6615.3	Ic		M
6585.5	Id		M
6556.3	Ie		W
6693.6	IIa	14.5	W
6622.1	IIc	15.5	W
6593.3	IId	17.9	M
6674.5	IIIb	37.4	W
6722.3	IVb	78.3	W

[a] S = strong, M = medium, and W = weak intensity

Table 3.7: $^3H_6 \rightarrow {}^3F_2$ Transition Lines in $TmCrO_3$ $T \geq 5$ K, Zero Field

Wavelength (Å)	Identification	Ground-state energy separation (cm^{-1})	Polarization[a] $\vec{E} \parallel \vec{Z}$, $\vec{E} \parallel \vec{Y}$
6940.7	Ia		S
6940.0	Ib		S
6902.8	Ic		M
6902.3	Id		M
6891.8	Ie		W
6874.4	If		M
6863.8	Ig		M
6950.0	IIa	19.1	M
6950.0	IIb	20.7	S
6911.1	IIc	17.4	M
6910.3	IId	16.8	W
6961.3	IIIa	42.5	S
6961.2	IIIb	43.9	S
6922.7	IIIc	41.6	M
6896.4	IIIf	46.3	W
6883.3	IIIg	41.3	M
6977.8	IVa	76.5	M
6998.7	Vb	120.9	M
7014.0	VIb	152.0	M
7024.0	VIIa	170.7	S
7036.4	VIIIa or VIIIb	195.8	M

[a] S = strong, M = medium and W = weak intensity

Table 3.8: $^3H_6 \rightarrow {}^3F_3$ Transition Lines in $TmCrO_3$ $T \geq 5$ K, Zero Field

Wavelength (Å)	Identification	Ground-state energy separation (cm^{-1})	Polarization[a] $\vec{E} \parallel \vec{Z}$, $\vec{E} \parallel \vec{Y}$	
7986.8	Ia		W	S
7967.9	Ib		S	
7924.5	Ic		W	S
7904.9	Id		M	S
7895.1	Ie		S	W
7857.4	If		M	W
7813.5	Ig			S
7774.2	Ih		S	
7761.4	Ii			S
7998.4	IIa	18.1	S	W
7979.8	IIb	18.7		S
7936.3	IIc	18.6	W	
7915.9	IId	17.6	S	W
7896.8	IIf	20.1		M
7784.1	IIh	16.3		S
8010.7	IIIa	37.2		S
7950.0	IIIc	40.3	W	M
8036.2	IVa	76.8	W	
8080.0	VIa	144.3		W
8095.3	VIIa	167.7	W	

[a] S = strong, M = medium, W = weak intensity

Table 3.9: $^3H_6 \rightarrow {}^3F_4$ Transition Lines in $TmCrO_3$ $T \geq 5$ K, Zero Field

Term	Mean Energy (cm^{-1})	Identification	Representation labels and transitions from which they were deduced		
			$^3H_6 \rightarrow {}^3F_2$	$^3H_6 \rightarrow {}^3F_3$	$^3H_6 \rightarrow {}^3F_4$
$^3H_6$	0	I	A_2	A_1	A_1
	17.7 ± 4	II	A_1	A_2	A_2
	41.3 ± 5	III	A_2	A_1	A_1
	77.2 ± 2	IV		A_2	A_2
	120.9 ± 1	V		A_1	
	148.2 ± 5	VI	A_2	A_1	A_1
	169.2 ± 3	VII		A_2	A_2
	195.8 ± 1	VIII		A_1 or A_2	
$^3F_4$	12520.5 ± 2	a			A_1
	12550.3 ± 3	b			A_2
	12618.9 ± 2	c			A_1
	12650.4 ± 3	d			A_1
	12666.1 ± 2	e			A_2
	12726.8 ± 1	f			A_2
	12798.3 ± 1	g			A_1
	12862.9 ± 2	h			A_2
	12884.3 ± 2	i			A_1
$^3F_3$	14407.6 ± 1	a		A_1	
	14409.2 ± 2	b		A_2	
	14486.8 ± 1	c		A_2	
	14487.9 ± 1	d		A_1	
	14509.9 ± 1	e		A_1	
	14546.6 ± 1	f		A_2	
	14569.1 ± 1	g		A_2	
$^3F_2$	14954.1 ± 1	a	A_1		
	15019.6 ± 2	b	A_1		
	15116.4 ± 2	c	A_1		
	15184.8 ± 1	d	A_2		
	15252.5 ± 1	e	A_2		

Table 3.10: Energy levels of Tm^{3+} in $TmCrO_3$, as determined by optical spectroscopy. Representations of levels are those deduced from spectra at temperature $T \geq 5$ K in the absence of an external magnetic field

$\vec{E}||\vec{z}$ corresponds to A_1 to A_2 or A_2 to A_1 (Table 3.4), $\vec{E}||\vec{y}$ corresponds to A_1 to A_1 or A_2 to A_2. The initial state for these transitions I, must be A_2 and consequently II is A_1. Had there been two lines in $\vec{E}||\vec{z}$ and three lines in $\vec{E}||\vec{y}$, the Γ_f's will be A_2 for the former and A_1 for the latter and since $\vec{E}||\vec{z}$ and $\vec{E}||\vec{y}$ still correspond respectively to A_1 to A_2 or A_2 to A_1 and A_1 to A_1 or A_2 to A_2, I must be A_1 and so II is A_2. In the next section this situation occurs.

3.9.2.2 Spectra at $3.4 < T \leq 4.0$ K, zero field and 5 K at ~ 900 Oe

The above inconsistency can indeed be removed by experiments between 3.4 and 4.0 K in the absence of magnetic field and at 5 K in an external field of about 900 Oe parallel to the $\vec{c}$ crystallographic axis. To avoid repetition, the details of such spectral changes are presented later in Chapter 4, where effects of spin reorientation on Cr^{3+} spectra are also presented and discussed. For the purpose of the present chapter, it suffices to just enumerate the changes in the Tm^{3+} spectra. The line Ia of $^3H_6 \longrightarrow {}^3F_2$ with $\vec{E}||\vec{z}$ is reduced to negligible intensity in both types of experiments and so one does have <u>three</u> lines with $\vec{E}||\vec{y}$ and <u>two</u> lines with $\vec{E}||\vec{z}$; a fact implying that I and II are A_1 and A_2 and hence III is A_1, VI is A_1. Hence the optical analysis under the conditions of the new experiments agrees with the results of magnetic measurements

(Hornreich et al, 1973).

It is also observed that the spectra at temperatures higher than 5 K are not affected by the ~ 900 Oe field and Ia remains as a relatively strong line. The only other change in the Tm^{3+} spectra at 4 K in the absence of the field and at 5 K in a 900 Oe external field is the reduction to negligible intensity of the line If of $^3H_6 \longrightarrow {}^3F_3$ belonging to $\vec{E}||\vec{z}$ (Chapter 4, Figure 4.14). Therefore, the selection rules are not obeyed strictly above 5 K in magnetic fields less than about 1 Koe, and it appears that the $\Gamma_2(F_x)$ configuration, indeed occurs at higher temperatures and that there is mixing of state b of representation A_2 with state a of representation A_1 and so lifting the selection rules for the $^3H_6 \longrightarrow {}^3F_2$ transitions. The degree of mixing is in principle temperature dependent since the overlap of the electronic wavefunctions and the interactions between the magnetic ions depend on temperature. Table 3.11 gives the energy level scheme as deduced for spectra at temperatures from 3.4 to 4.0 K in the absence of an external magnetic field.

3.10 Discussion

Optical absorption spectroscopy of the Tm^{3+} ions in $TmCrO_3$ single crystals have been used to find the Tm^{3+} crystal field energy levels and to associate each state with the appropriate irreducible representations of the $C_s(m)$ site

Term	Mean Energy (cm^{-1})	Identification	Representation labels and transitions from which they were deduced		
			$^3H_6 \rightarrow {}^3F_2$	$^3H_6 \rightarrow {}^3F_3$	$^3H_6 \rightarrow {}^3F_4$
$^3H_6$	0	I	A_1	A_1	A_1
	17.7 ± 4	II	A_2	A_2	A_2
	41.3 ± 5	III	A_1	A_1	A_1
	77.2 ± 2	IV		A_2	A_2
	120.9 ± 1	V		A_1	
	148.2 ± 5	VI	A_1	A_1	A_1
	169.2 ± 3	VII		A_2	A_2
	195.8 ± 1	VIII		A_1 or A_2	
$^3F_4$	12520.5 ± 2	a			A_1
	12550.3 ± 3	b			A_2
	12618.9 ± 2	c			A_1
	12650.4 ± 3	d			A_1
	12666.1 ± 2	e			A_2
	12726.8 ± 1	f			A_2
	12798.3 ± 1	g			A_1
	12862.9 ± 2	h			A_2
	12884.3 ± 2	i			A_1
$^3F_3$	14407.6 ± 1	a		A_1	
	14409.2 ± 2	b		A_2	
	14486.8 ± 1	c		A_2	
	14487.9 ± 1	d		A_1	
	14509.9 ± 1	e		A_1	
	14546.6 ± 1	f		A_2	
	14569.1 ± 1	g		A_2	
$^3F_2$	14954.1 ± 1	a	A_1		
	15019.6 ± 2	b	A_2		
	15116.4 ± 2	c	A_2		
	15184.8 ± 1	d	A_1		
	15252.5 ± 1	e	A_1		

Table 3.11: Energy levels of Tm^{3+} in $TmCrO_3$, as determined by optical spectroscopy. Representations of levels are those deduced from spectra at temperature from 3.4 to 4.0 K in the absence of an external magnetic field

symmetry group. It is seen that the crystal field level scheme of Tm^{3+} obtained is consistent with the level schemes of the same ion introduced as an impurity e.g. in $YAlO_3$ (Antonov, 1973). Furthermore the splittings between the three lowest-lying singlets of Tm^{3+} found in this work are in good agreement with the calculated splittings deduced from the magnetization and susceptibility data on $TmCrO_3$ single crystals (Hornreich et al, 1973) and the experimental values reported from inelastic neutron scattering experiments (Shamir et al, 1977b). The results also confirm that the lowest-lying Tm^{3+}singlets I and II in $TmCrO_3$ beong to the irreducible representation A_1 and A_2 respectively of the site group as found in the analysis of the magnetization and susceptibility data (Hornreich et al, 1973). This finding is different from that for Tm^{3+} in the isostructural $TmFeO_3$ where the two lowest-lying singlets were reported to belong to the same irreducible representation (Malozemoff, 1970).

Since Tm^{3+} is a rare-earth ion, the splitting of its levels by the crystal field is substantially smaller than that by the spin-orbit interaction. This is why the energy level diagram of Tm^{3+} in $TmCrO_3$ obtained in this work is similar, in terms of positions of levels, to that found for Tm^{3+} in the isostructural $TmFeO_3$. The two energy level diagrams are quite different however in the classification of the levels by the irreducible representations of the site symmetry group. This

difference, when combined with the selection rules can account for the differences between the Tm^{3+} absorption spectra of $TmCrO_3$ and $TmFeO_3$. It should be noted that the selection rules are expected to be strictly observed in the G_xF_z (Cr^{3+}) f_z (Tm^{3+}) configuration where the Cr^{3+} .... Tm^{3+} effective field (molecular field) at the Tm^{3+} sites is along the $\vec{c}$ direction and therefore does not result in any mixing of the A_1 and A_2 states. In the G_zF_x ... c_yf_x configuration, however, the effective field exerted by the transition-metal ions on the Tm^{3+} spins is in the a-b plane and therefore results in a mixing of the A_1 and A_2 states. Although the Tm^{3+} singlet states are in principle a linear combination of the A_1 and A_2 states, they can be practically regarded as belonging to either the A_1 or A_2 representation since the mixing from the Tm^{3+}-transition metal interaction is relatively small. The selection rules can therefore be expected to be valid to a first approximation also in G_zF_x .... c_yf_x configuration. This fact is confirmed by our analysis of the spectra. A close examination of the $TmCrO_3$ spectra in the G_zF_x.... c_yf_x configuration and the spectra of $TmFeO_3$ studied in the same configuration, reveals that the validity of the selection rules is more pronounced in the latter. This feature is to be expected since the effective magnetic field exerted on the Tm^{3+} ions by the transition ions which is responsible for the mixing of the Tm^{3+} A_1 and A_2 states is approximately 15 KOe in $TmCrO_3$ and

only 3 KOe in $TmFeO_3$ at low temperature (Hornreich et al, 1973; Malozemoff, 1970). The temperature-dependent effective field from the Tm^{3+} - Cr^{3+} interaction has in principle an additional effect on the Tm^{3+} levels, viz., to change the positions of the Tm^{3+} levels as a function of temperature. This change however is estimated to be less than 0.8 cm^{-1} and was not observable in the $TmCrO_3$ absorption spectra in the $G_zF_x.... c_yf_x$ configuration.

In conclusion, in this chapter, the interpretation of $TmCrO_3$ optical absorption spectra has been presented and analysed. The results are in agreement with the results obtained on the lowest-lying singlets by other methods. In addition the positions and irreducible representation classification of the other levels in the $^3H_6$, $^3F_2$, $^3F_3$ and $^3F_4$ multiplets of Tm^{3+} ions in $TmCrO_3$ have been determined. On the differences between the $TmCrO_3$ and $TmFeO_3$ spectra, it has been shown that some can be attributed to the different magnetic properties of the two materials, in particular to their different Tm^{3+}-transition-metal interaction. However temperature and field induced spin reorientation has only been discussed with regard to its effect on the validity of the selection rules. That the selection rules for a lower temperature (3.4 - 4.0 K) are valid does suggest that the zero-field configuration is $G_xF_z... f_z$ at such temperatures.

This aspect will be discussed in detail in the next chapter; the effect of spin reorientation on the Cr^{3+} spectra will also be discussed.

CHAPTER IV

Cr^{3+} TRANSITIONS AND SPIN REORIENTATION IN $TmCrO_3$

4.1 Introduction

In this chapter, the spectra resulting from transitions among Cr^{3+} levels together with the Tm^{3+} lines exhibiting abrupt changes will be presented. Only the Cr^{3+} lines in the ~ 7300 Å and the 5000 - 5200 Å range will be discussed. These lines in turn can be divided into two groups. The first is insensitive to the change of spin configurations, whereas the latter is critically dependent on spin configurations and hence can be used to detect spin reorientation. The first category consists essentially of magnon sidebands and phonon sidebands. The latter category is most conveniently discussed with the abrupt changes observed in the rare-earth spectra. Thus the discussion will be divided into two sections: The non-abruptly changing and the abruptly changing lines. But first the energy level scheme and the group theoretical description of the Cr^{3+} ions will be described.

4.2 Cr^{3+} in $TmCrO_3$

4.2.1 Site symmetry of Cr^{3+}

The Cr^{3+} ions in rare-earth orthochromites are at sites of C_i symmetry (Sugano et al, 1971). This is the group consisting of the elements E and I (the identity and the

inversion operator respectively). Since a Cr^{3+} ion consists of three d electrons it is a Kramer's ion and so has half-integral spin angular momentum numbers. This fact necessitates the use of the double group and the double-valued representations. The group character table C_i and DC_i (D for double group) are given in Table 4.1. In the group C_i, there are just two irreducible representations Γ_1^+ and Γ_1^-, the + and - signs referring to even and odd parity. Since inversion is a symmetry element of the site group, the wavefunctions of the ions at such sites will have definite parity. The wavefunctions with even and odd parity will form basis functions of the irreducible representations Γ_1^+ and Γ_1^- respectively. This is clearly illustrated in the character table. For example under "I" in the row Γ_1^-, there is a "-1" signifying that the basis functions change sign under inversion. The table for DC_i can be related to that of C_i in a simple manner. First of all there are two new double-valued representations. Since the number of irreducible representations have to be equal to the number of classes, there must be two more classes. In this case, each of the two new classes consists of one element, $\bar{E}$ and I respectively. The element E now corresponds to a rotation of 4π radians and the usual identity element of a rotation by 2π radians, previously denoted by E now denoted by $\bar{E}$, is no longer the identity element. An ion with an odd number of electrons, hence

C_i	E	I
Γ_1^+	1	1
Γ_1^-	1	-1

DC_i	E	$\bar{E}$	I	$\bar{I}$
Γ_1^+	1	1	1	1
Γ_1^-	1	1	-1	-1
Γ_2^+	1	-1	1	-1
Γ_2^-	1	-1	-1	1

Table 4.1 Character tables of C_i and DC_i

half-integral angular momentum quantum numbers will have its wavefunctions change sign under a 2π rotation, and thus needs another 2π (a total of 4π) radians to regain its original sign. This can be proved by using the equation 3.5 for the rotational group and extending it to include half-integral J values. The element I has the same meaning as before. The element $\bar{I}$ has the same effect as the product of $\bar{E}$ and I. Another feature of the DC_i table is that the characters under E and $\bar{E}$ are the same for the single-valued irreducible representations Γ_1^+ and Γ_1^-; similarly for those characters under I and $\bar{I}$. But the characters under E and $\bar{E}$ and similarly for I and $\bar{I}$ are opposite in sign for the double-valued representations Γ_2^+ and Γ_2^-. Ions with an even number of electrons (a non-Kramer's ion) will only belong to functions which are basis functions of the irreducible representations Γ_1^+ and Γ_1^-, whereas those ions with an odd number of electrons (a Kramer's ion) will only have wavefunctions which form basis functions of the representations Γ_2^+ and Γ_2^-.

4.2.2 Level scheme of Cr^{3+}

In orthochromites and similarly in a lot of other chromium compounds, the Cr^{3+} ion can be considered, as a first approximation, to be at a site of the cubic group since the true site symmetry (C_i in this case) can be treated as a reduction from cubic symmetry (Sugano et al, 1970). This

cubic group, O_h, will split the different electronic configurations into different levels and the other non-cubic symmetry components of the crystal field can then be introduced together with the spin-orbit coupling to further split these cubic group levels. Group theoretically, beginning with the cubic site group the resultant levels belong to the single-valued representations of O_h. This occurs since, before the spin-orbit coupling is introduced, the spin of the ion is not considered. Thus the cubic crystal field only affects the orbital angular momentum whose quantum numbers are always integral whether the ion is Kramer's or non-Kramer's. It is only when the ion has an odd number of electrons and when spin-orbit coupling is introduced that levels belonging to the double-valued representations occur. If the ion is non-Kramer's, introduction of spin-orbit coupling will still give levels whose symmetries are characterized by the single-valued representations (Cracknell, 1975).

Optical transitions for the Cr^{3+} ion can be divided into the interconfigurational and the intraconfigurational (Sugano, et al, 1970). The first type is among levels of different electronic configurations and the second among levels of the same electronic configuration. In the present work, the configurations of interest are t_2^3 and t_2^2e. The symbol t_2^3 means that the three d electrons are all in the orbital t_2 and t_2^2e means that two electrons are in orbital t_2 and one in

orbital e. Under the cubic field t_2^3 is split into the levels $^4A_2$, ^2E, $^2T_1$, and $^2T_2$ whereas t_2^2e will be split into a number of levels, two of which fall within the visible regions, namely $^4T_1$ and $^4T_2$. The relative positions of the levels are schematically given in Figure 4.1. The subscript g denotes that the wavefunctions of Cr^{3+} have even parity. Each level is identified by two other symbols. The capital letters T_1, T_2, E, and A_2 denote the orbital degeneracy whereas the superscripts signify the spin degeneracy 2S + 1 of the levels where S is the spin quantum number. Orbitally the T_1 and T_2 levels are three-fold degenerate and the E level two-fold whereas the A_2 level is an orbital singlet. Thus $^4A_2$ has a spin degeneracy of four, i.e. 2S + 1 = 4 or S = 3/2 and as orbital and spin degeneracies are taken together it is four-fold degenerate. Similarly $^2T_2$ is three-fold orbitally degenerate and two-fold spin degenerate, a total six-fold degeneracy.

In the above discussion, the levels can be characterized with both spin and orbital quantum numbers because the spin-orbit interaction has not been introduced so that the spin and orbital angular momenta are still good quantum numbers. When spin-orbit interaction is introduced, J, the total angular momentum number is the appropriate one. If the spin-orbit coupling and the non-cubic crystal field (symmetry C_i in this case) are present some or all of the orbital

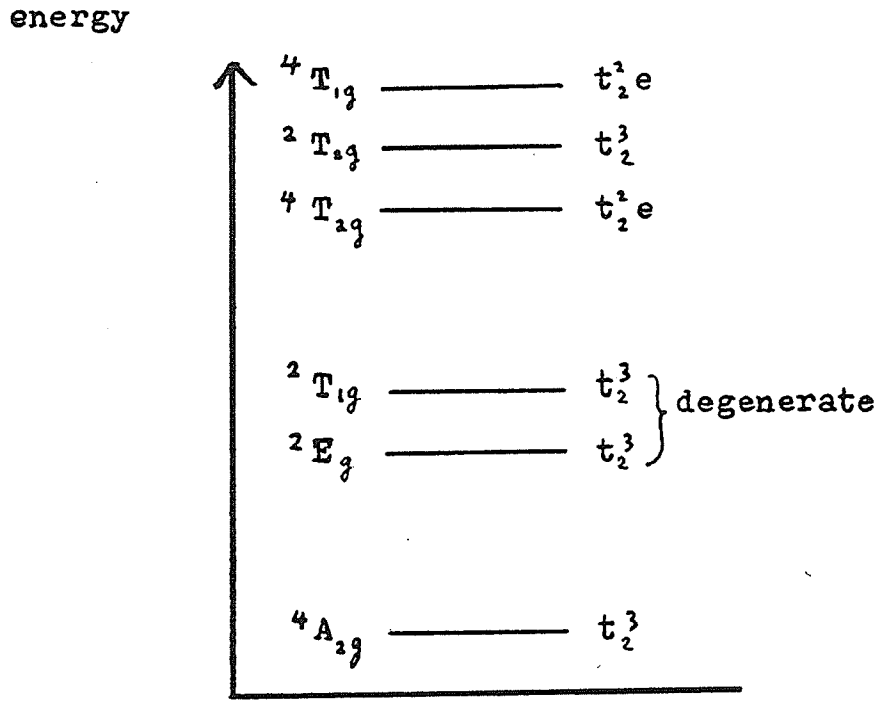

Figure 4.1: The cubic field Cr^{3+} levels

degeneracies are lifted. However the spin degeneracies for the Kramer's Cr^{3+} ion can only be lifted by an externally applied magnetic field or by the internal molecular field when the material is ordered magnetically. In $RCrO_3$, with the very low symmetry of C_i and spin-orbit coupling, all the cubic levels are split. The splittings are indicated in Figure 4.2. Since the spectra to be presented later are those from $^4A_2$ to ^2E and $^2T_2$ (the subscript g will hereafter be omitted) only these levels are given in the figure. Although this figure is just schematic, in a lot of situations the middle level of $^2T_2$ is indeed closer to the lower energy level. Also the spin-orbit coupling shifts the $^4A_2$ level by a small amount. When the compound is ordered, these levels will be split further into levels characterized approximately by the z-component of the spin, namely -3/2, -1/2, 1/2, 3/2 for the $^4A_2$ and -1/2, 1/2 for the ^2E and $^2T_2$ levels.

4.2.3 Selection rules for Cr^{3+} transitions

The transitions of interest $^4A_2 \rightarrow {}^2E$ and $^4A_2 \rightarrow {}^2T_2$ are among levels of the same parity (even in this case) so electric dipole transitions are parity forbidden. As mentioned before, this selection rule can be relaxed by admixing states of odd parity by odd crystal field components or by odd lattice vibrations. The former is absent in this case but the latter remains a possibility, which will be discussed

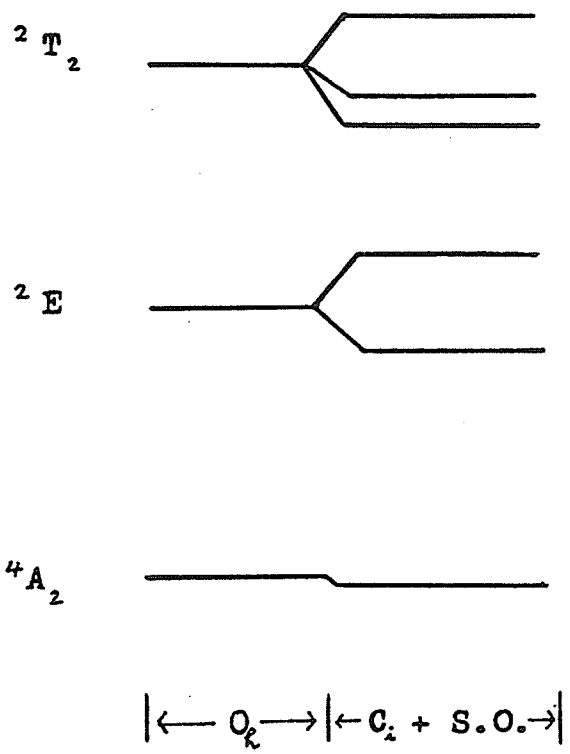

Figure 4.2: C_i and S.O. split cubic levels

later. The transitions mentioned above are also forbidden for another reason because they are among levels of different spin degeneracies, 4 and 2 respectively, (these are also intraconfigurational) since none of the electric dipole, magnetic dipole and electric quadrupole moments have matrix elements between the states of different spin multiplicities. So this rule is more strict than the parity rule which just forbids electric dipole transitions. Thus the $^4A_2 \rightarrow {}^2E$ and $^2T_2$ are <u>doubly</u> forbidden whereas the $^4A_2$ $^4T_1$ and $^4T_2$ are only parity forbidden. The spin selection rule is however relaxed slightly if the spin-orbit interaction is taken into account because such interaction can connect terms with S and S' where $|S-S'| = 0,1$ (Sugano et al, 1970). Therefore the term with S may have small components of the terms with $S \pm 1$ if the spin-orbit interactions is taken into account, and the presence of these small components allows the spin forbidden transitions $S \nrightarrow S + 1$ to occur. The degree of admixture of the S term with the $S \pm 1$ term is approximately given by $\langle V_{so} \rangle / \Delta E_{ee}$, where $\langle V_{so} \rangle$ is the matrix element of the spin-orbit interaction between the S and $S \pm 1$ terms and ΔE_{ee} is the energy separation between them. Because of the spin selection rule, the transitions among levels of different spin degeneraces are considerably weaker than those among levels of the same spin degeneracies.

4.3 Assisted electric dipole Cr^{3+} transitions

Single-ion Cr^{3+} transitions in $RCrO_3$ as noted are strictly parity and spin forbidden in the case of levels of different spin multiplicities. However electric-dipole transitions can occur in the form of a simultaneous creation or destruction of quasi-particles like phonons and magnons, giving rise to phonon sidebands and magnon sidebands respectively. The term sideband just refers to a spectral line which appears by the side of the parent zero phonon or magnon line. Thus such transitions involve a single-ion transition as well as a quasi-particle. However, the appropriate single-ion transition is not among the single-ion levels of Cr^{3+}, but among exciton levels (Loudon, 1968). Finally, simultaneous transitions involving the Cr^{3+} excitons and the excitation of the R^{3+} from ground to excited levels can also result in electric dipole transitions. If the R^{3+} is a Kramer's ion, its levels are Kramer's doublets each of which will be split into two levels, approximately described by the spin quantum numbers 1/2 and -1/2. In such cases the rare-earth ion may, for example be promoted from the -1/2 to the 1/2 level; hence such transitions are also called Cr^{3+} exciton and R^{3+} spin flip absorptions.

4.3.1 Excitons and magnons

When a species of magnetic ion is introduced as an impurity into a host, the interactions among the impurity ions can be ignored, since the concentration of these ions are usually low enough so that the ions are far apart. Hence the energy level scheme and selection rules are mainly dictated by the symmetry of the site of the impurity ions. The transitions are essentially among single-ion crystal field levels. This interaction, however cannot be ignored for the magnetic ions in concentrated substances. In such cases the crystal field levels will first be split or shifted by the exchange (molecular) field. Secondly, due to the inter-ion interactions, any transitions to the excited states can be transferred from ion to ion. This means that these single-ion crystal field levels are no longer the eigenstates of the crystal. The interactions give rise to levels which can be thought of as stemming from the single-ion levels. These new levels are known as the excitons. They are thus collective excitations of the crystal and so are characterized by the set of allowed and distinct $\vec{k}$ vectors of the Brillouin zone. Since the $\vec{k}$ vectors form a quasi-continuous band in $\vec{k}$- space, each exciton level is actually a quasi-continuous band. The number of such $\vec{k}$ vectors is determined by the number of magnetic ions in the crystal whereas the number of exciton bands are determined by the number of inequivalent magnetic ions in the unit cell. This splitting of a single-ion level into exciton bands is known as the Davydov splitting. Figure 4.3

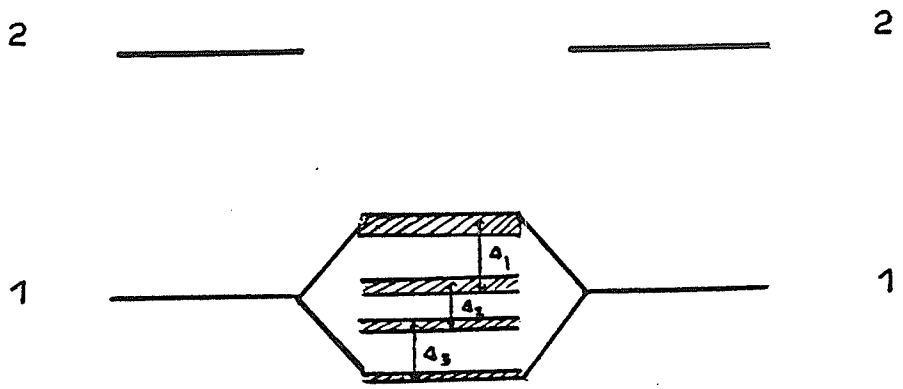

Figure 4.3: The relationship between exciton bands and Davydov splitting

illustrates the relation between the single-ion levels and the exciton bands. Here 1 and 2 are the single-ion levels and in this case there are four bands with Davydov splittings characterized by Δ_1, Δ_2 and Δ_3. The thickness of a shaded band is the dispersion of the exciton in the band because of the energy dependence on $\vec{k}$ vectors. If it happens that the single-ion level belongs to the lowest crystal-field-plus-exchange split level of the ion the exciton is usually called a magnon. The exciton and the magnon have no formal difference. This difference in terminology is illustrated schematically in Figure 4.4 for Cr^{3+} for an excited level, a level of ^2E, and a level of $^4A_2$.

4.3.2 Symmetry of the excitons and the magnons

The excitons and magnons being collective excitations must reflect the symmetry of the crystal. In other words their symmetry must be compatible with that of the space group of the crystal, meaning that the exciton and the magnon wavefunctions must belong to (form basis functions of) the irreducible representations of the space group. The particular symmetry of the excitons depends on the particular $\vec{k}$ vector of interest. In the case of the transitions in the optical and infrared the photon $\vec{k}$ vector is ≈ 0. Conservation of $\vec{k}$ vectors (a form of conservation of momentum) requires that the excitons involved be also of $\vec{k} \approx 0$. This simplifies the

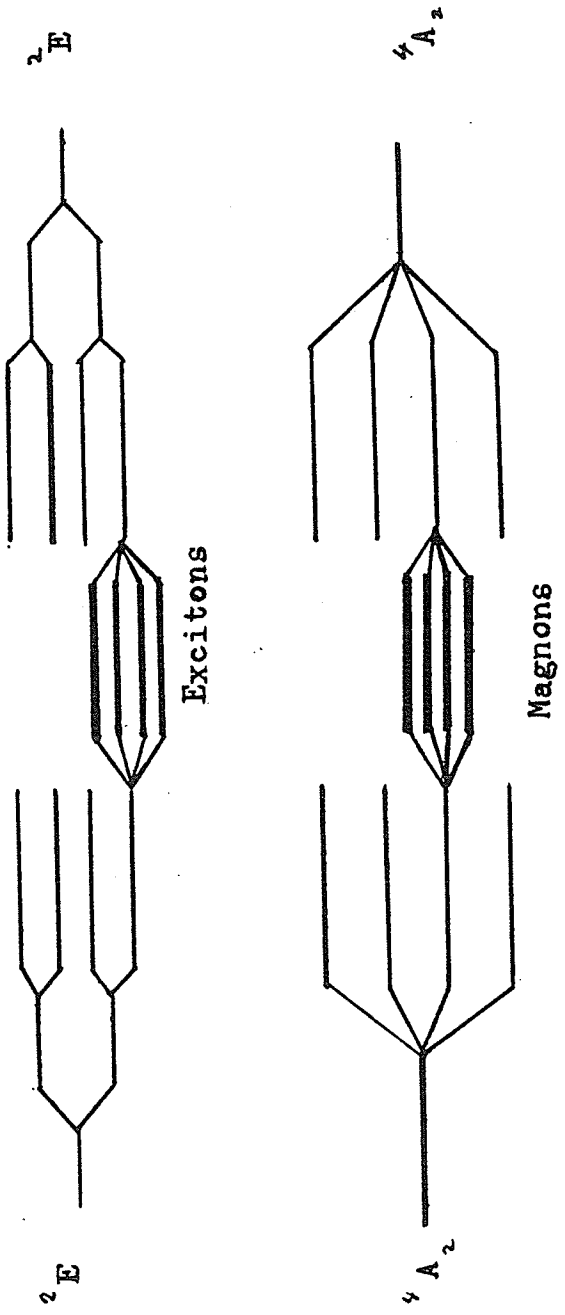

Figure 4.4: Relationships between excitons and magnons

symmetry consideration and offers an easy way to find the irreducible representations of the space group. In this case the irreducible representations of the space group coincide with those of the factor group of the space group (Burns and Glazer, 1978). This factor group is, in turn, always isomorphic to a certain point group. (Two groups are isomorphic if there is a one-one correspondence among the elements of the two groups). This isomorphism implies that the character tables are the same for the two groups. It should be mentioned that in a magnetic crystal, the appropriate group is the magnetic group. Thus the irreducible representations must be those of the magnetic space group. These representations are known as the corepresentations. However a magnetic group has a unitary subgroup and it is only necessary to know the irreducible representations of this unitary subgroup to determine selection rules. Thus for $\vec{k} \approx 0$ it is only necessary to know the unitary factor group isomorphic with the unitary subgroup of the magnetic group which is of course spin-configuration dependent. For $RCrO_3$ detailed group theoretical investigations show that for $\vec{k} \approx 0$ the factor group for both the Γ_2 and Γ_4 phases is isomorphic to the C_{2h} group which has the operations E, C_2, σ_h and I (Sugano et al, 1971), where the symbols have the same meaning as in Chapter 3. Since exciton levels arise from the single ion levels, they must have the same parity

as the parent levels and so are also parity forbidden and hence are mainly observed as magnetic dipole transitions. However the Γ_2 and Γ_4 excitons have different selection rules with respect to the polarizations of the incident light (Sugano et al, 1971).

It is seen that in general, for magnetic ions in concentrated substances, the exciton and magnon description is the more appropriate. This is most important for the lowest lying excited states because the electronic spins of neighbouring ions can significantly reduce the excitation energy below its molecular-field value. It will be seen that the magnon energies deduced from the present work are significantly different from the exchange split levels of the $^4A_2$ level. But as the parent single-ion level becomes higher in energy, the Davydov splittings become smaller and smaller. Experiments on $RCrO_3$ excitons derived from ^2E ($\sim$13700 cm^{-1}) have shown that the total splitting (sum of all the Davydov splittings) is ~ 7 cm^{-1} (Sugano et al, 1971; Kajiura et al, 1975; Aoyagi et al, 1976; Meltzer, 1970). Thus one expects that for the higher levels like $^2T_2$, this will be even smaller and the levels, in principle the excitons, are rather satisfactorily described by the single-ion model.

4.3.3 Magnon sidebands

4.3.3.1 Mechanism

There are two possible mechanisms which can give rise to magnon sidebands. The first arises from the multipole expansion of the Coulomb interaction between pairs of ions, and includes the dipole-dipole, dipole-quadrupole interactions, etc. These interactions have a long range, falling off as some power of the inverse separation between the ions. The second type of coupling is due to the exchange terms which result from the overlap of the electronic wavefunctions of the ions. Here the exchange mechanism will be invoked to explain the two-ion interaction and instead of the four sublattices, a two-sublattice approximation will be adopted following Aoyagi (1974). The sidebands can be explained as due to the non-diagonal exchange interaction involving a pair of ions i and j on opposite sublattices. This is illustrated in Figure 4.5, for the ^2E level excitons. Here g is the ground state with magnetic spin quantum number -3/2 for the i sublattice with down spin (↓) and with magnetic spin quantum number + 3/2 for the j sublattice with up spin (↑). Similarly e denotes one of the exciton levels derived from the single-ion level ^2E and u is an excited level of odd parity and of spin quantum number -3/2 and m denotes a magnon level. Both m and g belong to the ground orbital level $^4A_2$ with quantum numbers +1/2 and + 3/2 respectively. The direct transition

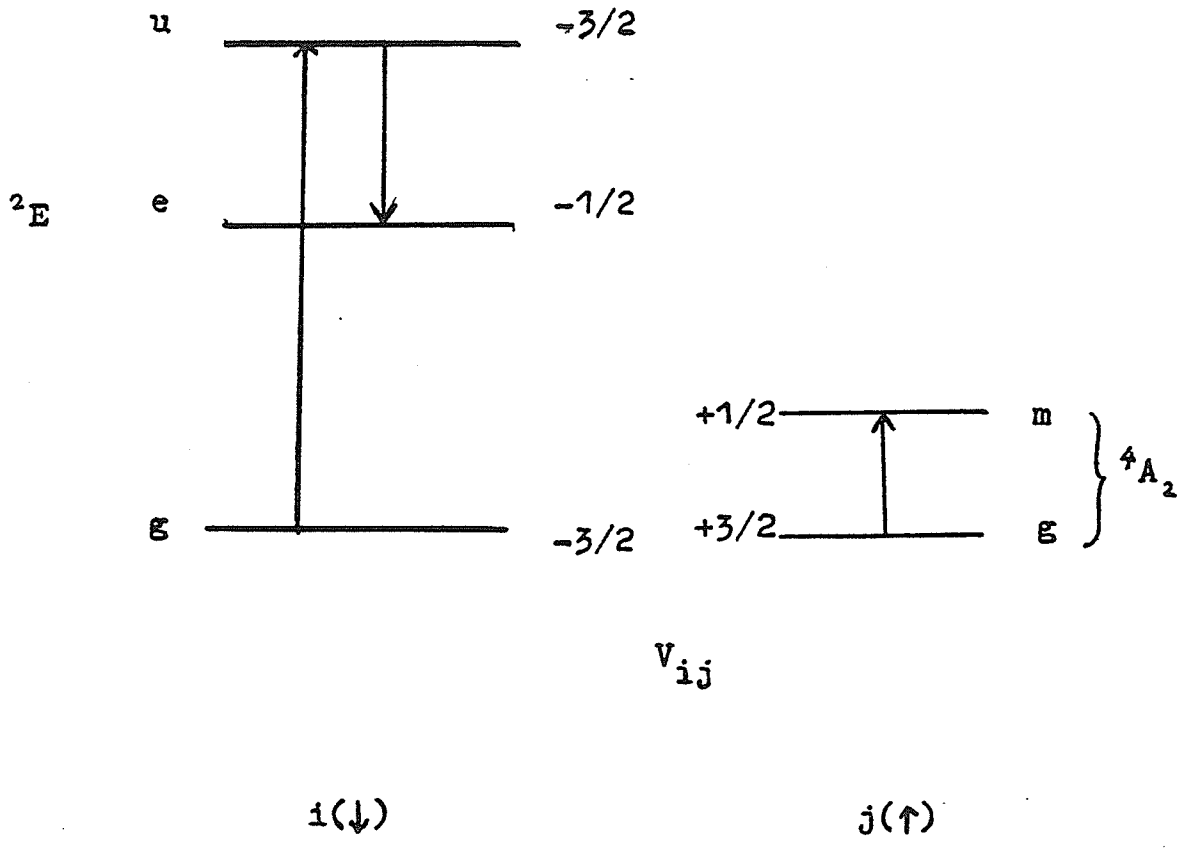

Figure 4.5: Non-diagonal exchange interaction mechanism for ^2E exciton magnon sidebands

from g to e for the i ion corresponding to the excitons observed are magnetic dipole. However magnon-assisted electric-dipole transitions are also possible. The ion i goes to an odd parity excited state u while the ion j goes from g to m. Then ion i deexcites from state u to state e. Spin angular momentum components are conserved since for the ith ion the change in spin momentum component $\Delta S_{zi} = -1/2 - (-3/2) = 1$ and for the jth ion, $\Delta S_{zj} = 1/2 - (3/2) = -1$. This is achieved by the exchange interaction $\hat{V}_{ij}$ coupling the two ions. This coupling induces an electric dipole moment (Loudon, 1968) and explains the observed electric dipole character of the sidebands. The two-ion transition differs also from the exciton transition, in that the restriction of the wave-vector to $\vec{k} \approx 0$ is no longer required and the only requirement is that $\vec{k}_{ex} = -\vec{k}_{mag}$, where ex and mag denote respectively the exciton and the magnon. This conserves the momentum since $\vec{k}_{ex} + \vec{k}_{mag} = 0$ as required by the $\vec{k} \approx 0$ photon absorption.

4.3.3.2 Selection rules for magnon sidebands

The intensity of the exciton-magnon absorption line is proportional to the product of the joint density of state of the exciton and the magnon and the square of the transition moment. In general, the joint density of state has its maximum value at the high symmetry points of the Brillouin

zone. Therefore unless the transition moment is zero at a particular point, the absorption intensity is also a relative maximum at those symmetry points. The Brillouin zone is shown in Figure 4.6, where the symbols for the various points are those of Van der Ziel and Van Uitert (1969a). Only the points Γ, X, Y, S, R, U, T, Z will be discussed. These points have the following meanings:

$\Gamma = (0, 0, 0)$, $X = (\pi/a, 0, 0)$, $Y = (0, \pi/b, 0)$, $S = (\pi/a, \pi/b, 0)$

$R = (\pi/a, \pi/b, \pi/c)$, $U = (\pi/a, 0, \pi/c)$, $T = (0, \pi/b, \pi/c)$, $Z = (0, 0, \pi/c)$

where a, b, c are the lattice parameters of the real lattice. In Chapter 3, Table 3.6 only the magnetic point groups are given for the explanation of the spin configurations because that was adequate for that purpose. Now the full magnetic space group elements for the two spin configurations will be given:

Γ_2: $\{E|0\}$, $\{C_{2x}|t_1\}$, $\{I|0\}$, $\{\sigma_x|t_1\}$, $\{RC_{2z}|t\}$, $\{R\sigma_z|t\}$, $\{RC_{2y}|t_2\}$, $\{R\sigma_y|t_2\}$

Γ_4: $\{E|0\}$, $\{C_{2z}|t\}$, $\{I|0\}$, $\{\sigma_z|t\}$, $\{RC_{2x}|t_1\}$, $\{RC_{2y}|t_2\}$, $\{R\sigma_x|t_1\}$, $\{R\sigma_y|t_2\}$

where $t = \frac{1}{2} c\hat{z}$, $t_1 = \frac{1}{2}(a\hat{x} + b\hat{y})$ and $t_2 = \frac{1}{2}(a\hat{x} + b\hat{y} + c\hat{z})$. The symbols E, C_{2x}, etc. have the same meaning as in Table 3.6. If all the non-primitive translation vectors (t, t_1, t_2) are set to zero in the group elements, the magnetic point groups

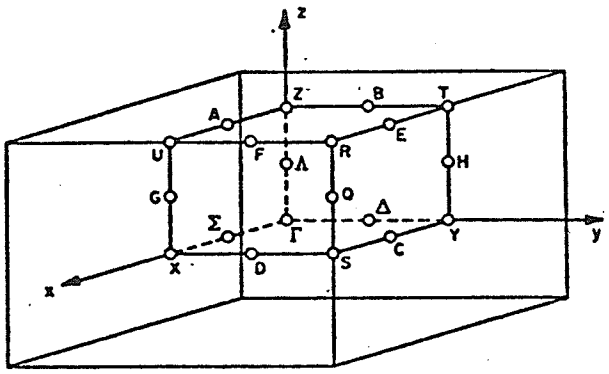

Figure 4.6: Brillouin zone of the orthorhombic lattice

given in Table 3.6 is obtained. In the case of the magnetic space groups, the unitary subgroups for Γ_2 and Γ_4 are respectively $G(\Gamma_2) = \{\{E|0\},\{C_{2x}|t_1\},\{I|0\}, \{\sigma_x|t_1\}\}$ and $G(\Gamma_4) = \{\{E|0\}, \{C_{2z}|t\},\{I|0\},\{\sigma_z|t\}\}$. It is the irreducible representations of these subgroups which determine the selection rules. These selection rules have been worked out for the Γ_4 spin configuration (Aoyagi, 1974; Van der Ziel and Van Uitert, 1969a) and it has been shown that electric-dipole transitions with $\vec{E}||\vec{a}$, $\vec{b}$ or $\vec{c}$ are allowed for the creation of magnons at each of the symmetry points Z, R, U and T but points Γ, X, Y and S are all forbidden. The results for the Γ_2 configuration have not been worked out. However, our experimental results seem to indicate that the selection rules may also be similar, for the Γ_2 configuration.

4.3.4 Phonon sidebands

Phonon sidebands of excitons are simultaneous creation of an exciton and a phonon. That is, they are phonon-assisted transitions. These are also known as vibronic (vibrational electronic) transitions. In general there are several mechanisms for such transitions. One possibility is that if the charge distributions of the initial and final electronic states are different, the equilibrium positions of the ions will be different for the two electronic states. Another mechanism, which is particularly important when the electronic transition is forbidden, as in the Cr^{3+} case, is

that the phonon may distort the environment of the ion in such a way that the transition is allowed. This is the appropriate mechanism since the Cr^{3+} ion is at an inversion center and so there is no admixture of odd crystal field components.

For d electrons, the transitions most likely to have strong phonon sidebands can often be determined by an inspection of the diagrams showing how the energy levels of an ion change with the size of the cubic crystal field parameters (Sugano et al, 1970). For Cr^{3+} the states $^4T_1$ and $^4T_2$ are quite sensitive to such parameters and can give rise to very broad and strong absorptions. On the other hand the levels ^2E, $^2T_1$ and $^2T_2$ are quite insensitive to such parameters. Transitions to these states therefore display a zero - phonon line (the exciton) and a highly structured phonon sideband, whose structure can be correlated with known phonon frequencies.

Phonons are also related to a number of temperature dependent effects of the crystal spectra (di Bartolo, 1968). Line shifts can occur because of the change of the crystalline field parameters, which in turn depend upon the internuclear separations. Thus the anharmonic interaction of the thermal phonons, giving rise to lattice parameter changes due to thermal expansion, is a possible origin of line shifts. In addition, line shifts occur because the

strains associated with thermal phonons can induce fluctuations in the crystal field parameters about their average values. For Cr^{3+}, line shifts of the $^4T_1$ and $^4T_2$ transitions are probably due to the anharmonic effect since their energies depend sensitively on the crystalline field parameters. For the ^2E, $^2T_1$, $^2T_2$ transitions the second mechanism is probably more important. The same mechanism which causes the line shift is also likely to be responsible for the broadening of these lines at higher temperatures.

4.3.5 Rare-earth ion assisted Cr^{3+} transitions

Co-operative absorptions also occur which involve the absorption of a photon with the simultaneous creation of an exciton and the promotion of the rare-earth ion to an excited state or band. This is similar to the Cr^{3+}-rare-earth ion pair emission that has been observed (Van der Ziel and Van Uitert,1969b), In this case the Cr^{3+} ion deexcites from the ^2E exciton state to the ground state $^4A_2$ and the rare-earth ion is promoted from the ground to an excited level. In $RCrO_3$, pair absorptions with the excitation (Kojima et al, 1980) and de-excitation (Aoyagi, 1974) of the rare-earth ion have been observed. These are called Cr^{3+} exciton-rare-earth ion spin-flip simultaneous absorptions. Again, exchange seems to be a possible mechanism, giving rise to an electric dipole moment. For these transitions the two following characteristics are

observed: I. They are electric dipole and form a band with a steep cut-off on the lower energy side of the band. II. The intensity of these transitions depends on the product of the joint density of states of the Cr^{3+} exciton state and the rare-earth ion excited state and the transition moment squared, analogous to the case of the magnon sidebands.

4.4 The Cr^{3+} spectra and spin reorientation in $TmCrO_3$: Tm^{3+}, Cr^{3+} and Cr^{3+}-Tm^{3+} spectra

4.4.1 Non-abruptly changing transitions

4.4.1.1 Cr^{3+} transitions: 7100 - 7250 Å

The spectra in this region are presented in Figure 4.7 and Figure 4.8. These lines are all electric dipole transitions. Their wavelengths in Å and energies in cm^{-1} and separations Δ in cm^{-1} from the average $TmCrO_3$ exciton position, ~13700 cm^{-1} (~ 7300 Å) are given in Table 4.2; the excitons were observed by Aoyagi et al, 1976. These lines can be conveniently divided into one group within the interval of 7100 - 7140 Å with a weaker absorption and another group within the interval of 7160 - 7250 Å.

The spectral lines between 7160 - 7250 Å have the following characteristics. They are about ~100 cm^{-1} to ~200 cm^{-1} from the average exciton position (~13700 cm^{-1} for $TmCrO_3$) and have ~30 cm^{-1} half-widths for those lines which are less broadened and so better resolved. All of the lines

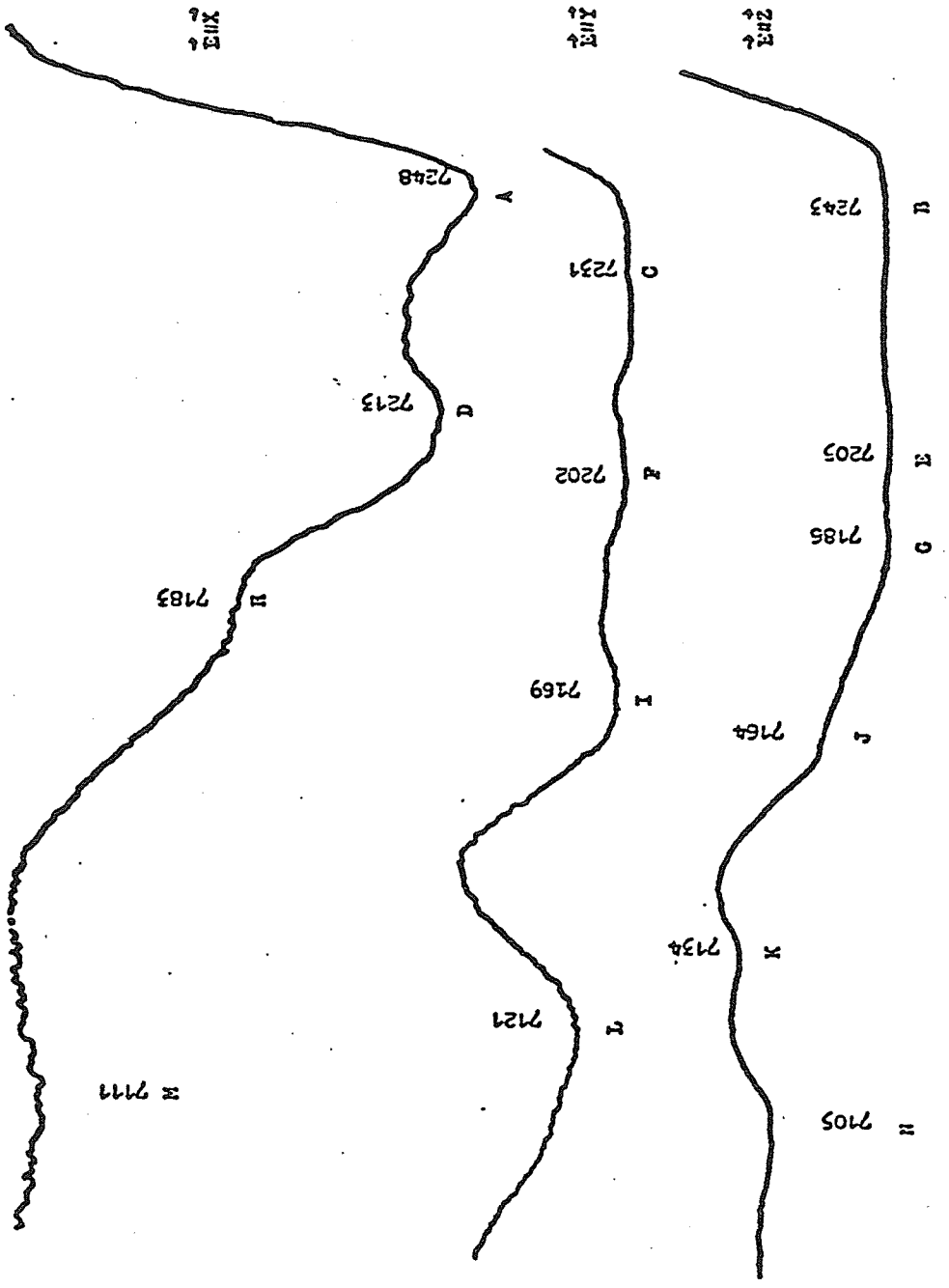

Figure 4.7: Cr^{3+} sidebands: 7100-7250 Å, 5 K

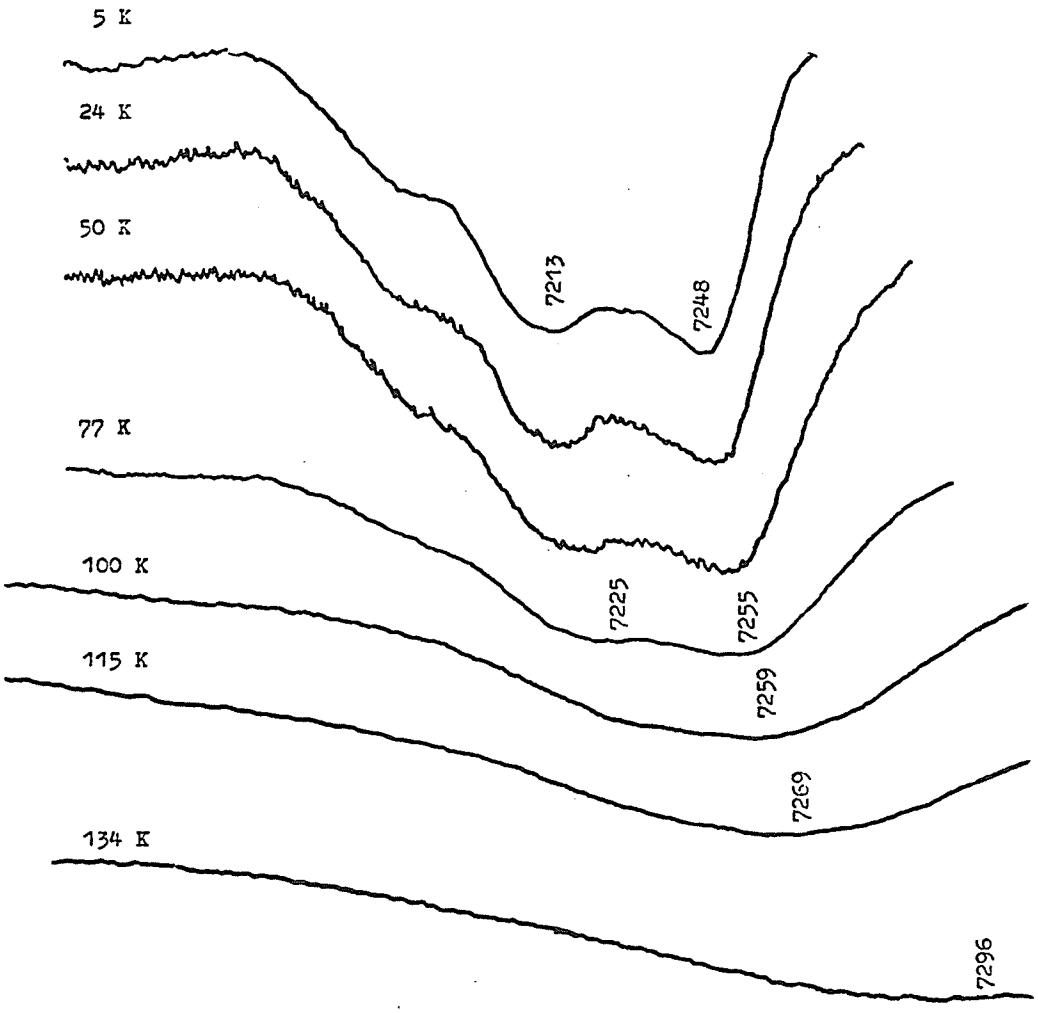

Figure 4.8: Temperature dependences of Cr^{3+} sidebands, $\vec{E} \| \vec{x}$

	Å	cm^{-1}	$\vec{E}\|\|\vec{x}$	$\vec{E}\|\|\vec{y}$	$\vec{E}\|\|\vec{z}$	$\Delta(cm^{-1})$
N	7105	14075			x	375
M	7111	14062	x			362
L	7121	14043		x		343
K	7134	14017			x	317
J	7164	13959			x	259
I	7169	13949		x		249
H	7183	13922	x			222
G	7186	13916			x	216
F	7202	13885		x		185
E	7205	13879			x	179
D	7213	13864	x			164
C	7231	13829		x		129
B	7243	13806			x	106
A	7248	13797	x			97

Table 4.2 Wavelengths, energies, polarization and separations of lines from excitons (~13700 cm^{-1}), of lines from 7100 - 7250 Å; x means transition is allowed.

exhibit distinct polarization characteristics. As the temperature is increased these lines broaden and merge into a single peak whose position shifts to a longer wavelength (Figure 4.8). The lines A, B and C (Figure 4.7) with separations respectively of 97, 106 and 129 cm^{-1} from the excitons, can be assigned to the absorption of a photon, with the simultaneous creation of an exciton and a magnon of respective energies 97, 106 and 129 cm^{-1}. These values are close to the predicted and observed magnon energies of 82, 109 and 121 cm^{-1} of $YCrO_3$ at the symmetry points Z, R, T and U respectively (T and U have the same energy), (Aoyagi, 1974). The lines D to J, separated from the exciton at about twice the energy of some of the one magnon energies, are probably one-exciton and two-magnon absorptions (e.g. 216 = 2 x 108). The temperature dependences of the positions of the lines in this group can be explained qualitatively with the help of Figure 4.9. When the temperature is increased the exchange splittings of the levels concerned, characterized by Δ_1 and Δ_2 respectively will decrease, since the substance becomes less ordered magnetically. This occurs since the molecular field, which is proportional to the existing sublattice magnetization, must decrease, thus decreasing the exchange splittings. When the temperature approaches T_N, the Néel temperature, all the exchange splittings vanish and a transition corresponding to energy

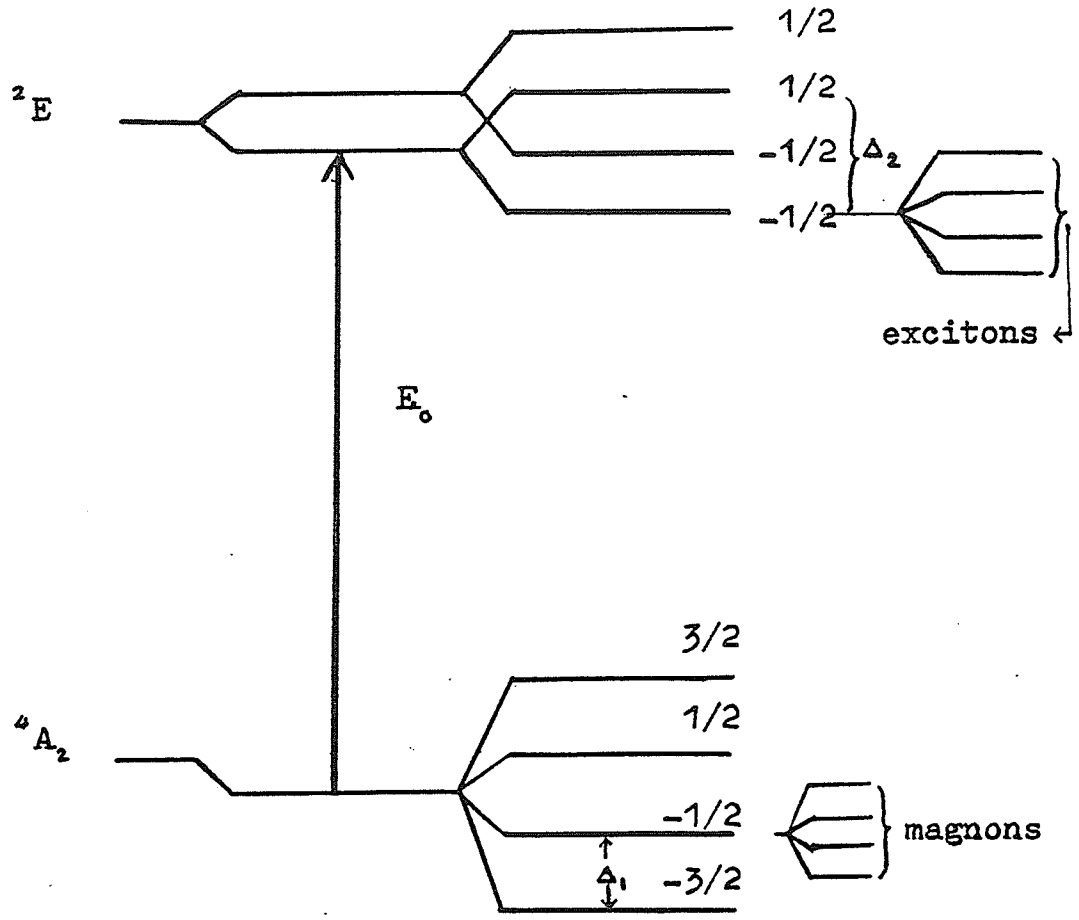

Figure 4.9: Schematic diagram of exciton and magnon splittings of ^2E and $^4A_2$ respectively

E_o will be observed. In fact, long before T_N is reached the magnon sidebands have already broadened into a large peak. Turning now to the lines K, L, M and N, it is observed that these lines are weaker and broader and are separated about 300 - 400 cm^{-1} from the exciton lines. Broadening of these lines is much more rapid compared with the magnon sidebands. Such characteristics show that these transitions are probably phonon sidebands of the excitons since the energies coincide with the range of phonon energies deduced from the Raman spectra of $ErCrO_3$ (Ullrich et al, 1977), $YCrO_3$ and $GdCrO_3$ (Udagawa et al, 1975).

4.4.1.2 Cr^{3+} transitions: 5000 - 5100 Å

In this section the absorption lines in the range 5000 - 5100 Å will be discussed. These lines together with the abruptly changing lines in the range 5100 - 5200 Å are clearly transitions of Cr^{3+} from the ground level ($^4A_2$, -3/2) to the levels related to the crystal field and exchange split levels of the cubic level $^2T_2$. This is about 19000 cm^{-1} for most Cr^{3+} ions as an impurity or in concentrated substances (Sugano et al, 1970). The spectra for these transitions are given in Figures 4.10, 4.11 and 4.12. The wavelengths, wavenumbers and polarization characteristics of this set of lines are given in Table 4.3 The lines A, B and C form one group and line D behaves separately. Since

	Å	cm^{-1}	$\vec{E}\|\|\vec{x}$	$\vec{E}\|\|\vec{y}$	$\vec{E}\|\|\vec{z}$
D	5020	19920	x	x	x
C	5046	19818	x	x	x
B	5066	19739	x	x	x
A	5087	19658	x	x	

Table 4.3 Wavelengths, energies and polarization of lines from 5020 to 5090 Å

x means that transition is allowed.

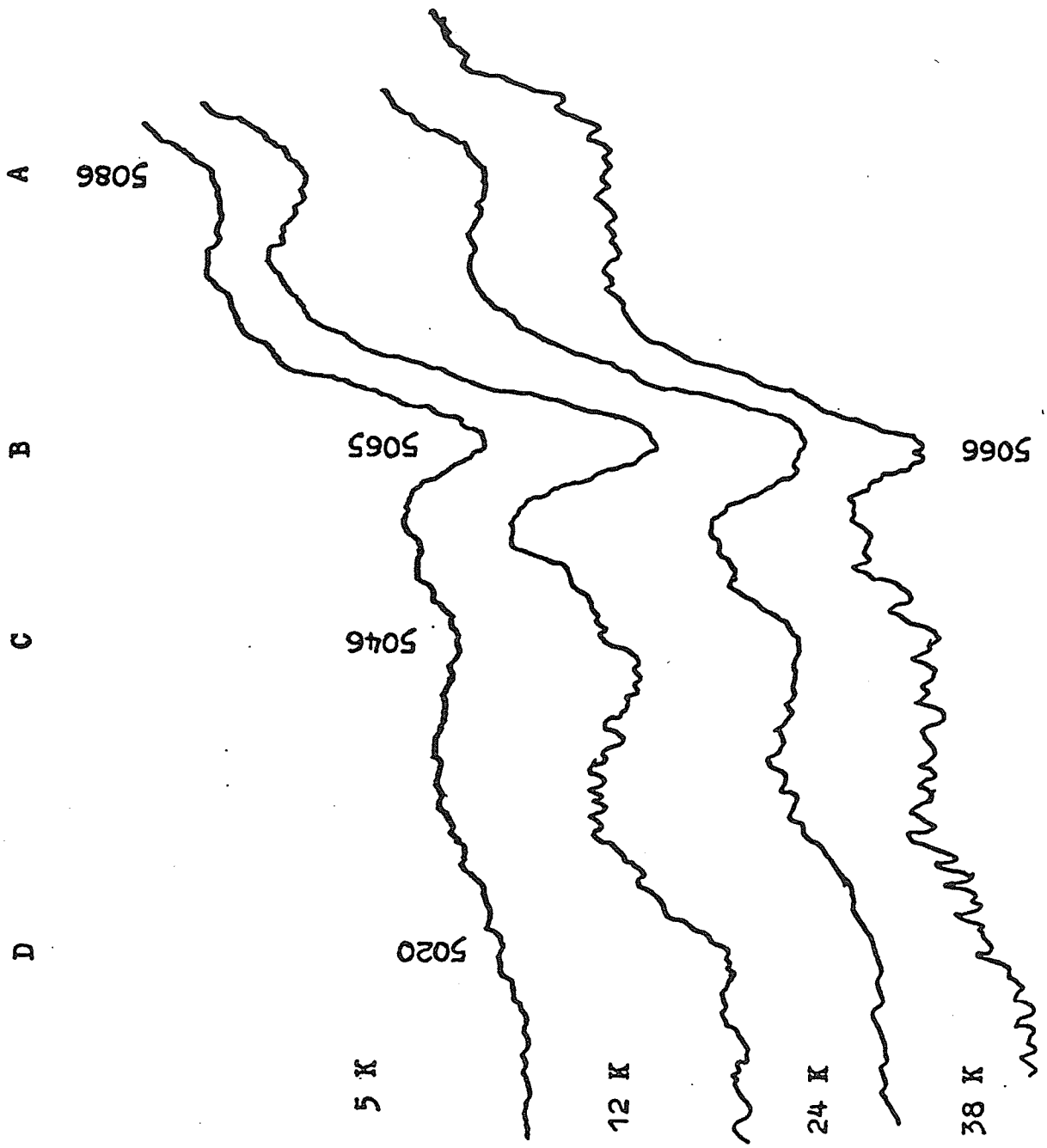

Figure 4.10: Cr^{3+} sidebands: 5000-5100 Å, $\vec{E}||\vec{x}$

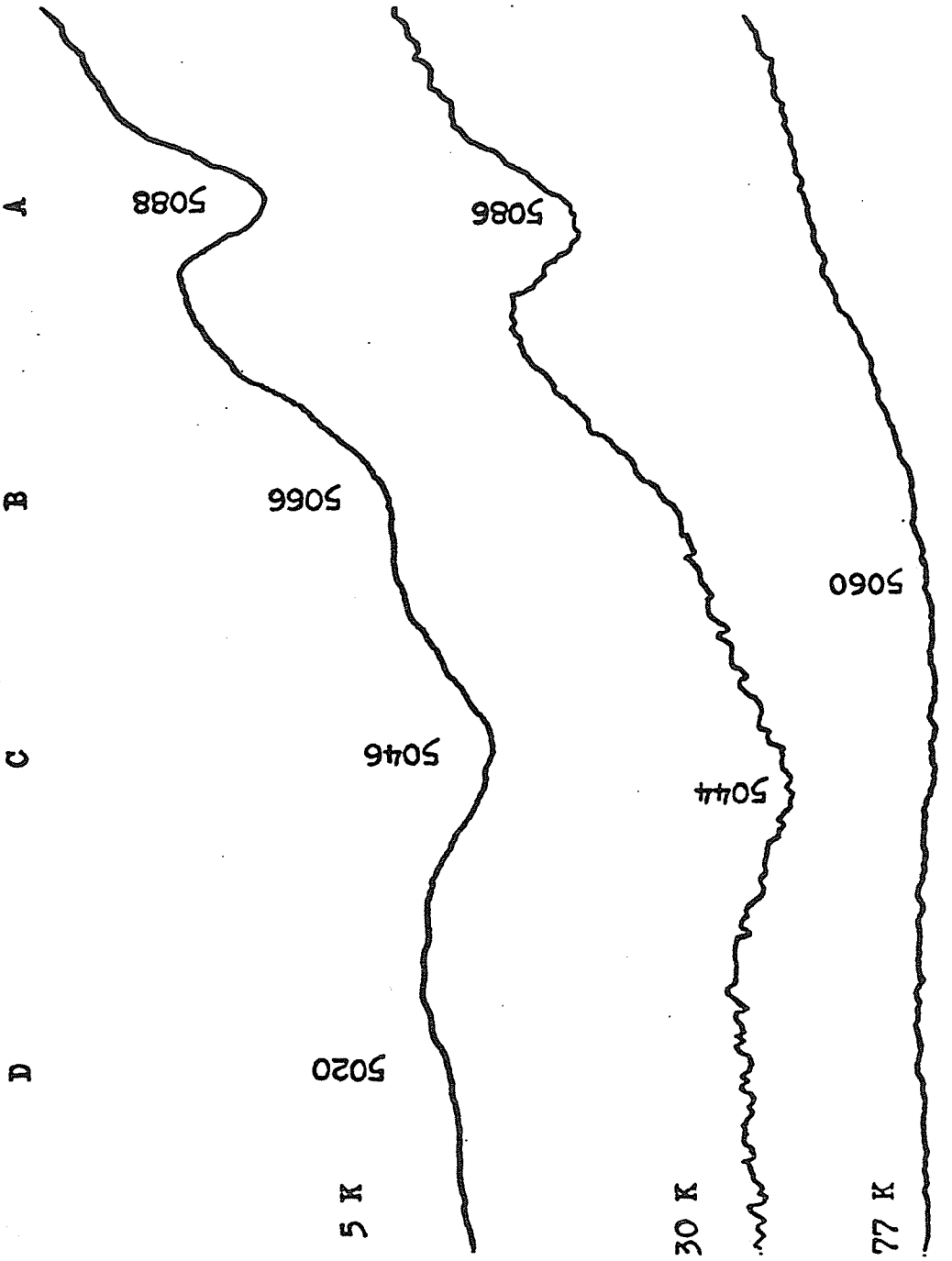

Figure 4.11: Cr^{3+} sidebands: 5000-5100 Å, $\vec{E}||\vec{y}$

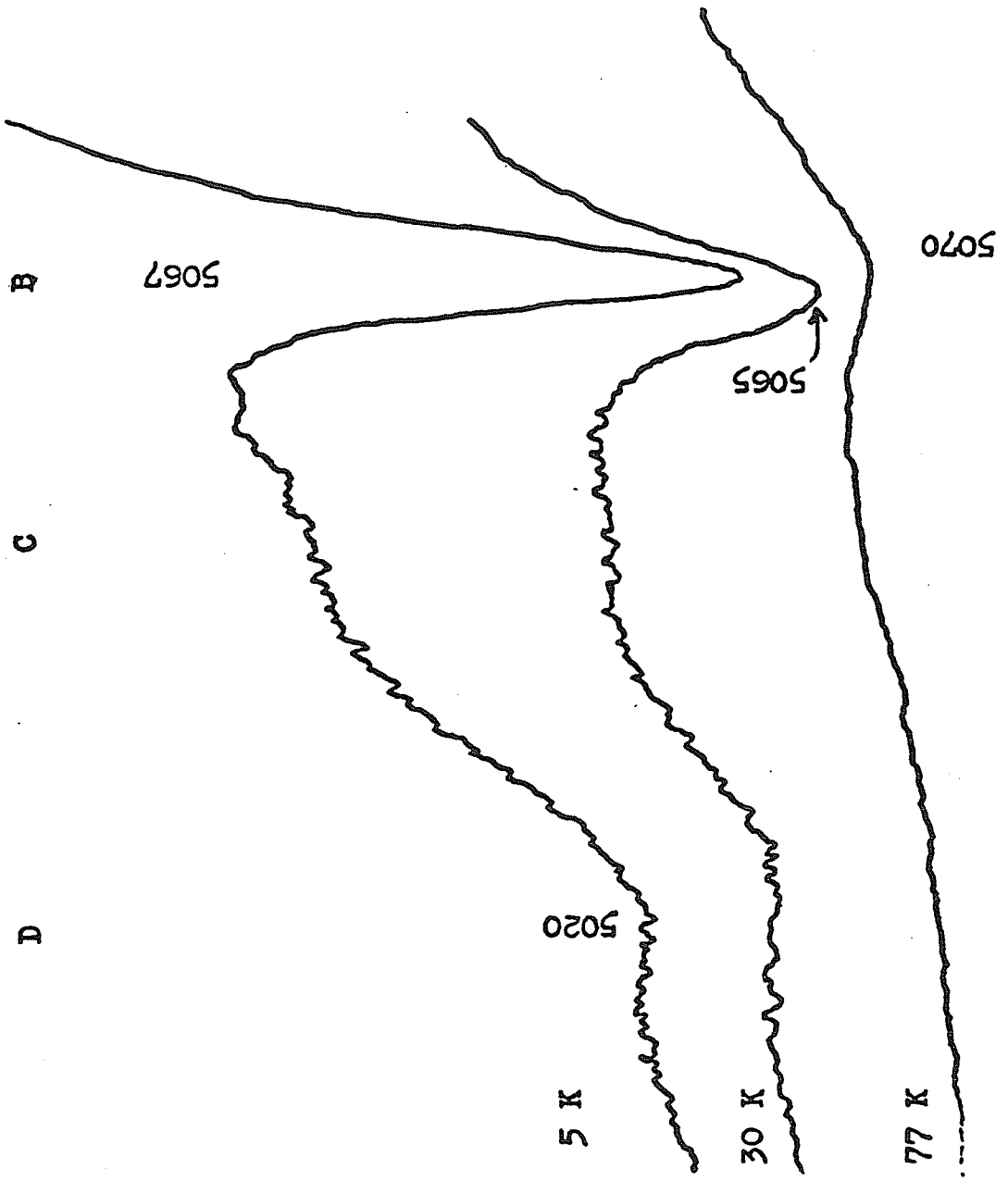

Figure 4.12: Cr^{3+} sidebands: 5000-5100 Å, $\vec{E}||\vec{z}$

$$A = 19658 = 19561 + 97 \ cm^{-1}$$

$$B = 19739 = 19560 + 179 \ cm^{-1}$$

$$C = 19818 = 19559 + 259 \ cm^{-1} ,$$

these lines can also be interpreted as magnon sidebands corresponding to the absorption of a photon with the simultaneous creation of an exciton at about 19560 cm^{-1} and one magnon of 97 cm^{-1} and two magnons of energies 179 and 259 cm^{-1} respectively. Line D can be visualized as D = 19920 = 19558 + 362 cm^{-1} where 362 cm^{-1} was the phonon energy deduced in the last section. The temperature dependences of the spectra also show that A, B and C are similar to magnon sidebands. However line D broadens very rapidly as it should if it is a phonon-assisted transition. Again the excitons are too weak to be observed. There are other transitions in the range 5100 - 5200 Å which can also be interpreted as magnon sidebands. However, since these also exhibit abrupt changes, they will be discussed in the next section together with the Tm^{3+} transitions and the other transitions showing abrupt changes.

4.4.2 Abruptly changing transitions

The following transitions, which will be discussed in the order Tm^{3+}, Cr^{3+} and Cr^{3+} - Tm^{3+} respectively, have the common feature that they can be either temperature or

field induced at about a fraction of a degree Kelvin below 4.2 K. The change in intensity when the critical temperature is crossed, is in all cases very abrupt signifying a change in spin configuration. However abrupt changes are not observed for the a-b sample.

4.4.2.1 Tm^{3+} transitions: 6687 and 6876 Å

The 6876 Å (Figure 3.4 If) transition of $^3H_6 \rightarrow {}^3F_3$ and the 6687 Å (Figure 3.3 Ia) transition of $^3H_6 \rightarrow {}^3F_2$ show an abrupt decrease to vanishing intensity as the temperature is decreased through the critical temperature, hereafter denoted by T_c. There is practically no shift in line position during the change which is complete in about half a degree Kelvin. The temperature dependences of these lines are shown in Figure 4.13 and 4.14. As mentioned in Chapter 3 at 4.2 K an external magnetic field, parallel to the z direction and of magnitude ~900 Oe, is sufficient to suppress these transitions. It is also observed that their intensities remain almost unchanged, after heating above T_c, except for the usual line broadening. However the broadening is slight compared with those of the Cr^{3+} magnon sidebands and phonon sidebands reported earlier. These two lines can indeed be followed up to 77.7 K with line widths of approximately 13 cm^{-1} compared with the magnon sidebands whose line widths are about 30 cm^{-1}. Thus they are definitely not magnon or

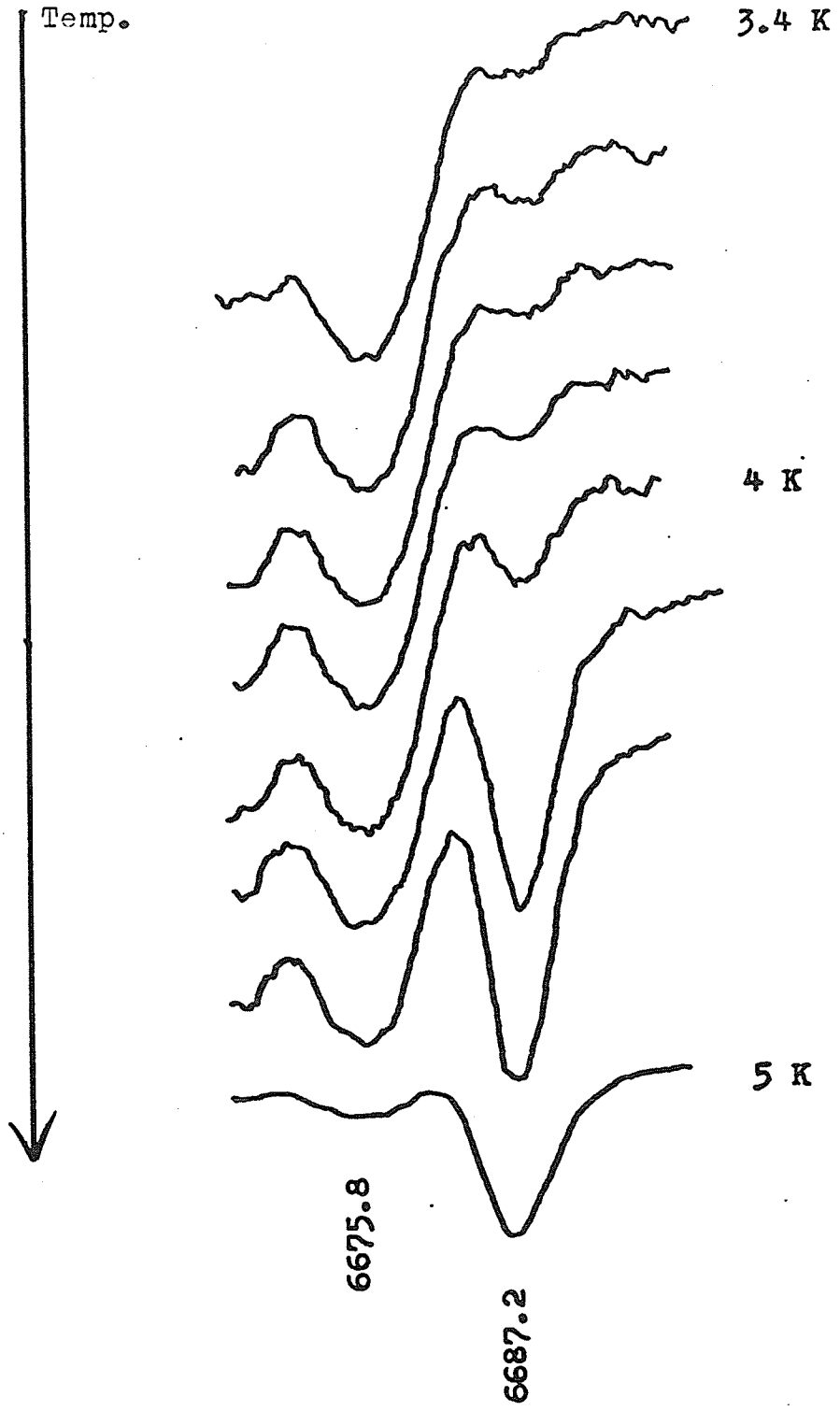

Figure 4.13: Tm^{3+} transition: 6687 Å, $\vec{E}||\vec{z}$; absorption curve at 5 K is recorded with a recorder sensitivity 1/5 of that of the other curves; spectra taken continuously as the sample temperature increases from 3.4 to 4 to 5 K, but the in between temperatures were not determined

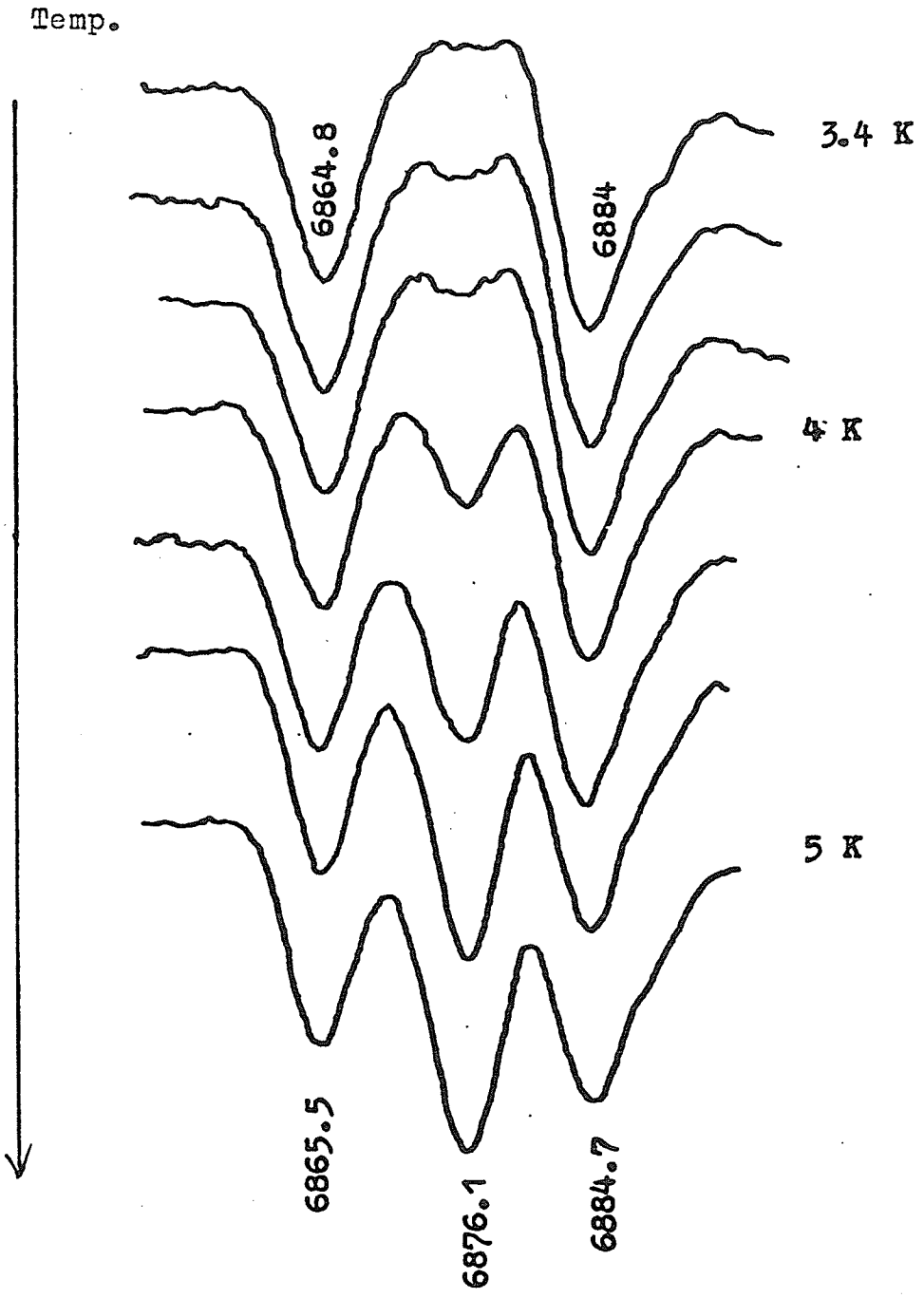

Figure 4.14: Tm^{3+} transition: 6876 Å, $\vec{E}||\vec{z}$; see caption of Figure 4.13

phonon sidebands superimposed on the Tm^{3+} spectra. Furthermore the 6687 line, as discussed in Chapter 3, is essentially a manifestation of the relaxation of the selection rules for the Tm^{3+} transitions which are strictly valid if the spin configuration is $\Gamma_4(F_z)$. In this case the molecular field causes no mixing of states of different representations. On the other hand at higher temperatures the stable configuration is $\Gamma_2(F_x)$, whose molecular field mixes states of different representations which causes the relaxation of the selection rules. The appearance of this line, as discussed in Chapter 3, results in an inconsistent assignment of representation labels to the Tm^{3+} levels. In particular levels I and II of $^3H_6$ have labels A_1 and A_2 as deduced from transitions to $^3F_3$ and $^3F_4$, but A_2 and A_1 from transitions to $^3F_2$. However on lowering the temperature, or with the application of the small magnetic field this very intense line is suppressed and as a consequence all the inconsistencies are removed and the selection rules are obeyed. Furthermore, levels I and II have A_1 and A_2 respectively, agreeing with the result deduced from magnetization measurements (Hornreich et al, 1973). The interpretation of the abrupt changes as spin reorientation $\Gamma_2 \leftrightarrow \Gamma_4$ is also consistent with the results of Cr^{3+} exciton studies of $TmCrO_3$ (Aoyagi et al, 1976). They reported exciton observations consistent with the Γ_4 configuration while the application of a magnetic field induced spin reorientation making the

observations consistent with the Γ_2 configuration. The ~4 K critical temperature observed in the present work also agrees with the temperature reported for the temperature and field induced spin reorientation of Cr^{3+} in $TmCrO_3$ (Tamaki et al, 1977). The line 6876 Å which does not, as discussed before, affect the selection rules and assignment of representation labels will not be discussed further.

4.4.2.2 Cr^{3+} transitions: 5100 - 5200 Å

The Cr^{3+} transitions in the range 5100 - 5200 Å are to part of the levels of the Cr^{3+} $^2T_2$ cubic level. Due to the combined effect of the C_i site symmetry and the spin-orbit interaction the level is split into three crystal field levels, each of which is split into two levels by the exchange field. Transitions from the $^4A_2$ (-3/2) ground level to these levels are parity and spin forbidden. However they can occur as assisted electric-dipole transitions in the form of magnon and phonon sidebands. The magnon and phonon sidebands with wavelengths from 5000- 5100 Å have been discussed. It was observed that they could be interpreted as one-magnon and two-magnon sidebands or phonon sidebands of an exciton level at ~19560 cm^{-1}. In this section it will be seen that the lines in the 5100 - 5200 Å could also be interpreted as magnon sidebands of other exciton levels.

The positions, energies, and polarizations of the above lines are given in Table 4.4 with the spectra shown in Figure 4.15 and 4.16. The $\vec{E}||\vec{x}$ spectra from the a-b sample are only just resolved and as mentioned at the beginning, do not show abrupt changes. Therefore they are not shown. (Their positions are approximately 5135, 5144, 5166 and 5176 Å). Since the behaviour of the spectra with $\vec{E}||\vec{x}$ or $\vec{E}||\vec{y}$ are similar to that with $\vec{E}||\vec{z}$, only the temperature dependences of the lines with $\vec{E}||\vec{z}$ are given (Figure 4.17). Table 4.4 also shows how the lines can be "decomposed" into two energies, one of which is the one or two-magnon energies obtained earlier. The other energy can be interpreted as unobserved exciton levels at ~19260 and ~19230 cm^{-1} for $T < T_c$ and at ~19262 and ~19223 cm^{-1} for $T > T_c$. Apart from the abrupt changes at T_c, these lines remain essentially unchanged in relative intensities for higher temperatures. At 77.7, however, they are so broadened that they cannot be traced. Also near T_c the absorption lines have half-widths of about 25 cm^{-1}. Thus they are magnon sidebands of these hitherto unobserved excitons. (So far magnon sidebands and excitons of $RCrO_3$ have only been reported in literature for the ^2E levels). These magnon sidebands behave very differently from those in the ~7200 Å region and in the 5000 - 5100 Å region. The 5100 - 5200 Å sidebands exhibit abrupt changes whereas the other sidebands just mentioned do not. This can be explained by assuming that the $^4A_2$ g

	Å	cm^{-1}	$\vec{E}\|\|\vec{y}$	$\vec{E}\|\|\vec{z}$	Interpret. cm^{-1}	Temp.
H	5122	19524	x		19266+258	$T<T_c$
G	5136	19470		x	19258+212	$T<T_c$
F	5143	19444		x	19444+212	$T<T_c$
E	5148	19425		x	19231+194	$T<T_c$
D	5158	19387		x	19258+129	$T<T_c$
C	5164	19365	x	x	19259+106	$T<T_c$
B	5174	19327		x	19230+ 97	$T<T_c$
A	5135	19324	x		19227+ 97	$T<T_c$
G'	5135	19474	x	x	19262+212	$T>T_c$
F'	5144	19440		x	19228+212	$T>T_c$
E'	5146	19432	x		19220+212	$T>T_c$
D'	5156	19395	x		19266+129	$T>T_c$
C'	5166	19357	x	x	19260+ 97	$T>T_c$
B'	5176	19320		x	19223+ 97	$T>T_c$
A'	5177	19316	x		19219+ 97	$T>T_c$

Table 4.4 Magnon sidebands : 5100 - 5200 Å ;
x means that transition is allowed.

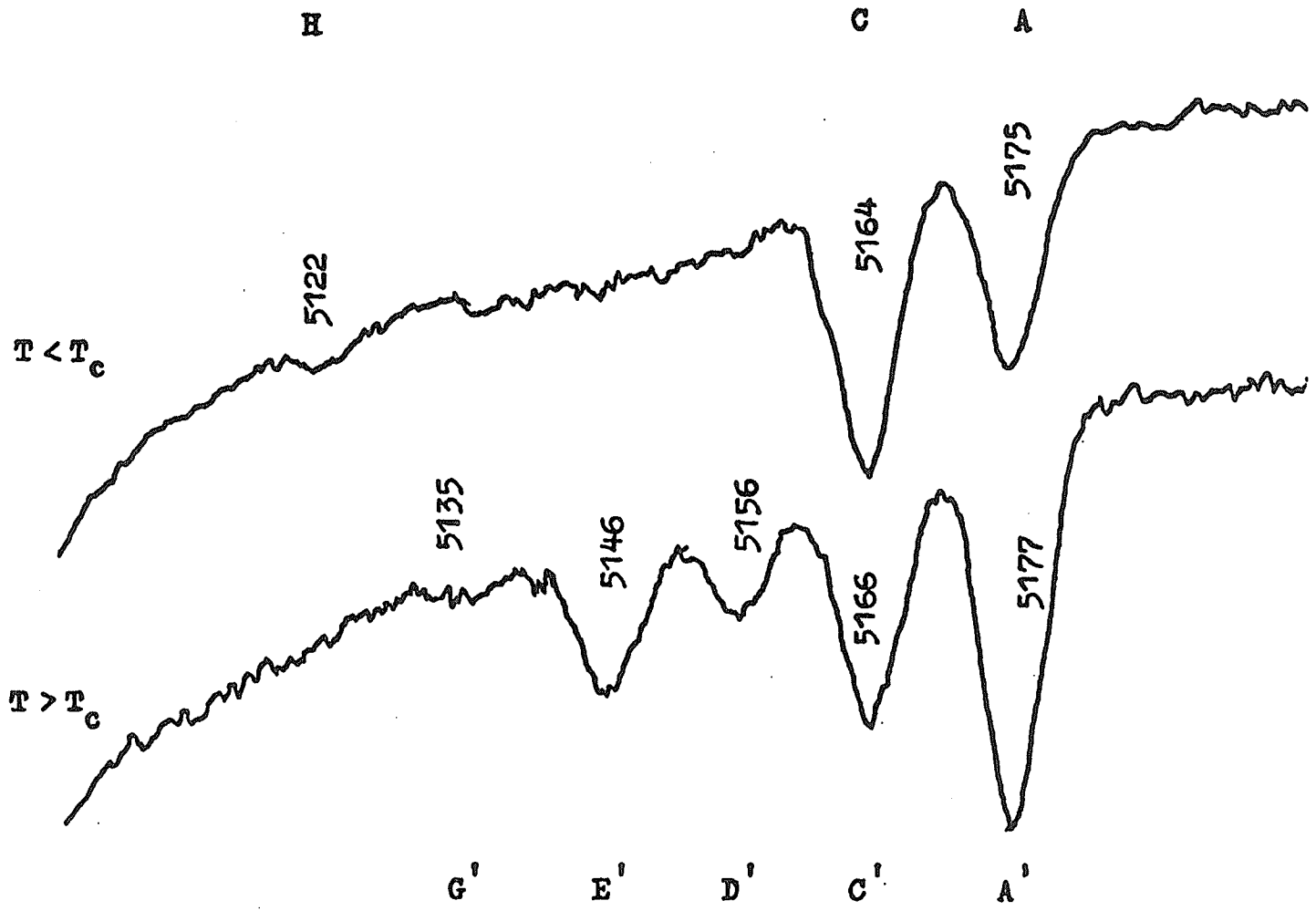

Figure 4.15: Cr^{3+} sidebands: 5100-5200 Å, $\vec{E}||\vec{y}$; T_c is the critical temperature for the abrupt changes

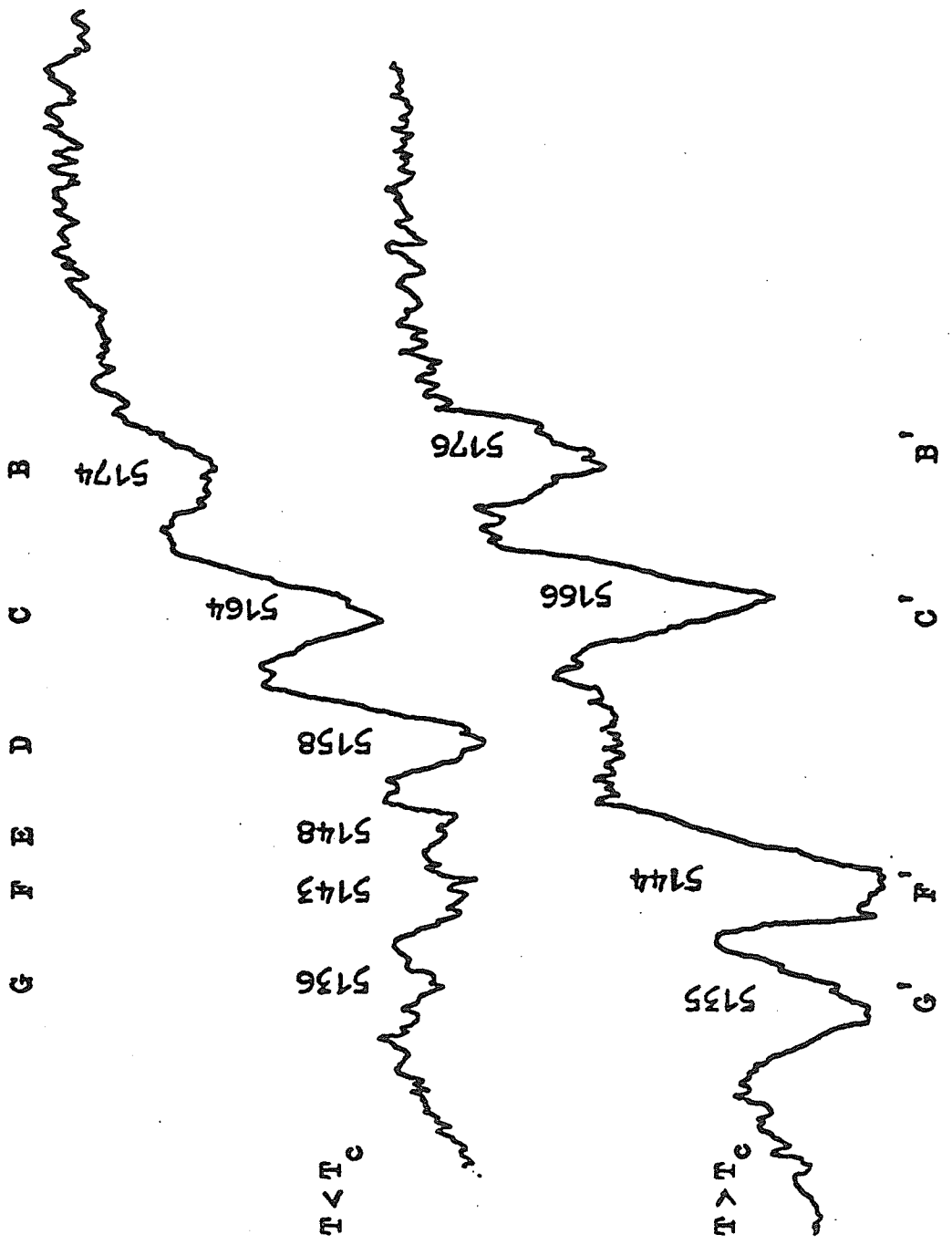

Figure 4.16: Cr^{3+} sidebands: 5100-5200 Å, $\vec{E}||\vec{z}$; T_c is the critical temperature

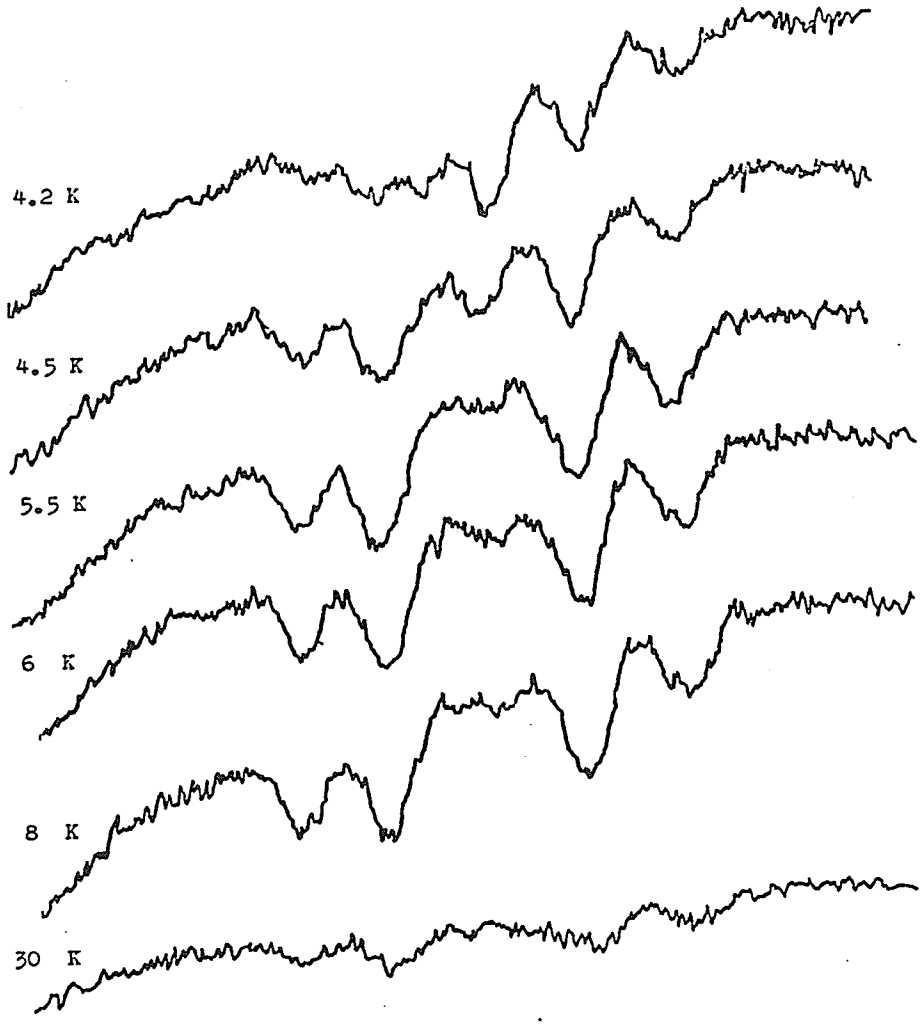

Figure 4.17: Cr^{3+} sidebands: 5100-5200 Å, $\vec{E}||\vec{z}$, $\vec{H}_o||\vec{z}$, showing field induced abrupt changes and temperature dependences where $\vec{H}_o$ is the applied field of ~900 Oe

factors (the magnons are derived from levels of this level) and hence the magnitude of the exchange splittings due to the molecular field are isotropic and do not depend on spin configurations as in $LuCrO_3$ (Kajiura et al, 1975). Some of the exciton levels derived from the exchange-split levels and the exchange-split levels themselves of the excited level $^2T_2$ are however dependent on spin configurations and so the magnon sidebands depend on the spin configurations because of the excitons. The exciton levels predicted are however too far apart to be exciton levels of the same exchange-split level. They probably belong to two separate single-ion exchange-split levels, since the Davydov splittings of such excited states are very small if those of the ^2E level are just about 7 cm^{-1} for $RCrO_3$.

4.4.2.3 Cr^{3+} - Tm^{3+} transitions

This group of lines is presented in Figure 4.18 and 4.19. These spectra are however quite weak and only an unresolved band is observed for the a-b sample. The positions, wavenumbers and polarization characteristics of the corresponding excited levels are given in Table 4.5. In this case the polarization is given in both the $\vec{E}$ and $\vec{H}$ vector since spectra from two samples of two crystallographic orientations are needed for a determination of the dipole nature of the transitions. However similar transitions of

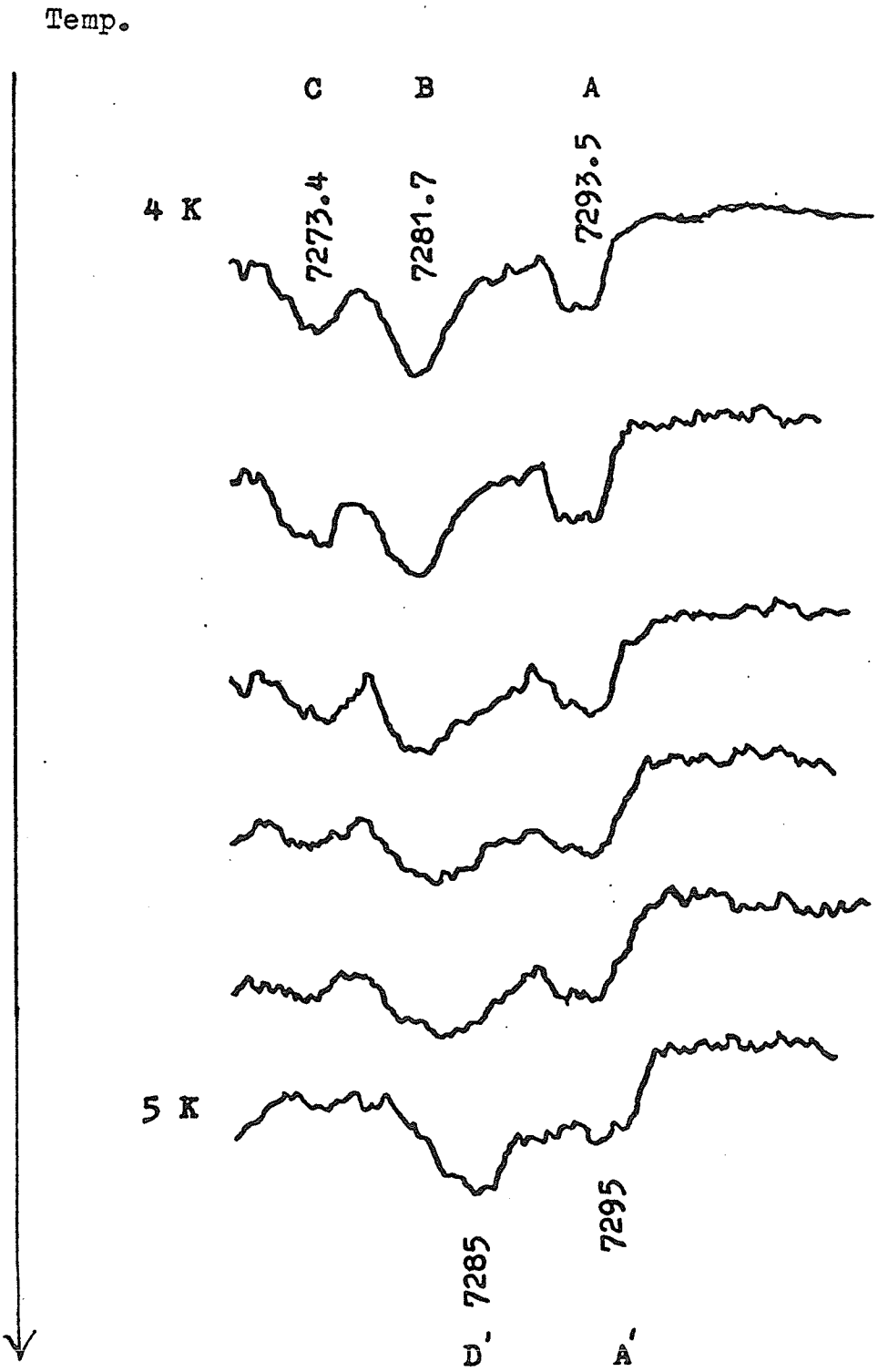

Figure 4.18: Cr^{3+} - Tm^{3+} transitions 7270-7300 Å, $\vec{E}||\vec{y}$, $\vec{H}||\vec{z}$; see caption of Figure 4.13

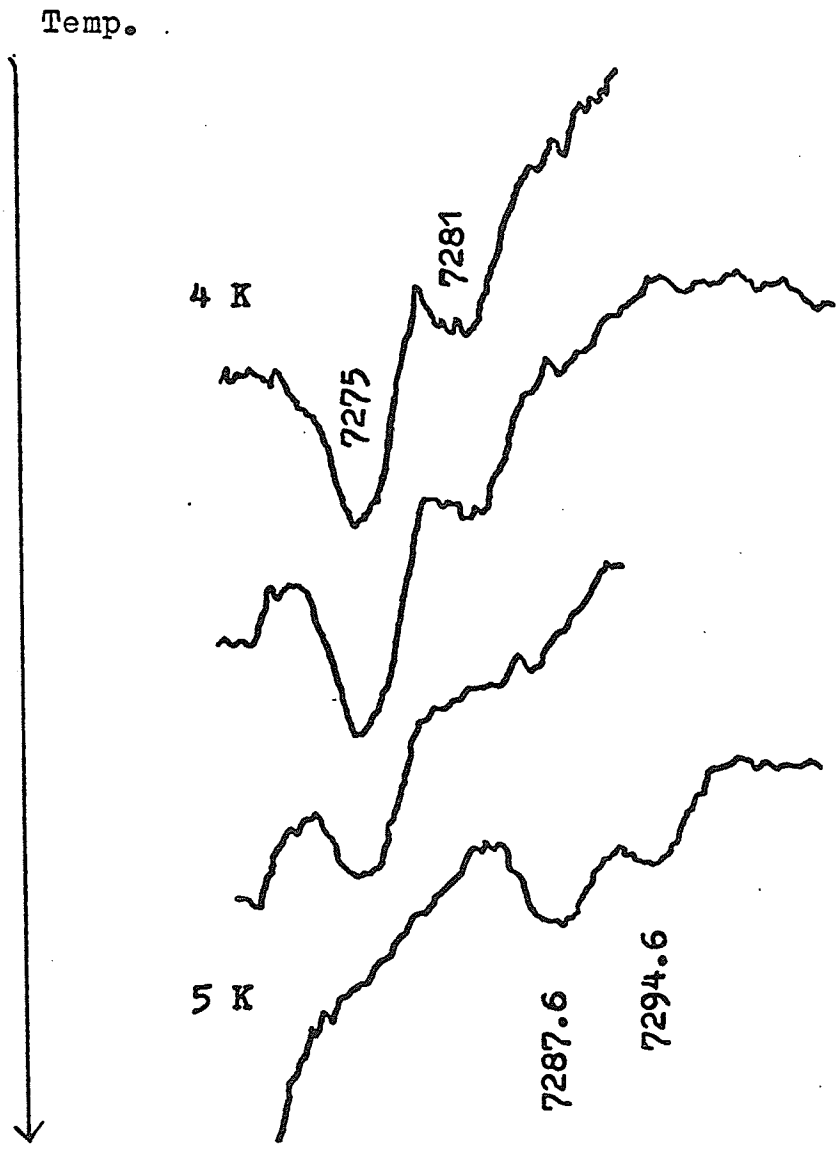

Figure 4.19: Cr^{3+} - Tm^{3+} transitions 7270-7300 Å, $\vec{E}||\vec{z}$, $\vec{H}||\vec{y}$; see caption of Figure 4.13

	Å	cm^{-1}	$\vec{E}\|\|\vec{y}$ $\vec{H}\|\|\vec{z}$	$\vec{E}\|\|\vec{z}$ $\vec{H}\|\|\vec{y}$	Interpret.cm^{-1}	Temp.
D	7273.4	13748.8	x		13709+40	$T<T_c$
C	7275	13745.7		x	13705+41	$T<T_c$
B	7281.7	13733.1	x	x	13711+22	$T<T_c$
A	7293.5	13710.8	x		13705+ 6	$T<T_c$
D'	7285	13727	x		13703+24	$T>T_c$
C'	7287.6	13721.9		x	13700+22	$T>T_c$
B'	7294.2	13709.5		x	13703+ 7	$T>T_c$
A'	7295	13708	x		13701+ 7	$T>T_c$

Table 4.5 Cr^{3+} - Tm^{3+} transitions: 7270 - 7300 Å; x means transition is allowed.

electric dipole origin have been observed in the same region for the other $RCrO_3$ (e.g. Kojima, 1980). So these transitions are likely to be electric dipole. These lines are close in position to the exciton levels of $TmCrO_3$ reported (Aoyagi, 1976). However, their line widths are about 13 cm^{-1}, whereas the excitons have half-widths ~1 cm^{-1} and the total Davydov splittings for the four excitons are ~7 cm^{-1}. Besides, these lines like the magnon sidebands (which however have half-widths of ~25 to 30 cm^{-1}) persist up to more than ~30 K and they too broaden and disappear into the back ground at higher temperatures. At the temperatures at which they can be traced, their relative intensities remain relatively constant.

The four exciton levels can be estimated from the observation reported by Aoyagi et al (1976). These are approximately 13711, 13709, 10705 and 13704 cm^{-1} for the Γ_4 configuration and 13703, 13701, 13700 and 13698 cm^{-1} for the Γ_2 configuration. The transitions reported here can then be interpreted in terms of these excitons and they are shown in Table 4.5. It is seen that these lines, whatever their origin, clearly "follow" the shift of the excitons in the reorientation $\Gamma_2 \leftrightarrow \Gamma_4$. They are characterized by two energies of ~23 and ~7 cm^{-1} which remain more or less unaffected by the change of spin configurations. The energy

of ~40 cm^{-1} is probably a similar quantity. The origin of these transitions cannot be determined in the present work. Such determination needs more detailed knowledge of the excitons which for $TmCrO_3$ are only very briefly reported (Aoyagi et al, 1976). However, as mentioned before, similar transitions have been observed and accounted for as Cr^{3+} exciton - rare-earth ion spin flip absorptions for the other $RCrO_3$.

4.5 Summary

In this chapter the spectra of $TmCrO_3$ other than those reported in Chapter 3 or briefly mentioned there, have been discussed and elaborated. It has been argued that these spectra can be conveniently grouped into those exhibiting abrupt changes at low temperature and those that do not. The first group consists of Cr^{3+}, Tm^{3+} and Cr^{3+} - Tm^{3+} transitions whereas the second consists only of Cr^{3+} transitions. In both groups the Cr^{3+} transitions however are mainly magnon-assisted electric dipole transitions with some additional sidebands due to phonons. Magnon energies found are consistent with those obtained for $YCrO_3$ (Aoyagi, 1974). However the present work also reports the magnon sidebands in the 5000 - 5200 Å region, which to the present, have not been reported in literature for any $RCrO_3$. Exciton levels, again not reported in literature, have been predicted. Transitions of

Cr^{3+} and Cr^{3+} - Tm^{3+} exhibiting abrupt changes have been interpreted in terms of excitons derived from Cr^{3+} cubic cubic levels $^2T_2$ and ^2E respectively. These changes are interpreted as indications of spin reorientation. The Cr^{3+} and Cr^{3+} - Tm^{3+} transitions show the spin reorientation directly through the spin-configuration dependent positions of the exciton levels whereas the Tm^{3+} transitions change in such a way that the selection rules are better obeyed at the lower temperature - more stable Γ_4 configuration. All the transitions are observed in both a-b and b-c samples, but abrupt spin reorientation is only observed in the b-c sample, which in the $\Gamma_4(F_z)$ configuration has a net moment along the z direction i.e. in the plane of the sample. On the other hand, the a-b sample in the $\Gamma_4(F_z)$ configuration has the net moment perpendicular to the plane of the sample. Therefore it needs more energy and a higher field, for a given temperature, to reorientate the moment from the x to the z axis. Apparently the small field of ~900 Oe is just sufficient, at 4.2 K, to bring about the reorientation of the moment for the b-c sample and so is not high enough for the a-b sample.

CHAPTER V

SUMMARY AND SUGGESTION FOR FURTHER WORK

5.1 Summary

In this thesis optical absorption spectroscopy has been used to study $TmCrO_3$ single crystals. The energy levels, and the corresponding group representation labels, of the multiplets $^3F_2$, $^3F_3$ and $^3F_4$ together with those of some of the $^3H_6$ ground multiplet have been determined. The level positions as expected are close to those of the isomorphous $TmFeO_3$, but the allocation of the representation labels to corresponding levels in the two compounds are very different. In particular, the representation labels of the two lowest Tm^{3+} levels in $TmCrO_3$ are different, agreeing with the results of magnetization studies, whereas those of the corresponding levels in $TmFeO_3$ have the same labels. This fact, as discussed in Chapter 3 explains the differences in low temperature behaviour of these two compounds.

Spin reorientations have been detected by observation of Tm^{3+} transitions, Cr^{3+} magnon assisted transitions and Cr^{3+} - Tm^{3+} spin-flip type pair transitions. These transitions all undergo directly or indirectly (except the ~7200 Å magnon sidebands) abrupt changes, which have been interpreted as manifestations of a spin reorientation.

Furthermore, these changes are indeed abrupt, being complete in a tiny fraction of a degree Kelvin. The stable, zero field, configuration at helium temperature is the $\Gamma_4(F_z)$ spin configuration agreeing with the results of exciton studies on $TmCrO_3$.

Magnon sidebands are found for $TmCrO_3$ excitons at ~7300 Å. From these sidebands magnon energies have been deduced, which are close in values to those found in $YCrO_3$. Neither the excitons at ~13700 cm^{-1} (~7300 Å) nor those at 20000 cm^{-1} (~5000 Å) have been observed in this work, but the magnon sidebands of the latter excitons are identified in this work (the excitons at ~13700 cm^{-1} have been observed by Aoyagi et al, 1976).

5.2 Suggestion for work

It is instructive to investigate the Zeeman effect of all the transitions reported. In particular, as proved by Malozemoff, 1970, this can help confirm the representation labels of the Tm^{3+} crystal levels.

Temperature-induced phase transitions have been the focus of this thesis, although it has also been demonstrated that at helium temperature, a magnetic field of less than 1000 Oe can also bring about these changes. A detailed study of field-induced transitions has been done by Tamaki

et al, 1977 using magnetization studies; the critical field as a function of temperature has been determined. It is therefore meaningful if similar dependences can be obtained spectroscopically.

The spin reorientation detected in this work is of the type $\Gamma_2(F_x) \rightarrow \Gamma_4(Fz)$ as the temperature decreases. According to theoretical studies (Yamaguchi, 1974) such a phase transition is not possible. Thus it is important that the corresponding theory be re-examined. (Hornreich, 1978 also has provided other instances which are contradictory to the predictions of this theory, regarding the order of the phase transitions). It is also very meaningful to investigate further the order of the transition detected in this work since the abruptness of the changes suggests a phase transition of the first order.

Spin reorientations can also be confirmed by the method of Faraday rotation. In the case of a $\vec{b}$-$\vec{c}$ platelet, for example, with the $\vec{k}$ vector of the incident light parallel to the $\vec{a}$ crystallographic axis, Faraday rotation of the plane of polarization of the incident light is expected for the $\Gamma_2(f_x)$ configuration, but not for the $\Gamma_4(F_z)$ configuration (there is no net component of magnetic moment parallel to the $\vec{k}$ vector). There are two general methods to study Faraday rotation. In one method the intensities of the

transmitted light for the cases $\vec{k}||\vec{M}_k$ and $\vec{k}||-\vec{M}_k$, are compared where $\vec{M}_k$ is the component of the net magnetic moment in the direction of wave vector $\vec{k}$. From such a comparison, the angle of Faraday rotation can be deduced; these two intensities will not be equal if $\vec{M}_k = 0$. Alternatively, the transmitted light, which is in general elliptically polarized, can be converted to a plane polarized light with a Babinet compensator. The orientations of the phane of polarization are different for the cases $\vec{k}||\vec{M}_k$ and $\vec{k}||-\vec{M}_k$. In both methods the angle of Faraday rotation is zero if $\vec{M}_k = 0$ as in the case of a spin reorientation.

Finally, Raman spectroscopy can also be conducted with $TmCrO_3$ to obtain the phonon energies and so providing a means to confirm the phonon energies deduced from phonon sideband measurements of this work.

REFERENCES

Allen, J.W., 1970, Solid State Commun. 11, 53.

Antonov, V.A., Arsenev, P.A., Bienert, K.E. and Potemkin, A.V., 1973, Phys. Stat. Sol(a) 19, 289.

Aoyagi, K., Tsushima, K. and Sugano, S., 1969, Solid State Commun. 7, 229.

Aoyagi, K., 1974, NHK tech. Reports, 26, 2,Ser. 141.

Aoyagi, K., Kajiura, M., Morishita, T. and Tsushima, K., 1976, Ann. Conf. Phys. Soc., Japan 5a-Q4.

Aoyagi, K., Kajiura, M., Tsushima, K., Nakagawa, Y. and Tsujikawa, I., 1977, Physica, 86-88 B + C, pt. III, 1207.

di Bartolo, B., 1968, Optical Interactions in Solids, Wiley and Sons, Inc.

Bermudez, V.M. and McClure, D.S., 1979, J. Phys. Chem. Solids, 40, 129.

Bermudez, V.M. and McClure, D.S., 1979, J. Phys. Chem. Solids, 40, 149.

Bertaut, E.F. and Forrat, F., 1956, J. Phys. Rad., 17, 129.

Bertaut, E.F., 1963, in "Magnetism", ed. Rado, G.T. and Suhl, H., Vol. III, Academic Press.

Bertaut, E.F., Mareschal, J., de Vries, G., Aleonard, R., Pauthenet, R., Rebouillat, J.P. and Zarubicka, V., 1966, IEEE Trans. Mag., 2, 453.

Burns, G. and Glazer, A.M., 1978, Space Groups for Solid State Scientists, Academic Press.

Caird, J.A., Deshazer, L.G. and Nella, J., 1975, IEEE J. of Quan. Elect., QE-11, 11, 874.

Cohen, M.G. and Bloembergen, N., 1964, Phys. Rev. 135, 4A, 950.

Cooke, A.H., Martin, D.M. and Wells, M.R., 1974, J. Phys. C. Solid State Phys., 7, 3133.

Courths, R. and Hüfner, S., 1975, Z. Physik B, 22, 245.

Courths, R. and Hüfner, S., 1976, Z. Physik B, 24, 193.

Cracknell, A.C., 1975, Magnetism in Crystalline Materials, Pergamon Press.

Dzyaloshinski, I., 1958, J. Phys. Chem. Solids, 4, 241.

Fairbank, Jr., W.M. and Klauminzer, G.K., 1973, Phys. Rev. B 7, 7.

Geller, S. and Wood, E.A., 1956, Acta Cryst. 9, 563.

Geller, S., 1956, J. Chem. Phys., 24, 1236.

Gordon, D.J., 1976, Ph.D. Thesis, Weizmann Institute of Science.

Gordon, J.D., Hornreich, R.M., Shtrikman, S. and Wanklyn, B.M., 1976, Phys. Rev. B, 13, 3012.

Hasson, A., Hornreich, R.M., Komet, Y., Wanklyn, B.M. and Yaeger, I., 1975, Phys. Rev. B, 12, 5051.

Hornreich, R.M., Komet, Y. and Wanklyn, B.M., 1972, Solid State Commun., 11, 969.

Hornreich, R.M., Wanklyn, B.M. and Yaeger, I., 1973, Int. J. Magnetism, 4, 313.

Hornreich, R.M., Komet, Y., Nolan, R., Wanklyn, B.M. and Yaeger, I., 1975, Phys. Rev. B, 12, 5094.

Hornreich, R.M., 1978, J. of Magnetism and Magnetic Materials, 7, 280.

Hüfner, S., 1978, Optical Spectra of transparent Rare Earth Compounds, Academic Press.

Kajiura, M., Aoyagi, K. and Tamaki, T., 1975, J. Phys. Soc. Japan, 39, 1572.

Kaneko, M., Kurita, S. and Tsushima, K., 1977, J. Phys. C., Solid State Phys., 10, 1979.

Kaplyanskii, A.A. and Medvedev, V.N., 1968, Soviet Physics, Solid State, 9, 2121.

Kaplyanskii, A.A., Przhevuskii, A.K. and Rozenbaum, R.B., 1969, Soviet Physics, Solid State, 10, 1864.

Kaplyanskii, A.A., Rozenbaum, R.B., 1972, Soviet Physics, Solid State, 13, 2200.

Koehler, W.C., Wollan, E.O. and Wilkinson, M.K., 1960, Phys. Rev. 118, 58.

Kojima, N., Tsushima, K. and Tsujikawa, I., 1980 I, J. Phys. Soc., Japan, 49, 1449.

Kojima, N., Tsushima, K., Kurita, S. and Tsusjikawa, I., 1980II,J. Phys. Soc., Japan, 49, 1456.

Kojima, N., Aoyagi, K., Tsushima, K., Tsujikwa, I. and Sugano, S., 1980III, J. Phys. Soc. Japan, 49, 1463.

Loudon, R., 1968, Adv. in Phys., 17, 243.

Low, W., 1960, J. Chem. Phys., 33, 1162.

Malozemoff, A.P., 1970, Ph.D. thesis, Stanford University.

McClure, D.S., 1962, J. Chem. Phys., 36, 2757.

Meltzer, R.S., 1970, Phys. Rev. B, 2, 2398.

Meltzer, R.S. and Moos, H.W., 1970, J. Applied Phys., 41, 1238.

Morishita, T., Aoyagi, K., Tsushima, K. and Kigawa, T., 1976, Solid State Commun., 20, 123.

Morishita, T., Aoyagi, K., Tsushima, K. and Kigawa, T., 1977, Physica, 86-88B, 1209.

Nomura, S., 1978, Landolt-Bornstein, Numerical Data and Functional Relationships in Science and Technology, New Series Group III Vol. 12, edited by K.H. Hellwege, Springer-Verlag, p. 387.

Pataud, P. and Sivardiere, J., 1970, J. de Phys. 31, 803.

Reisfeld, R. and Jorgensen, C.K., 1977, Inorganic Chemistry Concepts, Vol. 1, Lasers and Excited States of Rare Earths, Springer-Verlag.

Satoko, C. and Washimiya, S., 1977, J. Phys. Soc. Japan, 42, 1888.

Shamir, N., Melamud, M., Shaked, H. and Shtrikman, S., 1977a Physica, 86-88B, 1037.

Shamir, N., Melamud, M., Shaked, H. and Shtrikman, S., 1977b, Physica, 90B, 217.

Shamir, N., Shaked, H. and Shtrikman, S., 1977c, Physica, 90B, 211.

Slobodsky, Philip, 1979, Ph.D. thesis, Weizmann Institute of Science.

Sugano, S., Tanabe, Y. and Kamimura, H., 1970, Multiplets of Transition Metal Ions in Crystals, Academic Press.

Sugano, S., Aoyagi, K. and Tsushima, K., 1971, J. Phys. Soc. Japan, 31, 706.

Sviridov, D.T., Sevastyanov, B.K., Orekhova, V.P., Sviridova, R.K. and Veremeichik, T.F., 1973, Opt. Spectrosc., 35, 59.

Tamaki, T., Tsushima, K. and Yamaguchi, Y., 1977, Physica, 86-88B, 923.

Tinkham, M., 1964, Group Theory and Quantum Mechanics, McGraw-Hill, N.Y.

Tsushima, K., Aoyagi, K. and Sugano, S., 1970, Applied Phys., 41, 1238.

Udagawa, M., Kohn, K., Koshizuka, N., Tsushima, T. and Tsushima, K., 1975, Solid State Commun., 16, 779.

Uesaka, Y., Tsujikawa, I., Aoyagi, K., Tsushima, K. and Sugano, S., 1971, J. Phys. Soc. Japan, 31, 1380.

Ullrich, D., Courths, R., and Von Grundherr, C., 1977, Physica, 89B, 205.

Van der Ziel, J.P. and Van Uitert, L.G., 1969a, Phys. Rev. 179, 343.

Van der Ziel, J.P. and Van Uitert, L.G., 1969b, Phys. Rev. 180, 343.

Washimiya, S. and Yamaguchi, T., 1975, J. Phys. Soc., Japan, 38, 1302.

Weber, M.J., 1973, J. Appl. Phys., 44, 4058.

Weber, M.J. and Varitimos, T.E., 1974, J. Appl. Phys., 45, 810.

Wood, D.L., Ferguson, J., Knox, K. and Dillon, J.F., 1963, J. Chem. Phys., 39, 890.

Wybourne, B.G., 1965, Spectroscopic Properties of Rare Earths, Interscience Publishers.

Yamaguchi, T. and Tsushima, K., 1973, Phys. Rev. B, 8, 5187.

Yamaguchi, T., 1974, J. Phys. Chem. Solids, 35, 479.

Yamaguchi, T., 1975, J. Phys. Soc., Japan, 38, 1270.

Zuk, J. and Piotrowski, K., 1977, Appl. Phys., 14, 119.

Zuk, J. and Piotrowski, K., 1978, Solid State Commun., 28, 381.